**UNIVERSITÄTSKLINIKUM HAMBURG-EPPENDORF**

Laboratory of Radiobiology and experimental Radioocology

Direktor/in der Einrichtung

Prof. Dr. rer. nat. Kai Rothkamm
Laboratory of Radiobiology and experimental Radioocology

# Unveiling the role of SPOP in DNA damage response and double strand break repair: From mechanistic insights to clinical application

**Dissertation**

zur Erlangung des Doktorgrades Dr. rer. biol. hum.

an der Medizinischen Fakultät der Universität Hamburg

vorgelegt von:

Shaimaa Fahmy (M.Sc.)

aus Giza, Ägypten

Hamburg 2023

**(wird von der Medizinischen Fakultät ausgefüllt)**

**Angenommen von der**
**Medizinischen Fakultät der Universität Hamburg am:** 02.11.2023

**Veröffentlicht mit Genehmigung der**
**Medizinischen Fakultät der Universität Hamburg.**

**Prüfungsausschuss, der/die Vorsitzende:** PD Dr. Wael Mansour

**Prüfungsausschuss, zweite/r Gutachter/in:** Prof. Dr. Gunhild Von Amsberg

## List of figures

## List of contents

# 1. Introduction

## 1.1. Prostate cancer (PCa)

Prostate cancer (PCa) affects millions of men worldwide and it is the second most common male cancer (14.1%) with an estimated number of new cases of 1,414,259; and mortality rate of 6.8% with an estimated number of deaths of 375,304 in 2020 according to the World Health organization (Fig. 1). In addition, in Germany, it is the most common male cancer with an incidence rate of 19.7% and the second leading cause of male cancer deaths (22.9%), after lung cancer (Globocan, 2020). PCa incidence increases with age, where it is more common in patients more than 60 years old and is characterized by elevated levels of androgen receptor (AR) signaling; that's why it is characterized by hormone dependency especially in its early stages.

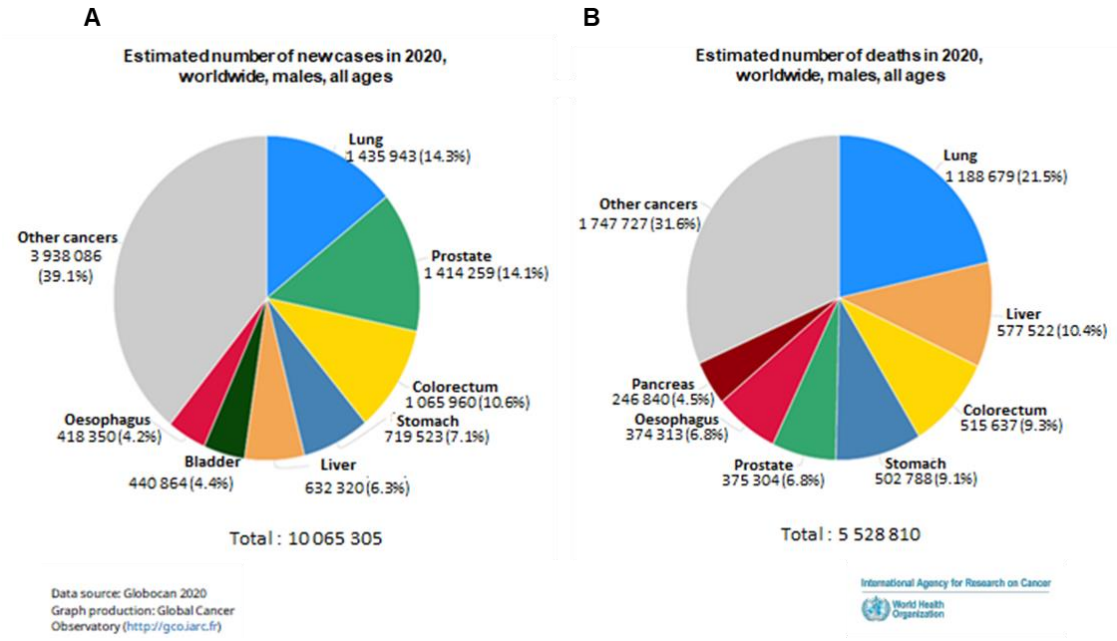


**Figure 1. Estimated incidence and mortality rates of different cancers in males worldwide.** (A) The estimated number of new cases of different cancers in all ages in men worldwide in 2020. (B) The estimated number of cancer related deaths in males in 2020. Source: GLOBOCAN 2020 (Globocan, 2020).

AR transcriptionally activates its downstream Prostate-specific antigen (PSA) that is used as a method for initial screening in PCa, as well as for follow up (Toivanen and Shen, 2017). Noteworthy, the worldwide incidence is estimated to increase in 2040 by 10,17,712 cases; which necessitates unraveling pathways included in prostate carcinogenesis, to personalize the treatments and improve the survival. Particularly

that the mechanisms behind PCa initiation and progression are still not clear (Feher et al., 1994; Toivanen and Shen, 2017).

PCa is mainly characterized by the presence of structural genomic rearrangements that includes genomic deletions, translocations, fusions, amplifications and copy number aberrations. The most common genomic alteration is the ETS related gene (ERG) fusion that is found in around 50% of the patients (Tomlins et al., 2005). In which, the androgen stimulated Transmembrane Serine Protease (TMPRSS) gene fuse with ERG that is a member of E-26 transformation- specific (ETS) transcription factor family on chromosome 21*q*, generating the ERG fusion (*TMPRSS2:ERG*). ERG is a transcription factor that regulate different genes and processes that promote PCa (Angeles et al., 2018). Other genomic aberrations in primary PCa include genomic deletions that involve the deletion at chromosome locus 10*q*23 that results in the deletion of the tumor suppressor gene Phosphatase and Tensin Homolog (PTEN) in 15-17% of the primary PCa. PTEN antagonizes phosphoinositide-3-kinase–protein kinase B/Akt (PI3K/AKT) pathway that regulates different processes as cell cycle, apoptosis, proliferation and invasion; therefore, the loss of PTEN promotes PCa (Jamaspishvili et al., 2018; Poluri and Audet-Walsh, 2018). In addition, other aberrations include the chromosome 5*q*21, which causes the loss of the chromatin remodeler chromodomain helicase DNA-binding protein 1 (CHD1) (17%). CHD1 plays role in maintaining accessible chromatin structure that is needed for transcription; additionally, it has been shown to have role in DNA double strand break (DSB) repair through enhancing homologous recombination (HR) repair pathway by mediating end resection through carboxy-terminal binding protein (CtIP) (Huang et al., 2012; Kari et al., 2016). Other structural rearrangements in primary PCa include amplification of genes such as AR and MYC Proto-Oncogene (MYC) (Barbieri and Rubin, 2015).

Noteworthy, unlike other tumors, PCa is rarely characterized by the presence of point mutations; around 0.7 per megabase (Mb) less mutations than other common cancers (Abeshouse et al., 2015). Some of these point mutations were found in the tumor suppressor gene TP53 (8%), in addition to mutations in DNA repair genes as in ataxia-telangiectasia mutated (ATM) (4.3%), breast cancer gene 1 (BRCA1) (0.69%), breast cancer gene 2 (BRCA2) (1.58%), and RAD51 Recombinase (RAD51) (0.88%) (Zhang et al., 2020; Hernández-Llodrà et al., 2021; Nientiedt et al., 2022). Furthermore, the advances in whole genome sequencing revealed new mutations in PCa, as in Forkhead box protein A1 (FOXA1) (3%) and Isocitrate dehydrogenase 1 (IDH1) (1%).

Intriguingly, the most common point mutation was discovered in a gene called Speckle-type POZ protein (SPOP) in around 15% of the primary PCa patients and 8% of the metastatic PCa (Barbieri et al., 2012; Frank et al., 2018).

## 1.2. Speckle-type POZ protein (SPOP)

SPOP gene encodes the substrate adaptor protein of Cullin-3-E3-ubiquitin ligase complex that binds different target proteins and mediates their polyubiquitylation and proteosomal degradation (Hernández-Muñoz et al., 2005; Jeong et al., 2006; Wei et al., 2018). SPOP is located on chromosome 17*q*21 and encodes for a 374-amino acids protein (Nagai et al., 1997; García-Flores et al., 2014). As depicted in Fig. (2), SPOP protein consists of three main domains: (i) the N-terminal MATH domain (meprin and TRAF-C homology) that recognizes the different substrates, (ii) the central BTB domain (broad-complex, tramtrack and bric-a-brac), which allows the binding between SPOP and Cullin-3 ring of the E3 Ubiquitin ligase complex, and (iii) the C-terminal BACK domain (BTB and C-terminal Kelch) that is thought to be responsible for extra CUL-3 recognition. Additionally, SPOP has NLS (nuclear localization sequence) in its C-terminal, through which, its localization in nuclear speckles occurs (Zhuang et al., 2009; Errington et al., 2012; Van Geersdaele et al., 2013).

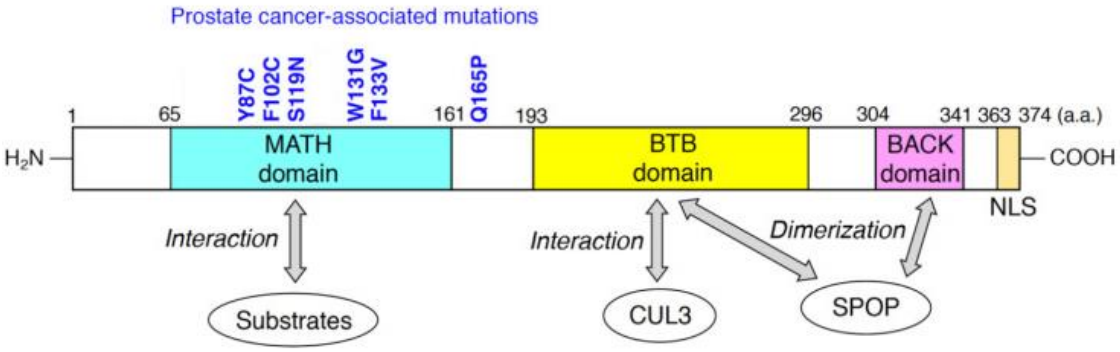


**Figure 2. Schematic illustration of SPOP protein structure.** The molecular structural arrangement of SPOP is shown. N-terminal meprin and TRAF homology (MATH) domain is responsible for selective binding with different substrates. BTB together with BACK domains are responsible for binding to the Cullin-3 ring (CUL3) and SPOP dimerization. The nuclear localization signal (NLS) domain is a C-terminal nuclear localization sequence. The most common somatic SPOP mutations in prostate cancer are shown in blue. These mutations are predominantly clustered in several key amino acids in the MATH domain, including Y87C, F102C, S119, W131, and F133. Modified from Maekawa and Higashiyama (Maekawa and Higashiyama, 2020).

A wide range of substrates have been identified for SPOP that play important role in different cancers by controlling different processes, such as regulation of hormone

signaling, transcription factors, epigenetics regulation and chromatin readers, immune response, in addition to cell cycle and apoptosis (Wei et al., 2018; Song et al., 2020; Zhang et al., 2021). On one hand, some of SPOP substrates may promote carcinogenesis; on the other hand, others could be tumor suppressors, which makes the role of SPOP in cancer contradictory.

### 1.3. SPOP in cancer

Protein degradation is critical for maintaining cellular homeostasis and abnormal accumulation of proteins may lead to various diseases including human cancers (Christianson and Ye, 2014). SPOP has been greatly explored for its dual functions in tumorigenesis (Brenner and Chinnaiyan, 2011; Christianson and Ye, 2014). An oncogenic function of SPOP has been reported in renal cell carcinoma (RCC). It has previously been shown that both transcriptional and translational levels of SPOP are significantly upregulated in RCC tissues (Zhao et al., 2016), which was associated with cancer metastasis in patients (Zhao et al., 2016). In line with its oncogenic function in RCC, the malignant behaviors of the RCC A498 and ACHN cells were reversed after siRNA-mediated SPOP knockdown (KD), as evidenced by apoptosis induction and migration inhibition (Liu et al., 2016). Normally, SPOP protein is a nuclear protein, however in RCC cells under hypoxia, it has been demonstrated to predominantly transfer to and concentrate in the cytoplasm (Li et al., 2014). Interestingly, normal HEK293 cells overexpressing cytoplasmic SPOP (cyto-SPOP) were able to generate tumor xenografts subcutaneously in about 80% of nude mice injected with HEK293-cyto-SPOP formed (Li et al., 2014). Mechanistically, cyto-SPOP promoted the ubiquitination and degradation of several tumor suppressors including PTEN, Dual specificity protein phosphatase 7 (DUSP7), Death-associated protein 6 (Daxx) and GLI Family Zinc Finger 2 (Gli2) in the cytoplasm, facilitating proliferation and inhibiting apoptosis in RCC cells (Li et al., 2014). Together, these findings confirm the oncogenic properties of SPOP in RCC cells via its cytoplasmic accumulation, resulting in degradation of several tumor suppressive genes.

On the contrary, several other studies revealed a tumor suppressor effect for SPOP in several types of human cancers as prostate, breast, lung, endometrial, colon, liver and gastric (Zeng et al., 2014; Boysen et al., 2015; Gao et al., 2015; Huang et al., 2015; ; Xu et al., 2015; Zhang et al., 2015; Li et al., 2017). The SPOP's tumor suppressor function in the aforementioned tumor types was linked to the finding that several discovered substrates of SPOP have role in cancer progression.

## 1.4. SPOP and PCa

SPOP mutations and hence, the loss of function were tightly correlated with a worse prognosis in patients with PCa (García-Flores et al., 2014). Somatic mutations in SPOP are the most common point mutations in PCa and they affect around 10-15% of the patients. Importantly, they are mutual exclusive with other alterations as ERG fusion (Berger et al., 2011; Barbieri et al., 2012). Additionally, they have been suggested to have role in the progression of PCa, as they are present in the early primary localized phase, not only in the metastatic PCa (Barbieri et al., 2012; Frank et al., 2018). Whole-genome and exome sequencing revealed the accumulation of loss-of-function-causing SPOP point mutations in primary prostate neoplastic tumors, but not in matched normal prostate cells (Berger et al., 2011; Barbieri et al., 2012). Most of these mutations are concentrated in the MATH domain of SPOP (such as Y87, F102, S119, Y123, F125, K129, W131, F133, and K134) (Barbieri et al., 2012), and these mutations have been linked to genomic instability and cancer in prostate (Boysen et al., 2015; Jung et al., 2016; Romanel et al., 2017; Hjorth-Jensen et al., 2018). These mutations inhibit the ability of SPOP to bind and degrade various target proteins. Consequently, they accumulate the downstream substrates and promote prostate tumorigenesis (Theurillat et al., 2014). Blattner et al., constructed a prostate-specific SPOP-F133 V mutation-carrying transgenic mouse and found that PCa was developed in part due to the activation of the PI3K/mTOR and AR signaling pathways, as well as, the loss of PTEN (Blattner et al., 2017). Additionally, the PCa-derived SPOP-F133 V mutation selectively damaged the homology-directed repair function mediated by wild type SPOP (Boysen et al., 2015). Extensive biochemical evidence has further indicated that SPOP functions as a tumor suppressor by promoting the degradation of oncogenic substrates in PCa, including steroid receptor coactivator-3 (SRC3) (Geng et al., 2013), AR (Geng et al., 2014), Tripartite Motif Containing 24 (TRIM24) (Groner et al., 2016), c-Myc (Geng et al., 2017), DEK Proto-Oncogene (DEK) (Theurillat et al., 2014), SUMO Specific Peptidase 7 (SENP7) (Zhu et al., 2015), Egl-9 Family Hypoxia Inducible Factor 2 (EglN2) (Zhang et al., 2017), Activating Transcription Factor 2 (ATF2) (Ma et al., 2018), Cell Division Cycle 20 (Cdc20) (Wu et al., 2017), ERG (Gan et al., 2015), Bromodomain-containing protein 4 (BRD4) (Dai et al., 2017; Janouskova et al., 2017; Zhang et al., 2017) Programmed death-ligand 1 (PD-L1) (Zhang et al., 2018), cyclin E1 (Ju et al., 2019) and G9a-like protein euchromatic methyltransferases (GLP) (Zhang et al., 2021).

Several studies revealed how SPOP mutations influence prostate cancer prognosis. Garcia-Flores et al., reported that SPOP mutations in primary prostate cancer were associated with poor prognosis as manifested by biochemical progression free survival and progression free survival (García-Flores et al., 2014). Furthermore, Boysen et al., demonstrated that SPOP mutations and its loss of function accumulate genomic rearrangements and instability. Interestingly, they mechanistically associated the loss of SPOP with an impairment of DNA repair via homologous recombination repair (HR), hence, accumulation of DNA double strand breaks (DSBs) and genomic instabilities (Boysen et al., 2015).

### 1.5. DNA damage and Genomic instability

Different endogenous, as well as, exogenous factors can insult DNA resulting in various types of DNA lesions that if left untreated can predispose to genomic instabilities. These factors include: (i) pathological endogenous conditions as erroneous replication and/or transcription deregulation, (ii) endogenous genotoxins such as reactive oxygen species (ROS), (iii) in addition to insults from exogenous genotoxins i.e. ionizing radiation (IR), ultraviolet light (UV) and DNA damaging agents as chemotherapeutics (Helena et al., 2018). In order to protect against the accumulation of DNA damages and genomic instabilities, mammalian cells have evolved different repair mechanisms and cell cycle checkpoints to halt cells with damaged DNA before cell division. Thereby, allowing for repair and preventing the propagation of genetic alterations to daughter cells (Zhou and Elledge, 2000; Wei Dai, 2014). Repair mechanisms include (Fig. 3): nucleotide excision repair (NER), which repairs the incorrect nucleotides in DNA produced after exposure to i.e. UV light or chemotherapeutic agents (Cleaver et al., 2009). Additionally, base excision repair (BER) that repairs the modified bases encountered in DNA from oxidative lesions (David et al., 2007). Another mechanism that mainly acts during replication is the mismatch repair (MMR), which corrects the base-base mismatches that interfere with the DNA structure (Jiricny, 2006). Moreover, there are different DSB repair mechanisms that specifically target the toxic DSBs (Jackson, 2002). Defects in DNA repair genes have been associated with different cancers. For example, MMR genes mutations that includes MutS homolog 2 (MSH2) and 6 (MSH6), MutL homolog 1 (MLH1), and PMS1 Homolog 2 (PMS2), increase the risk of particularly colorectal cancer, in addition to other cancers as breast, ovarian, endometrial and stomach (Yoshioka et al., 2021). Also, the loss of NER genes have been linked to enhanced

risk of different cancers. For example, germline mutations in Xeroderma pigmentosum complementation group C (XPC) predisposed to xeroderma pigmentosum and increased risk of skin cancer. Moreover, other cancers as leukemia and sarcomas can be caused by the loss of XPC (Jager et al., 2019; Yurchenko et al., 2020). Furthermore, defects in DSB repair genes, as will be discussed below, were associated with different cancers as prostate, breast, ovarian and pancreatic (Hopkins et al., 2022).

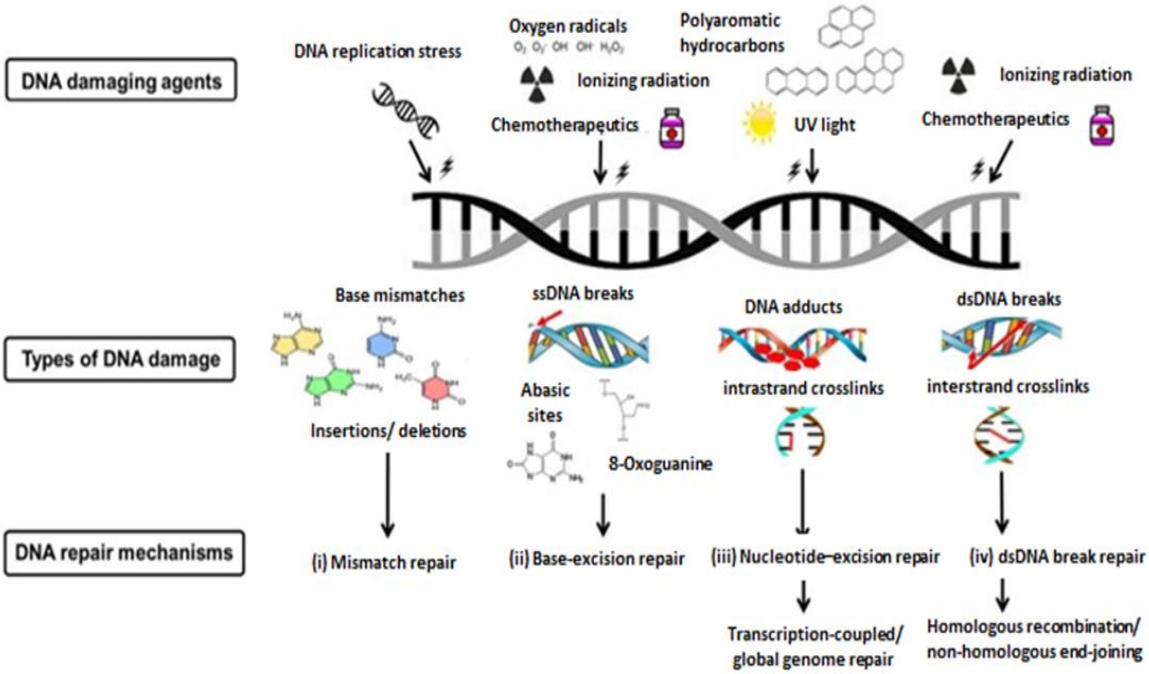


**Figure 3. Schematic illustration of different DNA damage types and repair mechanisms.** A range of DNA lesions are caused by various DNA damaging agents. Each DNA damage type is repaired by a specific repair mechanism**.** Base mismatches occur as a result of replication errors which are normally repaired by mismatch repair mechanism. DNA single strand breaks and base damages resulted from Ionizing radiation, oxygen radicals, as well as, chemotherapeutics are repaired by base excision repair. DNA adducts such as inter- or intra-strand crosslinks generated by UV light are repaired by the global or transcription coupled nucleotide excision repair. DSBs - another type of DNA lesions that results from ionizing radiation and several chemotherapeutic agents - are repaired by homologous recombination or non-homologous end joining. Modified from Helena et al (Helena et al., 2018).

## 1.6. Double Strand Breaks (DSBs)

Of the many types of DNA damage that exist within the cell, DNA DSBs are of the most deleterious that result in genomic instabilities. DSBs can result either (i) exogenously after exposure to IR and certain chemotherapeutic drugs, or (ii) endogenously by ROS. Additionally, studies showed that DSBs can be produced as a result of stresses as in replication and transcription (Ui et al., 2020). DSBs can occur at the termini of

chromosomes due to defective metabolism of chromosome ends (telomeres). In addition, programmed DSBs can be generated endogenously to initiate recombination between homologous chromosomes during meiosis and occur as intermediates during developmentally regulated rearrangements, such as V(D)J recombination and immunoglobulin class-switch recombination (Khanna and Jackson, 2001; Soulas-Sprauel et al., 2007).

Although cells can adapt to low levels of irrepairable damage (Lee et al., 1998), as little as one DNA DSB can be sufficient to kill a cell, if it inactivates an essential gene (Rich et al., 2000). The repair of DNA DSBs are considered to be particularly more difficult than that of other types of DNA damage. Moreover, erroneous rejoining of broken DNA DSBs may occur, leading to the loss or amplification of chromosomal material or under certain circumstances, to translocations in which, segments of chromosomal arms are exchanged, sometimes in a reciprocal fashion. These events can lead to tumorigenesis if, for example, the deleted chromosomal region encodes a tumor suppressor or if an amplified region encodes a protein with oncogenic potential. In the cases of chromosomal translocations, this can sometimes lead to a gene fusion that dysregulates or alters the functions of a proto-oncogene (Nikiforova et al., 2000). Notably, a large proportion of different malignancies exhibit chromosomal rearrangements, indicating that they have arisen through the inappropriate resolution of DNA DSBs. Several experimental evidences support the causal link between DSBs and the induction of gene mutations, chromosomal aberrations and cell transformation (Vamvakas et al., 1997). Consistent with these ideas, It has been shown that a defined chromosomal DNA DSB generated by the site-specific endonuclease I-SceI serves as a potent inducer of chromosomal translocations (Richardson and Jasin, 2000).

### 1.7. DSBs signaling

Upon sensing DSBs, cells activate a cascade of signals known as DNA damage response (DDR) that allow the accurate repair of damages and halt their progression. DDR consists of sensors, transducers and effectors, each of which includes different proteins that work in harmony to repair the DSBs. Interestingly, proteins that act as sensors, can also function as transducers (Khanna and Jackson, 2001). An important kinase family in DDR is phosphatidyleinositol 3-kinase-like protein kinase (PIKKs), which includes the ataxia-telangiectasia mutated (ATM), ataxia telangiectasia and RAD3 related (ATR) and DNA-dependent protein kinase (DNA-PK). ATM and ATR are considered the key players in DDR and DSB repair, intriguingly, they do not only act

as transducers, but also as sensors. They orchestrate different signal transductions and processes to allow for the accurate repair of DNA damages (Richardson and Jasin, 2000).

ATM detects mainly DSBs induced by i.e. IR or genotoxins, while ATR is mainly stimulated during replication fork stresses, which produce long single stranded DNA (ssDNA) (Canman et al., 1998; Jackson and Bartek, 2009). As shown in Fig. (4), induction of DSBs leads to ATM autophosphorylation of serine 1981 (ser1981), which causes dissociation of ATM dimers and enhancement of kinase activity. The activated ATM i.e. pATM is then recruited to DSBs through the sensing complex MRN. Kinase-activated ATM mediates a cascade of signals that include chromatin structure modifications; in which, the histone variant 'H2AX' is phosphorylated to form γH2AX and covers hundreds of kilobases around DSBs (Fernandez-Capetillo et al., 2004). This histone modification allows the activation of other mediators as the DNA damage checkpoint protein 1 (MDC1), which in turn further amplifies the γH2AX signal and allows the recruitment of other factors implicated in DDR such as p53-binding protein 1 (53BP1) and breast cancer gene 1 (BRCA1) that play an important role in regulating DSB repair (Lavin, 2008). Noteworthy, ATR also produces the same effect as with ATM on H2AX, however, with replication stress induced damages. In addition to chromatin changes, activated ATM and ATR phosphorylate and activate two important downstream serine–threonine checkpoint effector protein kinases 2 and 1, namely ChK2 and ChK1, respectively. The phosphorylated forms of ChK2 (pChK2) and ChK1 (pChK1) phosphorylate different downstream targets. For example, ChK2 substrates include p53 tumor suppressor protein (p53) leading to p53 stabilization, which promotes p21 expression. p21 then binds to and inhibits the cyclin and cyclin-dependent kinase (CDK) complexes leading to cell cycle arrest (Ou et al., 2005). CDC25 phosphatases are also substrates of both ChK1 and ChK2 (Uto et al., 2004). The inhibitory phosphorylation sites on CDK are dephosphorylated by Cdc25, which causes CDK activation. Consequently, Cdc25 inhibition results in cell cycle arrest (Boutros et al., 2007). In human cells, there are three Cdc25 paralogs (Cdc25A-Cdc25C). ChK1 phosphorylation of Cdc25A causes it to degrade in a way that is ubiquitin/proteasome-dependent (Mailand et al., 2000; Boutros et al., 2007). ChK1 inhibits the phosphatase activity of Cdc25B and Cdc25C by phosphorylating them (Boutros et al., 2007). Therefore, ATM/ChK2 and ATR/ChK1 are critical checkpoints in

mediating G1/S, intra S phase and G2/M arrest, thus allowing for efficient DSB repair (Kastan and Bartek, 2004).

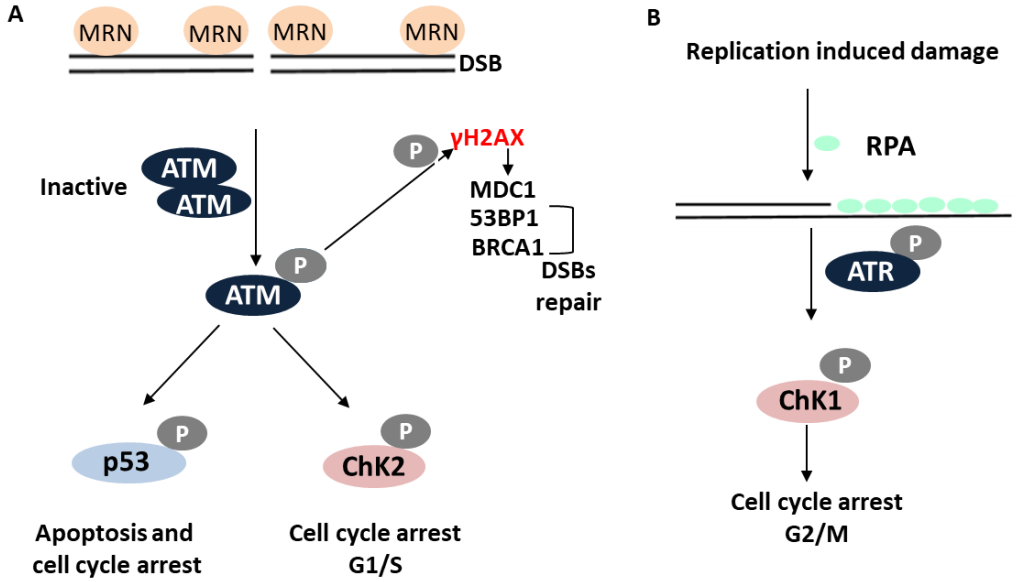


**Figure 4. ATM- and ATR- mediated DNA damage response (DDR).** The protein kinases ATM and ATR activate response networks after different genotoxic stress by phosphorylating key proteins in various signalling pathways. (A) ATM is activated mainly by DSBs induction. MRN complex is firstly recruited to the DSB sites to recruit and activate ATM. ATM activation – through its dissociation from the inactive dimer and auto-phosphorylation (pATM) – prompts a cascade of DDR signaling via phosphorylation of different downstream targets such as H2AX. ATM phosphorylates H2AX at serine 139 (γH2AX), which further activates other factors as MDC1, 53BP1 and BRCA1. Additionally, ATM regulates cell cycle checkpoints, senescence and apoptosis by phosphorylation of p53 and checkpoint kinase 2 (ChK2) at G1/S transition. These mechanisms promote DNA damage repair or lead to senescence or apoptosis in case of irreversible damages. (B) ATR is another important kinase which is activated by replication induced-damages that produce RPA-coated ssDNA. Activated ATR phosphorylates different downstream substrates including checkpoint kinase 1 (ChK1) at G2/M transition. This Figure is inspired from Frappart and McKinnon, in addition to, Menolfi and Zha (Frappart and McKinnon, 2006; Menolfi and Zha, 2020).

## 1.8. DSB repair pathways

There are two distinct and complementary mechanisms for DNA DSB repair: (i) Non homologous end joining (NHEJ) pathway, which joins the DNA double-stranded ends in the absence of a homologous sequence (Farlow et al., 2011; Zhao et al., 2020) and (ii) homologous recombination (HR), which requires the presence of a DNA template homologous to the damaged region (Helleday et al., 2008).The choice between both pathways depends on several factors as the cell cycle phase and the recruited proteins. Importantly, it should be precisely controlled; otherwise, will result in genomic instabilities (Scully et al., 2019).

NHEJ is considered a fast DSB repair mechanism as it takes place without end resection, it re-joins DNA ends independent from homology sequence (Takata et al., 1998). It takes place in all cell cycle phases and one of its main features is the end protection that is mediated by the end protection factor RAP1-interacting factor 1 (RIF1) (Zimmermann et al., 2013). The DDR factor 53BP1 directs the repair to NHEJ, through binding to chromatin at DSBs; thereby hindering the end resection mediated by BRCA1 and CtIP (Escribano-Díaz et al., 2013; Bakr et al., 2016). NHEJ includes mainly three steps: end binding, end processing and ligation (Fig. 5). In order to mediate NHEJ, two main complexes are included: the DNA-dependent protein kinase (DNA-PKcs) complex that includes the Ku70/Ku80 heterodimer and the DNA-PKcs catalytic subunit (Weterings and Chen, 2007). Additionally, for ligation, there is a complex of ligase IV with two cofactors, namely, X-ray cross complementation (XRCC4) and the XRCC4-like factor (XLF). End binding is initiated by the DNA-PK complex, where KU70/KU80 brings two ends in close proximity and with the help of other proteins as DNA-PK, a synapse is formed and the kinase activity of the complex is activated (Mari et al., 2006). Next, processing takes place by polymerases, i.e. pol μ and pol λ and nucleases, where both are needed to add and/or remove nucleotides, thus preparing the ends for ligation (Ramsden, 2011). An example of nucleases is Artemis that is 5'-3' exonuclease, and is activated by the kinase activity of DNA-PK. This exonuclease activity facilitates the removal of single stranded protruded regions from DNA ends, preparing for a final ligation step, where, the two DSB ends join via the ligase complex (Löbrich and Jeggo, 2017).

HR is unlike NHEJ (Fig. 5), it is known to be of high fidelity, as it repairs using a template 'sister chromatid', therefore, it dominates in the late phase of S/G2. Additionally, in contrast to NHEJ, it starts with an end resection step, before proceeding into synapsis (Li and Heyer, 2008). For that reason, HR includes three main steps, in addition to a final ligation step, namely presynapsis, synapsis and postsynapsis. Presynapsis involves enzymes with endonuclease activity as CtIP and others with exonuclease activity as Meiotic recombination 11 (MRE11) and exonuclease 1 (EXO1), all together works on resecting the 5' ends of DSB, exposing the 3'end, thus producing 3' single stranded DNA (3'-ssDNA) overhangs (Eid et al., 2010). Next, Replication protein A (RPA) coats and stabilizes the generated long 3'-ssDNA, then RPA is displaced by RAD51, which plays the key role in the synapsis and invasion step. Therefore, RAD51 is considered a key marker for efficient HR (Cruz et al., 2018).

Synapsis takes place via the invasion of the 3'-ssDNA end (coated with RAD51) to the homologous sequence in the sister chromatid. Subsequently, the DSB and its homology connect, forming a displacement loop structure (D-loop) (Sun et al., 2020). Following, is a postsynapsis step, where DNA synthesis is mediated via polymerase η. Finally, the removal of flaps and filling gaps is enhanced in the ligation step through many proteins, such as polymerase η and ε, proliferating cell nuclear antigen (PCNA), and DNA ligase I, allowing for the recovery of the initial damaged sequence (Helleday et al., 2007).

## 1.9. DSB repair in PCa

Few mutations exist in PCa's genetic makeup when compared to other common solid cancer forms. Instead, PCa frequently exhibits structural alterations such as chromosomal deletions and translocations. DNA DSBs are known to have a role in the processes that lead to these rearrangements, placing DSBs and associated repair systems at the core of PCa carcinogenesis. DNA DSB repair has repeatedly been discovered to interact with AR pathway signaling, which has a substantial influence on PCa development and therapy response. Multiple studies have indicated that germline mutations in DNA repair genes are associated with a higher risk of developing PCa. Common germline mutated DDR genes in primary PCa or castration resistant Prostate cancer (CRPC) are found in the BRCA1 and BRCA2 genes. Various studies have shown that the inactivating BRCA1/2 mutations, predominantly BRCA2, increase predisposition to PCa (Kote-Jarai et al., 2009; Gallagher et al., 2010). Loss-of-function mutations in BRCA1/2 lead to a deficiency in the error-free HR repair. Therefore, DSBs will be repaired alternatively by other non-conservative and potentially mutagenic mechanisms, such as the NHEJ pathway, resulting in genomic instability (chromosomal translocations and deletions) that explain the underlying mechanism of BRCA1/2 associated cancers.

Other heterogeneous panel of repair defects caused by homozygous mutations or copy number alterations was identified in primary prostate tumors compared to paired normal tissue. Such mutations include alterations in ATM, RAD51, MDC1, Poly [ADP-ribose] polymerase 1 (PARP1), and FA complementation group D2 (FANCD2), although the level of incidence varied between the studies (Bangma and Roobol, 2012; Irshad et al., 2013; Kamoun et al., 2018).

In our lab we could link some PCa-specific genetic alterations to individual DSB repair deficiency. For instance, PCa cells with deletion of either PTEN or CHD1 harbor HR-defect (Kari et al., 2016; Mansour et al., 2018). B-cell lymphoma 2 (BCl2) overexpression impairs NHEJ pathway and causes a repair switch to the alternative PARP1-depedent end joining (Oing et al., 2018). Interestingly, SPOP deficiency has previously been suggested to decrease RAD51 loading, thus impairing HR repair (Boysen et al., 2015).

Both preclinical and clinical studies have found that AR signaling regulates the expression and/or function of DDR genes. Several NHEJ factors were found to be positively regulated by the AR pathway, resulting in a slight increase in NHEJ activity upon androgen addition (Goodwin et al., 2013). Other studies have demonstrated that castration primarily reduces the expression of the NHEJ factor KU70 (Al-Ubaidi et al., 2013; Tarish et al., 2015) . In addition to direct regulation of the NHEJ pathway, other studies show that AR signaling regulates HR pathway (Goodwin et al., 2013; Polkinghorn et al., 2013; Li et al., 2017). In consistent with this idea, blocking the AR signaling by Enzalutamide was found to suppress the expression of the HR genes BRCA1, RAD54 Like (RAD54L), and RecQ Mediated Genome Instability 2 (RMI2) (Li et al., 2017).

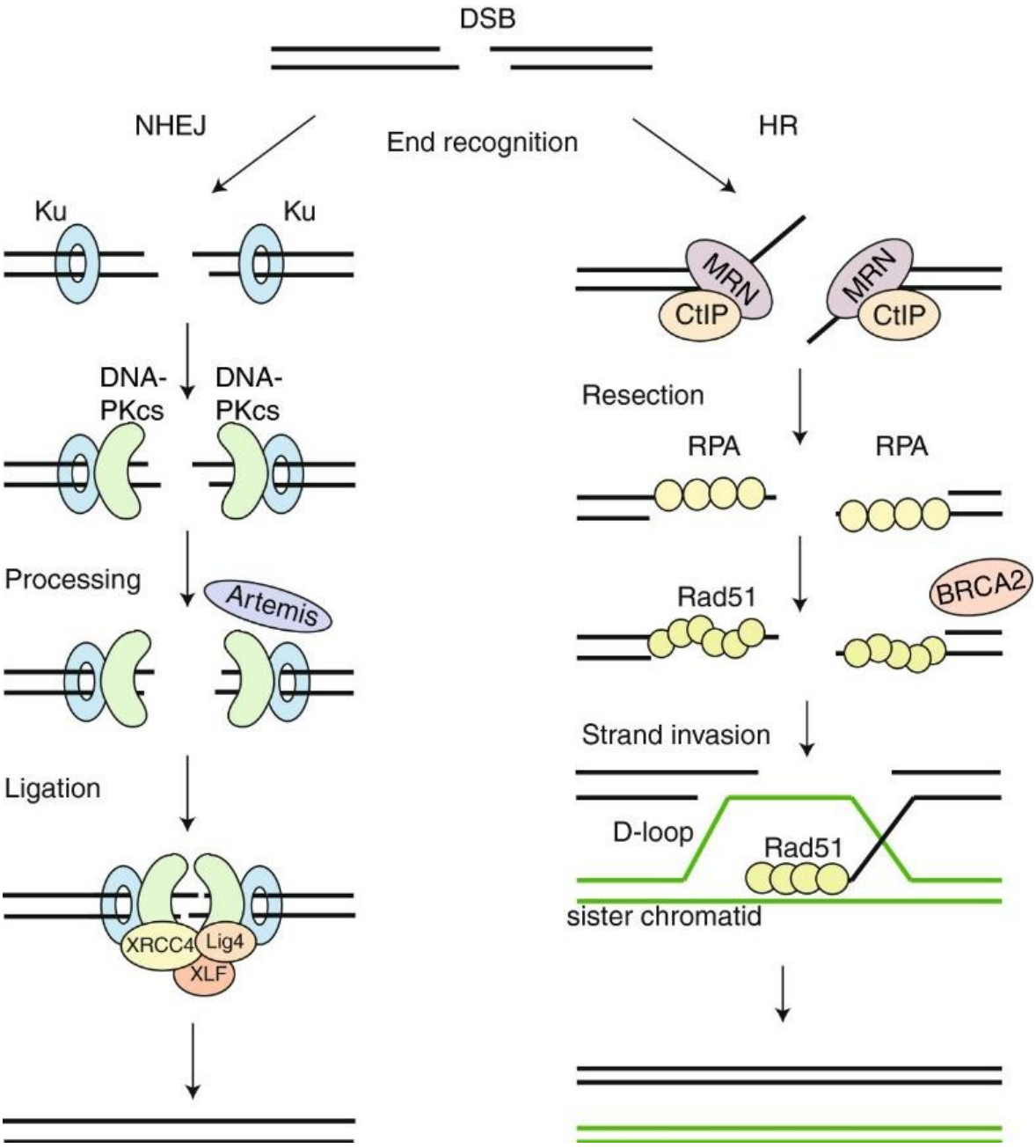


**Figure 5. The canonical DSB repair pathways of non-homologous end joining (NHEJ) and homologous recombination (HR).** NHEJ (left-hand side) starts with the recognition of the DNA ends by the Ku70/80 heterodimer, which in turn recruits and stimulates the kinase activity of the catalytic subunit of DNA protein kinase (DNA-PKcs). If the ends are incompatible, nucleases such as Artemis can trim the ends. The XRCC4-DNA Ligase IV-XLF ligation complex seals the break. HR (right-hand side) starts with end recognition and resection by MRN-CtIP-complex, generating 3'-single stranded DNA (ssDNA) overhangs. These ssDNA-overhangs are firstly coated by RPA, which is subsequently replaced by Rad51 with the help of BRCA2. These Rad51 nucleoprotein filaments mediate strand invasion on the homologous template (sister chromatid). Extension of the D-loop and capture of the second end lead to repair (Brandsma and Gent, 2012).

## 1.10. Transcription and R-loops related formation of DSBs

### 1.10.1. Transcription machinery

Transcription is a central aspect of DNA metabolism that takes place on the same strand as replication and repair processes, indicating a physical and functional connection between these processes. Transcription has proven to be a relevant player in the induction of genetic instability (Kim and Jinks-Robertson, 2012). Transcription basically includes three stages: (i) initiation, (ii) elongation, and (iii) termination (Fig. 6). In order for initiation to take place, DNA should be accessible. Therefore, transcription factors 'TFs', chromatin remodelers and coactivators such as histone acetyltransferases open the chromatin and activate transcription. Initiation starts with the recruitment of RNA polymerase II (RNA pol II) to the transcription start site (TSS) of the accessible chromatin via general transcription factors 'GTF' and mediator complex. To initiate transcription, CDK7 (cyclin-dependent kinase 7) phosphorylates RNA pol II on serine 5 (ser5) position of its C-terminal domain 'CTD'; CDK7 is a factor from the GTF 'Transcription factor II human (TFIIH)' (Hsin and Manley, 2012). Once RNA pol II is phosphorylated on ser5 (RNA Pol II ser5p), RNA pol II escapes promoter, hence, RNA synthesis starts. However, downstream of the TSS at around 25-50 nucleotide (nt) regions, RNA pol II enters a stage of pausing known as 'promoter proximal stalling', (Adelman and Lis, 2012). At this step, the DRB-sensitivity-inducing factor (DSIF) and Negative elongation factor (NELF) halt further elongation, enhancing RNA pol II pausing, thereby, pausing transcription (Yamaguchi et al., 1999).

In order to proceed into active elongation, the positive transcription elongation factor b (p-TEFb) phosphorylates the elongation inhibitory complex 'DSIF and NELF', thereby, releasing NELF and rendering DSIF in a form that enhances RNA pol II elongation (Canman et al., 1998; Peterlin and Price, 2006). Additionally, RNA pol II must be phosphorylated on ser2 position of its CTD (RNA Pol II ser2p), which is considered a marker of active transcription elongation; this step is carried out by p-TEFb that is also known as phosphorylated cyclin dependent kinase 9 (pCDK9) (Marshall et al., 1996; Brookes and Pombo, 2009; Lu et al., 2016). The kinase activity of cyclin dependent kinase 9 (CDK9) is necessary for the phosphorylation of RNA pol II at ser2. Importantly, CDK9 itself without being phosphorylated is inactive, i.e. can't phosphorylate RNA pol II at ser2. Therefore, CDK9 must be first autophosphorylated at threonine 186 (T186) of its T-loop, and forms a heterodimer with cyclin T (Cyc T) 1 or 2, this complex is known as p-TEFb (pCDK9). This heterodimer through binding to Hexamethylene Bis-

acetamide-inducible Protein 1 (HEXIM1), is incorporated into 7SK small nuclear ribonucleo-protein (snRNP) complex. p-TEFb kinase activity is inactive while in complex with HEXIM1 ,7SK snRNP, as well as, other proteins as La-related Protein 7 (LARP7) and 7SK snRNA Methyl Phosphate Capping Enzyme (MePCE). Hence, it is unable to phosphorylate RNA pol II on ser2 position (Baumli et al., 2008; Ni et al., 2008). In order to become active, it must be dephosphorylated to be freed from the complex. However, after dissociating from the complex, it must be again re-phosphorylated at its T-loop, hereby, forming the active kinase form of p-TEFb (pCDK9). This active form of p-TEFb is necessary for RNA pol II ser2p, and promotes the release from proximal promoter pausing, consequently, results in active elongation (Bacon and D'Orso, 2019). Eventually, termination takes place by the dissociation of RNA pol II from the transcription machinery (Proudfoot, 2016).

Several studies have reported higher mutation rates in highly transcribed regions of the genome. Some of these mutations may be due to elevated rates of DSB formation in these same regions. Variable rates of DSB formation across the genome are influenced by chromatin structure. However, some DSBs in heavily transcribed regions appear to result from transcription deregulation (Sebastian and Oberdoerffer, 2017). Transcription deregulation/ stress includes (i) transcription downregulation, in which RNA pol II pauses or stalls for long time. It can be triggered by different mechanisms as decreased chromatin accessibility, prolonged proximal promoter pausing, RNA pol II backtracking, in addition to, RNA-DNA hybrids (R-loops) accumulation. Longer pausing/stalling of RNA pol II and with that R-loops generation, may collapse with replication fork and generate DSBs. In addition, (ii) transcription upregulation on the other hand, which can be provoked by different mechanisms such as the increased signal of transcription factors as with AR and estrogen receptor in prostate and breast cancers, respectively (Stork et al., 2016; Nicholas et al., 2021; Rinaldi et al., 2021). Transcription upregulation causes accumulation of R-loops, which cause replication fork stalling, collapse and generation of DSBs. Collectively, deviation of transcription from its hemostasis; whether by transcription reduction or upregulation, will result in genomic instability and one main factor behind these genomic instabilities is the accumulation of R-loops.

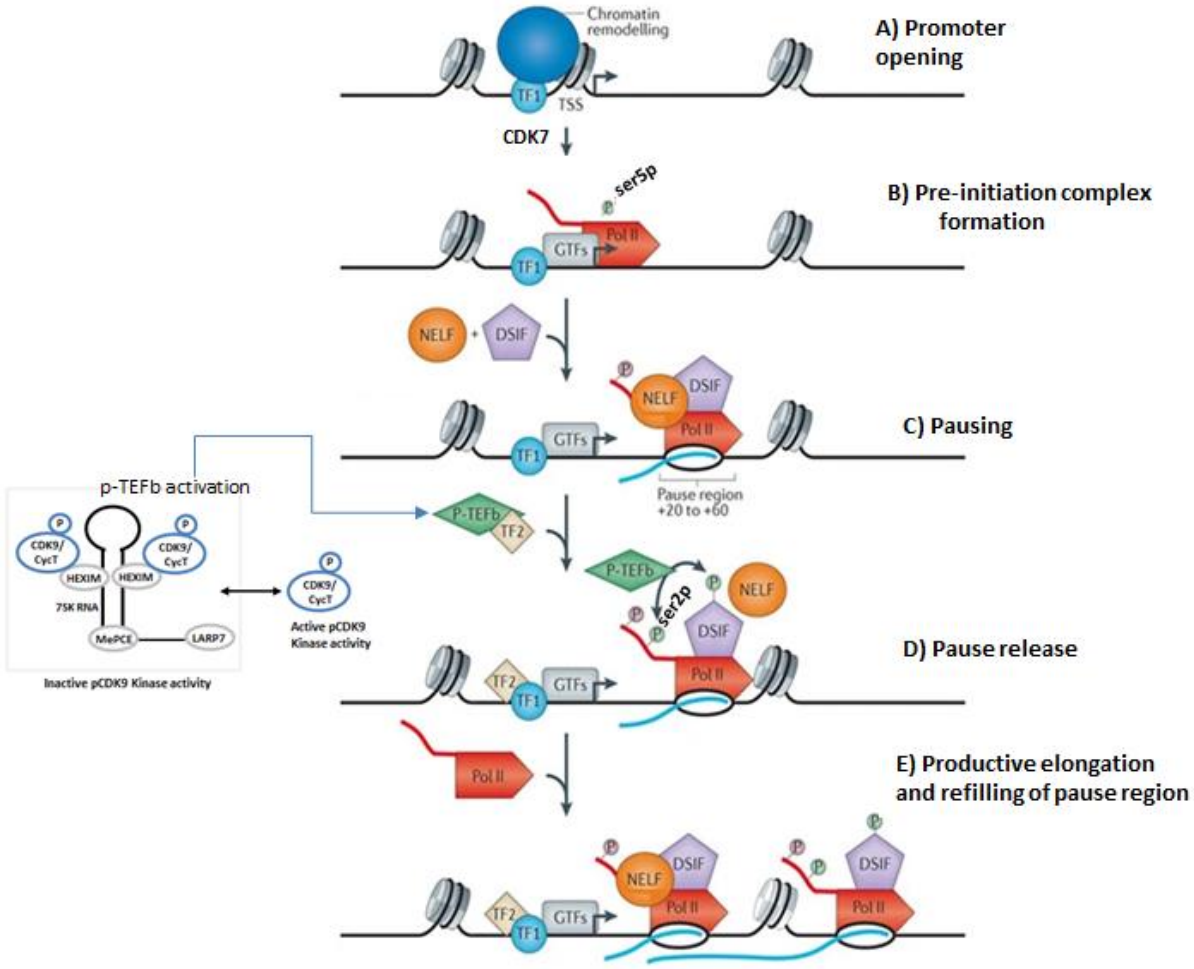


**Figure 6. Schematic representation of transcription process.** Shown are the main key steps and players implicated in transcription regulation. (A) Promoter opening starts with binding of a transcription factor (TF1) at the promoter site and recruitment of chromatin remodelers to open chromatin structure around the TSS. (B) Pre-initiation complex formation involves the recruitment of general transcription factors (GTFs), allowing the loading of RNA pol II, which is then phosphorylated by CDK7 at serine 5 position of its carboxy-terminal domain (CTD), thus initiating the transcription and RNA synthesis. (C) Pol II pausing occurs shortly after transcription initiation and involves the binding of pausing factors NELF and DSIF. (D) Pause release is initiated by activation of p-TEFb, where CDK9 is phosphorylated, its kinase activity is stimulated through dissociation from HEXIM1, 7sK RNA, LARP7, MePCE. Activated CDK9 phosphorylates the DSIF–NELF complex, leading to NELF dissociation and transformation of DSIF into a positive elongation factor. Furthermore, CDK9 phosphorylates RNA pol II on serine 2. (E) Therefore, productive transcription elongation proceeds. Modified from Adelman and Lis (Adelman and Lis, 2012).

### 1.10.2. R-loops and genomic instability

R-loops are three stranded structure that are co-transcriptionally produced (Belotserkovskii et al., 2018). Where, the nascent RNA form a hybrid with the template DNA, displacing the single stranded DNA (ssDNA). They are considered harmless in normal levels, as they regulate physiological processes, such as gene expression,

DSB repair, replication and immunoglobulin class switching recombination in B-lymphocytes (Yu et al., 2003). Maintaining normal levels of R-loops is vital, and accumulation of R-loops results in genomic instabilities. R-loops hemostasis is obtained through (i) mechanisms that resolve and / or prevent R-loops formation. Resolving enzymes include: Ribonucleases H1 and 2 (RNAse H1 and RNase H2); which have 5'-3' exonucleases that specifically target and digest the RNA found in RNA-DNA hybrid (Wahba et al., 2011). In addition, helicases such as ATP-dependent nucleic acid helicase (DHX9), aquarius (AQR), senataxin (SETX), also resolve R-loops by unwinding RNA-DNA hybrids (Allison and Wang, 2019). Additionally, (ii) Transcription dynamics play pivotal role in R-loops hemostasis. Where, increase or decrease of transcription causes accumulation of R-loops and leads to genomic instabilities (Kotsantis et al., 2016; Stork et al., 2016; Core and Adelman, 2019; Zatreanu et al., 2019; Nicholas et al., 2021).

Although a programmed formation of R-loops plays important physiological functions, these structures can turn into source of DNA damage and genome instability when their homeostasis is altered. In general, there are several proposed mechanisms for unscheduled R-loops as a source of genomic instability (Fig. 7) (Rinaldi et al., 2021): (i) Induction of transcription stress, where accumulation of the unscheduled R-loops pauses RNA pol II that if prolonged, would result in transcription stress that predisposes to replication stress, DSBs and genomic instabilities (Aguilera and García-Muse, 2012; Rinaldi et al., 2021). (ii) Induction of replication stress. Since transcription and replication share the same DNA template, therefore, R-loops-mediated stalled RNA pol II may collide with the replication fork, leading to replication stalling. This effect is particularly provoked, when replication and transcription are in head-on direction more than in co-directional. Stalled replication forks can completely collapse resulting in DSBs, transcription stress, chromosomal aberrations and genomic instabilities (Aguilera and García-Muse, 2012; Hamperl et al., 2017). (iii) Generation of ssDNA stretches. ssDNA stretches are generated on the non-template strand as a result of R-loops formation (Rinaldi et al., 2021). Such vulnerable ssDNA structures can lead to DNA mutations or DNA breaks that result in replication stress and DSBs (García-Muse and Aguilera, 2016; Hamperl et al., 2017; Rinaldi et al., 2021). For example, if the exposed ssDNA processed by DNA daminases, cytidine will be converted to uracil, that if removed by BER, would result in DNA nicks, that eventually lead to DSBs. In addition, when the ssDNA is processed by endonucleases as xeroderma pigmentosum

type F (XPF) and xeroderma pigmentosum type G (XPG), SSBs form, which process into DSBs. (iv) Induction of DSBs. As explained different deregulations induced by R-loops can indirectly result in DSBs; however, R-loops can directly generate DSBs. Processing of the accumulated R-loops by the transcription coupled NER pathway nucleases XPG and XPF generates DSBs and hence, genomic instabilities (Aguilera and García-Muse, 2012; Rinaldi et al., 2021). Altogether, despite the physiological role of R-loops, their hemostasis is vital, otherwise, leads to genomic instabilities, through causing transcription stress, replication stress and DSBs.

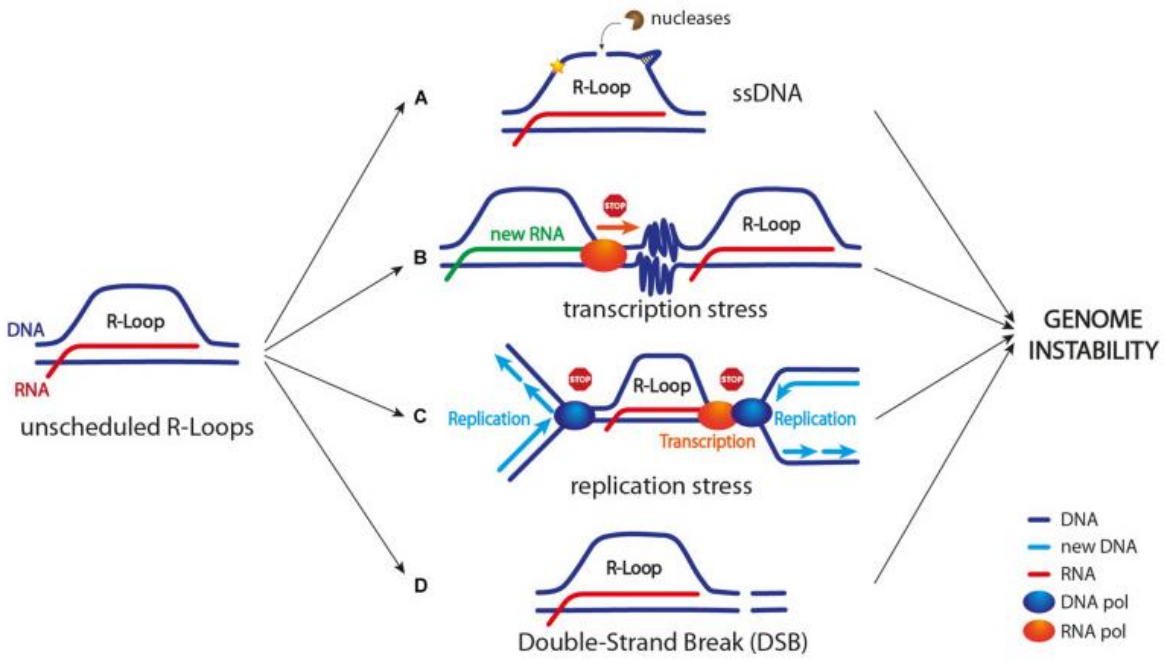


**Figure 7. R-loops accumulation results in genomic instabilities**. Accumulation of unscheduled R-loops causes genomic instabilities through different mechanisms: (A) ssDNA exposure that can be processed by different nucleases leading to DNA breaks that might cause several mutations. Accumulation of ssDNA can also cause harmful secondary structures such as G-quadruplexes and hairpins. (B) R-loops accumulation in front of the transcription machinery can result in transcription block through stalling RNA pol II. Unscheduled R-loops can also result in chromatin condensation (zig zag lines). (C) R-loops accumulation and with that stalled transcription and chromatin condensation can stall the replication fork, resulting in replication stress. (D) R-loops might lead to DSB formation when processed by the transcription NER pathway proteins XPG and XPF (Rinaldi et al., 2021).

## 1.11. Transcription deregulation and genomic instabilities in PCa

Alteration in transcription has been shown to be one of the major processes that predisposes to genomic instabilities in PCa (Barbieri and Rubin, 2015). The deregulations in many transcription factors, as in AR can lead to genomic aberrations. AR is a transcription factor that is pivotal for the normal growth of prostate, however, its amplifications and aberrant levels lead to changes in the transcription program and result in structural genomic rearrangements. Among these rearrangements, gene fusions play important roles in PCa tumorigenesis. The TMPRSS2 fusion with ERG and other ETS family genes are the most frequent gene fusions in PCa (Tomlins et al., 2005). Previously, it has been shown that AR signaling could promote spatial genome reorganization and contribute to the generation of the *TMPRSS2:ERG* fusion. In general, genomic rearrangements induced by AR signaling have been linked to the incorrect repair of the DSBs generated by Topoisomerase 2B (TOP2B) (Labbé and Brown, 2018). TOP2B associates with many transcription factors including AR and produce transient DSBs, in order to relax the topological constraints. Upon stimulation of AR signaling, TOP2B induces DSBs at the junctions that allow the AR regulated promoter of TMPRSS2 fusion with the ERG gene (Haffner et al., 2011). If these DSBs are incorrectly repaired by the error prone NHEJ mechanism, this would result in the generation of the *TMPRSS2:ERG* gene fusion (Haffner et al., 2011; Adamo and Ladomery, 2016; Labbé and Brown, 2018). Furthermore, AR negative PCa cells also showed aberrant transcription through the presence of genomic aberrations in transcription factors as the tumor suppressor gene TP53 (Labbé and Brown, 2018). Intriguingly, Jensen et al., showed that SPOP deficiency resulted from its Knockdown (KD), decreased the mRNA level of some DNA repair genes as ATR, ChK1, BRCA2 and RAD51, which they suggested as the reason behind accumulation of DSBs, replication stress and impaired HR repair in SPOP-KD cells. Additionally, they found that only SPOP wild type is in interactome with transcription machinery proteins (Hjorth-Jensen et al., 2018). Altogether, deeper understanding and revealing the mechanisms that contribute to genomic instabilities in PCa, can improve the treatment targeting and hence, halt the disease progress.

## 2. Aim of the work

The main goal of this study is to understand the role of SPOP in DSB repair and how this predisposes to genomic instabilities in PCa. Achieving this aim will not only increase our understanding of the crosstalk between DSB repair and PCa; but it will also provide a stratification strategy for a biomarker-derived personalized therapy in PCa.

# 3. Materials and Methods

## 3.1. Materials

### 3.1.1. Vectors and plasmids

| Vector | Manufacturer |
|---|---|
| SPOP Crispr guide RNA1 in plenticrispr v2_Genescript (CAAGCTTACCCTCTTCTGCG) | GenScript, USA |
| pDONR223_SPOP_WT- Homo sapiens | Addgene, USA |
| pEGFP-N1 | Clontech, BD Bioscience, Heidelberg, Germany |
| pGC | Previously constructed in our group (Mansour et al., 2008) |
| pEJ | Previously constructed in our group (Mansour et al., 2008) |

### 3.1.2. Oligonucleotide/primer sequence

| Primer | Sequence (5'-3') | Tm [°C] | Manufacturer |
|---|---|---|---|
| SPOP-Forward | CCA GAG AGT CAA CGG GC AT | 59.40 | Eurofins, Luxembourg |
| SPOP-Reverse | ACC AAT ACT CAT CAG ATC TGG GAA C | 60.14 | Eurofins, Luxembourg |

### 3.1.3. Antibodies

| Antibody | Species | Company | Number | Dilution |
|---|---|---|---|---|
| **Primary antibodies used in Western Blot** | | | | |
| SPOP | Rabbit | Proteintech, USA | #16750-1-AP | 1:1000 |
| ATR, monoclonal | Goat | Santa Cruz, USA | SC #1887 | 1:1000 |
| p-ATR, monoclonal | Rabbit | Cell signal, USA | CS #58014 | 1:1000 |
| ChK2, monoclonal | Mouse | Bioscience Europe, Netherlands | BD #611570 | 1:1000 |
| pCHK2-Thr68, monoclonal | Rabbit | Cell signaling, USA | CS #2661 | 1:1000 |
| ATM, monoclonal | Rabbit | Cell signaling, USA | CS #2873S | 1:1000 |
| pATM serine 1981, monoclonal | Rabbit | GeneTEX, USA | GTX # 132146 | 1:1000 |
| Chk1, monoclonal | Mouse | Cell signaling, USA | CS #2360S | 1:750 |
| pChk1, monoclonal | Rabbit | Cell signaling, USA | CS #2348 | 1:1000 |

| | | | | |
|---|---|---|---|---|
| RAD51, polyclonal | Rabbit | Calbiochem | PC130 | 1:1000 |
| HSC70, monoclonal | Mouse | Santa Cruz, USA | sc-7298 | 1:1000 |
| β-actin | Mouse | Sigma-Aldrich, Germany | A-2228 | 1:1000 |
| Histone H2B, polyclonal | Rabbit | IMGENEX | IMG-359/ NB100-56347 | 1:250 |
| GAPDH ( FL-335), polyclonal | Rabbit | Santa Cruz, USA | sc-25778 | 1:500 |
| Rpb1 NTD (D8L4Y), monoclonal | Rabbit | Cell signaling, USA | CS #14958 | 1:500 |
| pRNA polymerase II subunit B1 (phospho-CTD Ser-5) clone 3E8, monoclonal | Rat | Millipore | 04-1572 | 1:1000 |
| p-Rpb1-CTD (Ser2) (E1Z3G), monoclonal | Rabbit | Cell signaling, USA | CS #13499 | 1:1000 |
| CDK9 (C12F7), monoclonal | Rabbit | Cell signaling, USA | CS #2316 | 1:1000 WB<br>1:100 IP |
| pCDK9 (Thr186) =pTEFB, polyclonal | Rabbit | Cell signaling, USA | CS #2549 | 1:1000 |
| HEXIM1 (D5Y5K), monoclonal | Rabbit | Cell signaling, USA | CS # 12604 | 1:1000 |
| AR, monoclonal | Mouse | Invitogen, USA | MA5-13426 | 1:200 |
| PSA (8A12), monoclonal | Mouse | Invitogen, USA | MA5-17108 | 1:1000 |
| XPF (F-11), monoclonal | Mouse | Santa Cruz, USA | Sc #398032 | 1:500 |
| XPG (8H7), monoclonal | Mouse | Santa Cruz, USA | Sc #13563 | 1:200 |
| RNase H1, polyclonal | Rabbit | Abcam, UK | Ab #229078 | 1:1000 |
| **Secondary antibodies for Western Blot** | | | | |
| IRDye® 800CW goat anti-mouse, polyclonal | Mouse | LI-COR, USA | 926-32210 | 1:7500 |
| IRDye® 800CW Donkey anti-goat, polyclonal | Goat | LI-COR, USA | 925-32214 | 1:7500 |
| IRDye® 800CW Goat anti-rat, polyclonal | Rat | LI-COR, USA | 925-32219 | 1:7500 |
| IRDye® 800CW goat-anti-rabbit, polyclonal | Rabbit | LI-COR, USA | 926-32211 | 1:7500 |
| **Primary antibodies used in Immunofluorescence** | | | | |
| Anti-γH2AX (Ser139) monoclonal | Mouse | Millipore, Germany | #05-636 | 1:500 |

| | | | | |
|---|---|---|---|---|
| Anti-RAD51(AB-1), polyclonal | Rabbit | Calbiochem, USA | # PC130 | 1:500 |
| 53BP1 | Rabbit | Novus, USA | #100-305 | 1:500 |
| CenpF (Centromere protein F) | Rabbit | LSBio, USA | #B276 | 1:500 |
| DNA-RNA Hybrid, clone S9.6 (R-loops) | Mouse | Miilipore, Germnay | #1095 | 1:100 |
| **Secondary antibodies used in Immunofluorescence** | | | | |
| Alexa Fluor®488, Goat anti-Rabbit IgG (H+L), polyclonal | Rabbit | ThermoFisher, USA | #A32723 | 1:1000 |
| Alexa Fluor®594, Goat anti-Mouse IgG (H+L), Polyclonal | Mouse | ThermoFisher, USA | #A32742 | 1:1000 |
| **Primary antibodies used in DNA fiber assay** | | | | |
| Anti-BrdU (Bromodeoxyuridine), Rat monoclonal | Rat | Abd Serotec, UK | #ABT0030G | 1:1000 |
| Anti-BrdU (clone B44), Mouse, monoclonal | Mouse | Bexton Dickinson, USA | # 347580 | 1:1000 |
| **Secondary antibodies used in DNA fiber assay** | | | | |
| Alexa Fluor® 555, Goat-Anti-Rat IgG (H+L) | Rat | ThermoFisher, USA | # A21434 | 1:500 |
| Alexa Fluor® 488, Goat-Anti-Mouse IgG (H+L) | Goat | ThermoFisher, USA | # A-11001 | 1:500 |

### 3.1.4. Chemicals and kits

| **Product** | **Manufacturer** |
|---|---|
| 4′,6-Diamidin-2-phenylindol (DAPI) | Merck, Darmstadt, #124653100 |
| 5-Chloro-2'-deoxyuridine (CldU) | Sigma-Aldrich, Steinheim # C68910 |
| 5-Iodo-2´-deoxyuridine (IdU) | Sigma-Aldrich, Steinheim, #I7125 |
| AccuPower®2xGreenStarTMqPCR Master Mix | Bioneer, Korea, #K-6251 |
| Agarose, For Routine Use | Sigma-Aldrich, Steinheim, #A9539-500G |
| Ammonium bicarbonate (NH4C03) | Fluka, Biochemia, Sigma-Aldrich, Germany, #09830 |
| Ampicillin | Sigma-Aldrich, USA |
| AmpliSize™Molecular Ruler (50-2.000 bp) DNA Ladder | Bio-Rad Laboratories, München, #170-8200 |

| | |
|---|---|
| Bakterien One Shot™ TOP10 coli | ThermoFisher, USA |
| Bicinchoninic Acid solution | Sigma-Aldrich, USA |
| Bovine Serum Albumin | Sigma-Aldrich, Steinheim, #A7030 |
| Cell Lysis (10X) | Cell signalling, USA, #9803 |
| Click-iT®EdU imaging Kit (5-ethynyl-2'-deoxyuridine) | Life-Technologies, USA, #C10340 |
| cOmplete Mini | Roche, Switzerland |
| Copper(II) sulfate solution | Sigma-Aldrich, USA |
| Coulter ® Isoton® II solution | Beckmann Coulter GmbH, Krefeld, #8448011 |
| Dimethylsulfoxide (DMSO) | Sigma-Aldrich, Steinheim, #D2650 |
| Dithiothreitol (DTT) (diluted in dd.$H_20$; 1:200 from 200mM stock solution) | Sigma-Aldrich, Germany, #43816 |
| DMEM (Dulbecco`s Modified Eagle Medium) | Sigma-Aldrich, USA |
| DNeasy Blood & Tissue Kit (50) DNA extraction | Qiagen, Germany, #69504 |
| Enzalutamide (diluted in DMSO) | Selleckchem, Germany |
| Ethanol (99 %) | Th. Geyer, Germany |
| Ethidium bromide solution | Sigma-Aldrich, Steinheim, #E1510-10ML |
| Ethylenediamine tetraacetic acid (EDTA) | Serva, Heidelberg, #11280 |
| EU (5-Ethynyl-uridine) (diluted in dd.$H_20$) | Jena bioscience, CLK-N002-10 |
| Fetal Calf Serum (FCS) | ThermoFisher, USA |
| Fugene®HD Transfection Reagent | Promega, USA |
| FxCycle™ Far Red Stain | ThermoFisher, USA, #F10348 |
| Glycerol | Sigma-Aldrich, USA |
| Histone extraction kit | Abcam, USA, #113476 |
| Immersion oil | Zeiss, Göttingen, #444969-0000-000 |
| I-SceI Restriction enzyme | New England BioLabs, USA, R0694L |
| Isopropanol | Merck, USA |
| Kanamycin | Sigma-Aldrich, USA |
| MACS® Bleach Solution 1000 ml | Miltenyi Biotec, Bergisch Gladbach, #130-093-663 |
| MACSQuant® Washing Solution 1500 ml | Miltenyi Biotec, Bergisch Gladbach, #130-092-749 |
| MACSQuant®Running Buffer 1500 ml | Miltenyi Biotec, Bergisch Gladbach, #130-092-747 |
| MACSQuant®Storage Solution 1500 ml | Miltenyi Biotec, Bergisch Gladbach, #130-092-748 |
| MagicMark XP Western Standard | Life Technologies, USA |
| Methanol | J.T.Bakker, Pleasant Prairie, #8045 |
| MOPS buffer SDS Running Buffer (20X) | Invitrogen, USA, #2282440 |
| Odyssey Blocking Solution (Licor) | Li-COR, Nebraska, USA, #927-40000 |
| Opti-MEM | Roche, Switzerland |
| Paraformaldehyde (PFA) | Merck, USA |
| PBS (1x) | Sigma Aldrich, USA |

| | |
|---|---|
| Penicillin/Streptomycin (PS) | ThermoFisher, USA |
| phenylmethylsulfonyl fluoride (PMSF) | ThermoFisher, USA |
| Puromycin | Sigma-Aldrich, USA |
| Qiagen Plasmid Plus Maxi Kit | Qiagen, Germany, #12963 |
| RIPA buffer | Cell signalling, USA, #9806S |
| SeeBlue Plus2 Pre-stained Protein Standard | Life Technologies, Carlsbad, USA, #LC5925 |
| Sodium Chloride (NaCl) | Sigma-Aldrich, Steinheim, #S6150 |
| Sodium Hydroxide (NaOH) | Sigma-Aldrich, Steinheim, |
| Sodiumdodecylsulfat (SDS) | Sigma-Aldrich, Steinheim, #L4509 |
| Subcellular Protein Fractionation Kit for Cultured Cells | ThermoFisher, USA, # 78840 |
| SureBeads™ Protein G Magnetic Beads | Biorad, USA, #161-4023 |
| Trans-Blot Turbo 5X Transfer Buffer | Bio-Rad, USA, #10026938 |
| Tris- Acetate SDS Running Buffer (20X) | Invitrogen, USA, #2191722 |
| Tris/Glycin buffer (TG) | Bio-Rad, USA, #1610734 |
| Tris-Borat-EDTA | Sigma-Aldrich, Steinheim, #93290 |
| TritonX-100 | Sigma-Aldrich, Steinheim, #T8787 |
| Trypanblue solution, 0.4% | ThermoFisher, USA |
| Trypsin – EDTA 0.05 % | Life Technologies, USA, #25300054 |
| Tween20 | Sigma-Aldrich, Steinheim, #P1379 |
| UltraPure™ Distilled Water | Life Technologies, USA, #10977 |
| Vectashield® Mounting Medium | Vector Laboratories, Burlingame, USA, # H-1000 |
| Wizard® SV Gel and PCR Clean-Up System | Promega, Fitchburg, USA, #A9282 |

### 3.1.5. Consumables and products

| **Product** | **Manufacturer** |
|---|---|
| Bolt™ 4-12%, Bis-Tris Plus | Invitrogen, USA, #22041270 |
| Cell culture Flasks (T25, T75) | Sarstedt |
| Conical centrifuge tubes (15 mL, 50 mL) | Sarstedt |
| CriterionTMPrecastTris-HCl Gel, 4-15 % | Bio-Rad Laboratories, München, #345-0028 |
| Cuvettes | Sarstedt |
| Filterpaper CriterionTMBlotter | Bio-Rad Laboratories, München, #170-4085 |
| Inoculation loop | NeoLab, Germany |
| NuPAGE™ 3-8 % Tris-Acetate Gel | Invitrogen, USA, #EA03755BOX |
| Odyssey Nitrocellulose Membrane | LI-COR, Nebraska, USA, #926-31092 |
| Pipette serology, 1 ml sterile | Sarstedt, Nümbrecht, #86.1251.001 |
| Pipette serology, 10 ml sterile | Sarstedt, Nümbrecht, #86.1254.001 |
| Pipette serology, 2 ml sterile | Sarstedt, Nümbrecht, #86.1252.001 |
| Pipette serology, 25 ml sterile | Sarstedt, Nümbrecht, #86.1685.001 |
| Pipette serology, 5 ml sterile | Sarstedt, Nümbrecht, #861253001 |
| Pipette serology, 50 ml sterile | Sarstedt, Nümbrecht, #861689001 |
| Pipette tips, 0.5-20 µl | Eppendorf AG, Hamburg, #0030000854 |
| Pipette tips, 50-1000 µl | Eppendorf AG, Hamburg, #0030000919 |
| Reaction Tubes | Sarstedt, Nümbrecht, #72690001 |

| | |
|---|---|
| Reaction tubes, 1.5 ml | Sarstedt, Nümbrecht, #72.690.001 |
| Reaction tubes, 50 ml | Sarstedt, Nümbrecht, #62.554.501 |
| Reaction tubes,15 ml | Sarstedt, Nümbrecht, #62554502 |
| Realtime PCR-Plat-cover, (Microseal®) | Bio-Rad Laboratories, München, #MSB1001 |
| Realtime PCR-Plates, (Hard-Shell®PCR Plates, 96-well, thin-well) | Bio-Rad Laboratories, München, #HSP9601 |
| Serological pipettes | Sarstedt, Nümbrecht |
| Trans-Blot Turbo Midi-size Transfer Stacks | Bio-Rad Laboratories, USA |
| Transformation cuvette | Biozyme Scientific |
| Well plates (6, 12, 24) | Sarstedt, Nümbrecht |

### 3.1.6. Instruments

| | |
|---|---|
| Accu-jet Pro | Brand, Deutschland |
| Autoclave | Meditech, Norderstedt |
| Autoclave VE-150 | Systec, Wettenberg |
| Balance | P1200, Mettler Toledo, Giessen |
| Blot-Chamber Criterion Precast | Bio-Rad, München |
| Camera system | AxioCamMRm, Zeiss, Göttingen |
| Cell culture-Incubator MCO-18AIC | Sanyo, San Diego, CA, USA |
| Centrifuge | Biofuge 15 R, Heraeus, Hanau |
| Centrifuge 5415 C | Eppendorf, Hamburg |
| CFX96 Touch Real-Time PCR Detection System | Bio-Rad, München |
| Coulter Counter Z2 | Beckman Coulter, Krefeld |
| FACS device MACSQuant®X and MACSQuant Analyzer 10 | Miltenyi Biotec, Bergisch Gladbach |
| Fluorescence Microscope Axionvision Observer Z1 | Carl Zeiss, Microscopy GmbH, Göttingen |
| Freezer | Kryotec, Deutschland |
| Gel electrophoresis chamber CriterionCell | Bio-Rad, München |
| Heat block Thermomixer® comfort | Eppendorf, Hamburg |
| Heat block Thermostat 5320 | Eppendorf AG, Hamburg |
| Ice machine FM-120DE-50 | Hoshizaki Europe, Amsterdam |
| Ice machine MF 36 | Scotsman-FRIMONT S.P.A., Mailand, Italien |
| Incubator (CO2 Incubator) | SANYO Medical, Bad Nenndorf |
| Incubator Heracell 240 | Heraeus, Deutschland |
| Incubator Kelvitron®t | Heraeus Instruments, Hanau |
| Invitrogen chamber WB | Thermo Fisher, USA |
| Liquid suction system (pump) BVC 1 | Vakuumbrand, Wertheim |
| Magnet stirrer | Ikameg Ret, IKA Labortechnik, Staufen |
| NanoDrop ONE C | Thermo Fischer Scientific, Massachusetts, USA |
| pH-Meter | Beckman Coulter, Krefeld |
| Photometer (Bio-Photometer) | Eppendorf AG, Hamburg |

| | |
|---|---|
| Pipette 0,5 - 10 µl | Eppendorf AG, Hamburg |
| Pipette 10 - 100 µl | Eppendorf AG, Hamburg |
| Pipette 100 - 1000 µl | Eppendorf AG, Hamburg |
| Radiation device RS225 | Gulmay, Surrey, UK |
| Shaker | Edmund Bühler, Johanna Otto GmbH, Hechingen<br>Mini-Shaker, Modell Kühner, Braun, Melsungen<br>Polymax 1040, Heidolph, Schwabach |
| Sterile Herasafe work bench | Heraeus, Hanau |
| Thermocycler Primus 25 advanced® Thermocycler | Peqlab, VWR, Pennsylvania, USA |
| Trans-Blot Turbo Transfer System - Bio-Rad | Biorad, USA |
| Vortexer Vortex-Genie® 2 | Scientific Industries, Bohemia, USA |
| Water Bath | Haake W19/D3, Karlsruhe |

### 3.1.7. Software and online sources used in the analysis

| **Software** | **Manufacturer** |
|---|---|
| Axio-Vision Rel. 4.7 | Carl Zeiss Microscopy GmbH, Göttingen |
| CFX Manager TM Software #1845000 | Bio-Rad, München |
| Cytoscape Version 3.8.2 | Institute for Systems Biology, USA |
| FlowLogicTM, Flow Cytometry Analysis Software | Miltenyi Biotec, Bergisch Gladbach |
| Gene set enrichment analysis (GSEA) Version 4.1.0 | UC San Diego, Broad Institue, USA |
| GeneWise | EMBL, UK |
| Expasy | SIB Swiss Institute of Bioinformatics, Switzerland |
| GraphPadPrism 9 | GraphPad Software Inc, CA, San Diego |
| Image J | Wayne Rasband |
| Odyssey® Infrared Imaging System | LI-COR, Nebraska, USA |
| RStudio 2022.02.2+485 "Prairie Trillium" | RStudio, PBC |

### 3.1.8. Buffers and solutions

Double distilled water (dd.$H_2O$) was used for all buffer preparations

| **Immunofluorescence detection of RAD51, γH2AX, 53BP1** | |
|---|---|
| Blocking solution | 1x PBS, 3% BSA |
| Fixation | 1x PBS, 4% PFA |
| Wash I | 1x PBS, 1.5% BSA, 0.1% Tween20 |
| Wash II | 1x PBS, 0.5% Tween20 |

| | |
|---|---|
| **Immunofluorescence detection of R-loops** | |
| Blocking solution | 3% BSA, 1x PBS |
| Wash Buffer | 0.5% Tween20, 1x PBS |
| Pre-extraction | 0.1% TritonX, 1x PBS, 1:200 DTT (200 mM stock solution) |
| **Protein extraction and Western blotting** | |
| Phenylmethylsulfonylfluoride (PMSF) | 200 mM in isopropanol |
| 5x Laemmli | 50 mM Tris-HCL, pH 6.8,<br>2% SDS, 0.1% bromophenolblue |
| Transfer buffer | 10% 10x TG buffer, 10 % methanol |
| TBS-T buffer | TBS, 0.05% Tween20 |
| Running buffer | 10% 10x TG-buffer, 10% SDS |
| **DNA Fiber assay** | |
| Blocking solution | 1x PBS, 3% BSA, 0.1% Tween20 |
| Denaturation solution | 2.5M HCl |
| Fixation | 1x PBS, 4% PFA (paraformaldehyde) |
| Spreading buffer | 200mM Tris-HCL, PH 7.4, 50mM EDTA, 0.5% SDS |
| Fixation after spreading | Methanol/ Acetic acid 3:1 |
| Wash solution | 1x PBS, 1% BSA, 0.1% Tween20 |
| **Co-immunoprecipitation** | |
| Wash buffer | PBS-T (PBS+ 0.1% Tween20) |
| **Histone extraction** | |
| $NH_4HCO_3$ | Dissolved in dd.$H_2O$, 50mM, PH8 |
| **Transformation** | |
| LB medium (Lysogeny broth) | For 2 l: 20 g Bactotrypton<br>10 g Bacto Yeast Extract<br>20 g NaCl, 2 ml 1M NaOH, dd.$H_2O$ |
| LB Agar | LB medium<br>1.5 % Agar |
| **Agarose gel** | |
| 1% Agarose | Dissolved in 1x TBE buffer |
| **EU incorporation** | |
| Wash buffer | 1x PBS + 0.2% Triton X-100 + 1%BSA |

## 3.2. Methods

### 3.2.1. Cell culture

Cell culture was performed under sterile conditions in laminal flow hood to protect against contamination. DU145 and LNCaP prostate cancer cell lines were obtained from the American Type Culture Collection (ATCC, Manassas, VA, USA). Dulbecco's modified Eagle medium (DMEM) was used as cell growth medium, supplemented with 10% Fetal Calf Serum (FCS) and 1% penicillin streptomycin (PS). SPOP knockout subclones established from DU145 and LNCaP cells were cultured in the presence of 1 µg/ml puromycin for selection. For cell passaging, medium was aspirated from the flasks and adherent cells were washed with 5-10 ml pre-warmed phosphate buffer solution (PBS). After removing the PBS, 0.5 – 1.5 ml trypsin were added to T25 or T75 flasks, respectively. Next, cells were incubated at 37°C for 2-4 minutes, to detach from the flasks' surface. Once cells were detached, trypsin was inactivated by immediately adding 5-10 ml growth medium. 0.2 ml cell suspension were added to 9.8 ml cell counter solution for counting to determine the required cell number for each planned experiment.

### 3.2.2. Cell preservation

Similar steps were followed as for cell passaging until cell detaching. Once cells were detached, they were collected in falcon tubes and centrifuged at 1,200 rpm for 5 min. The supernatant was removed and cells were washed with 1x PBS before being centrifuged again as above to collect cell pellet. Cells were then re-suspended in 1 ml freshly-prepared preservation solution (FCS + 10% DMSO) and aliquots were prepared in cryotubes (3-5x$10^6$ cells/tube). Mr. Frosty was used to gradually freeze cells at -80 °C, before final storage in liquid nitrogen. For re-culturing, cells were thawed and transferred into falcon containing 10 ml growth medium, centrifuged at 1200 rpm for 5 min, then the supernatant was removed and cells were suspended in 5ml standard growth medium in T25 flasks.

### 3.2.3. Transformation

For plasmid preparation, 100 ng of each plasmid were mixed with 25 µl freshly thawed TOP10 E-coli (section 3.1.4) and dd.$H_2O$ in a total volume of 100 µl. The mixture was then electroporated (1.8kV, at a time constant of 4-5 sec).The transformed bacteria were incubated in LB medium for 1h at 37°C with agitation (225 rotations/min), spread on LB plates containing 50 mg/ml ampicillin (for pGC and SPOP plasmids) or 50 mg/ml

kanamycin (for pEJ and pEGFP-N1) and incubated 1h at 37˚C. 100 µl of the transformed bacteria were streaked on the agar plates containing the corresponding antibiotic and incubated overnight at 37°C. Single clones were picked from the plates and mixed with 4 ml LB medium (with antibiotic) in falcon tube and incubated at 37°C for 6-7 h at 230 rpm. Subsequently, 1ml of the grown bacterial suspension was added to 500 ml LB medium containing the corresponding antibiotic in a flask and incubated overnight at 37°C to multiply. Eventually, plasmid extraction took place using QIAGEN® Plasmid Plus Maxi Kit (section 3.1.4.), according to the manufacturer's protocol. The concentration and purity of the extracted DNA were analyzed using NanoDrop spectrophotometer.

### 3.2.4. Establishment of SPOP-knockout (SPOP-KO) clones using CRISPR/CAS9

The CRISPR (clustered regularly interspaced short palindromic repeats)/Cas9 (CRISPR associated protein 9) system has emerged recently as a novel tool for genome editing in any organism. It depends on the targeted introduction of DNA DSBs by the programmable Cas9 nuclease and subsequent exploitation of the DNA repair machinery of the host cell. DSB repair can be conducted by the error-prone non-homologous end joining pathway, which frequently results in small insertion/deletions (indel) mutations at the site of the DSB sites, thus leading to gene knockouts (Fig. 8). A specific guide RNA sequence (gRNA) that directs Cas9 nuclease was used to induce site-specific DNA DSB at specific genomic sites.

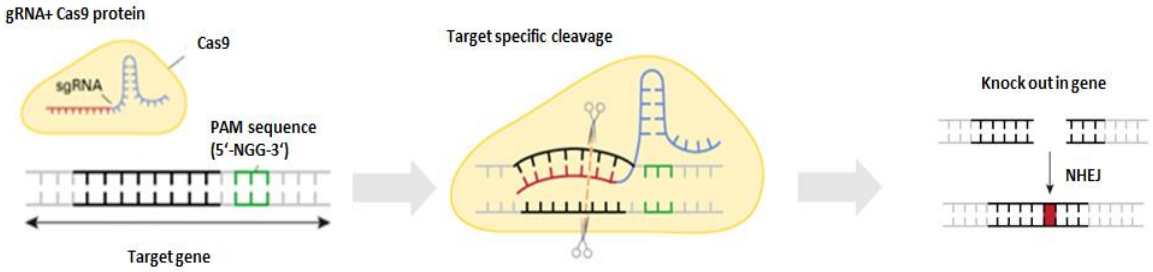


**Figure 8. Graphical illustration for CRIPSR/CAS9-mediated gene disruption.** Single guide RNA (sgRNA) binds to a recombinant Cas9 endonuclease, forming the cleavage complex. This complex recognizes a specific genomic sequence in DNA that contains a 2-6 base pair proto-spacer adjacent motif (PAM), where Cas9 introduces DSBs. When NHEJ repair this site-specific DSB, insertions/deletions (indels) might be produced, hence disturbing the gene function. Figure is modified from https://www.takarabio.com/learning-centers/gene-function/gene-editing/gene-editing-tools-and-information/introduction-to-the-crispr/cas9-system.

All-in-one vector (SPOP CRISPR guide RNA1 in plenticrispr v2_Genescript), which contains both Cas9 gene and SPOP-specific gRNA that target exon 5 (section 3.1.1), was used to establish SPOP-KO cells. The All-in-one vector has the advantage that transfection of cells takes place at once, with a ratio of 1:1 of Cas9 to the gRNA. This produces more efficiency, as it decreases the off targets. Where, once the Cas9 is transfected in the optimum concentration together with gRNA, it cleaves directly the target DNA sequence (Editing and Life Genescript, 2016). Briefly, $1x10^6$ cells were seeded in T25 flask in 5 ml normal growth medium and incubated at 37°C with 5% $CO_2$ until reaching 70-90% confluency (1-2 days). Transfection mixture was freshly prepared by mixing 8 µg of SPOP-targeted All-in-one CRISPR vector with 800 µl OptiMEM. Subsequently, 16 µl Turbofect were added to the transfection mixture and incubated for 20 min at RT in dark. Meantime, medium was removed from the confluent cells and replaced with DMEM medium containing 10% FCS without antibiotic. The transfection mixture was added dropwisely on the cells and incubated for 24h under normal growth conditions. Thereafter, cells were washed with 1x PBS, trypsinized and split into new T75 flasks with different cell numbers (25,000, 50,000, 100,000, 200,000) and incubated under normal growth conditions. 48h post-splitting, DMEM selection medium (10% FCS+ 1 µg/ml puromycin) was added to select cells that stably integrated the plasmid within their genome. Selection medium was changed twice weekly until clones started to appear within 2- 6 weeks. All cells without the integrated plasmid died and distinct clones of “survivors” were seen. Individual clones were trypsinized and transferred to 24-well plates for further propagation, then later into 6-well plate in the presence of selection medium. Cell pellets were prepared from each individual clone for western blot (section 3.2.11).

### 3.2.5. Puromycin sensitivity test

The sensitivity of the parenteral cells to puromycin was tested by seeding 200,000 under normal growth conditions in the presence of different concentrations of puromycin (0 µg/ml, 0.02 µg/ml, 0.04 µg/ml, 0.1 µg/ml, 0.2 µg/ml, 0.5 µg/ml, and 1 µg/ml). cell growth was monitored daily for up to 1 week. At a concentration of 1 µg/ml, neither DU145 nor LNCaP cells showed any viable cells. For further experiments, 1 µg/ml puromycin was used for selection of resistant clones.

### 3.2.6. Cell growth curve

Once the cell lines reached 80 to 90% of confluence, they were counted and plated at a density of 50,000 cells per well in a 6-well plate under normal growth conditions. Cell number was determined using the Cell coulter at different time points (0, 2, 4, 8, and 11 days). Three different readings were recorded to each sample at each time point.

### 3.2.7. Protein extraction using RIPA buffer

Cell pellets (section 3.2.2) were suspended in equal volumes of freshly prepared extraction buffer (for 1ml: 5 µl 200mM PMSF + 100 µl mini component protease inhibitor + 200 µl RIPA buffer 5x+ rest of volume dd.$H_2O$). The re-suspended cell pellets were incubated for 30 min on ice with frequent vortex, and sonicated for 10 sec. before being centrifuged at 14,000 rcf for 15 min at 4°C. Finally, supernatant containing the extracted proteins was collected and concentration was measured using BCA (section 3.2.9) and stored at -20°C till western blot.

### 3.2.8. Subcellular protein fractionation

Subcellular Protein Fractionation Kit for culture cells (Section 3.1.4) was used according to the manufacturer's instructions to isolate the cytoplasmic, membrane, nuclear and chromatin fractions. Concentration of extracts was measured using BCA method (section 3.2.9) and stored at - 20°C till processing in western blot.

### 3.2.9. BCA protein assay

BCA method was used to determine total protein concentration (Smith et al., 1985), which is based upon the use of Biuret-reaction. The Biuret reagent (copper sulfate dissolved in a strong base) changes to brown color upon reaction with peptide bonds. The BCA Protein Assay reagent was prepared by mixing reagent A and reagent B in a ratio of 50:1. Two µl of protein extracts were added to 48 µl dd.H2O. 50 µl of dd.H2O were used as a blank. One ml of the color reagent was added to the diluted samples and the blank as well, and after vortexing, they were incubated at 37°C for 30 minutes. The color intensity was determined using a spectrophotometer at a wave length of 562 nm.

### 3.2.10. Sodium dodecyl sulfate–polyacrylamide gel electrophoresis (SDS-PAGE)

50 µg of total protein or 12 µg of chromatin bound fraction were mixed with 3 µl of 5x laemmli (section 3.1.8) and dd.H2O in a final volume of 15 µl. The mix was then denatured at 95 °C for 5 min and pulse centrifuged before being loaded into Biorad 4-

15% gradient SDS-polyacrylamide gel, Invitrogen Bolt 4-12% (with MOPS buffer) or Invitrogen NoPage 3-8% (with Tris acetate buffer). Magic marker western protein standard and sea blue were used for molecular weight determination. The electrophoresis was performed for 10 min at 100V followed by 200 V for separation using Biorad system. For Invitrogen system, 160 V was used for 60 min for Invitrogen Bolt 4-12% and 120 V with NoPage 3-8% gel.

### 3.2.11. Western Blot (WB)

The electrophorized proteins were transferred onto nitrocellulose membrane using Trans-Blot Turbo transfer system for 15 min at High molecular weight program (12 V). The membrane was incubated for overnight in Licor blocking buffer (section 3.1.4) at 4°C with gentle shaking. Staining with the primary antibody specific (section 3.1.3) for each protein took place for overnight at 4°C with gentle shaking. Membrane was then washed 3 times using TBS-T (section 3.1.8) for 5 min, before staining for 1h at RT with the fluorescent secondary antibody (section 3.1.3). Finally, membranes were scanned by the Licor Odyssey CLx imaging system.

### 3.2.12. Co-immunoprecipitation (CoIP)

$2x10^6$ cells were lysed in 1x Cell Lysis buffer (section 3.1.4) according to the manufacturers' instructions. Briefly, after washing the cells 2 times with ice cold 1x PBS, 200 µl 1x Lysis buffer were added and cells were then incubated on ice for 5 min before being scraped. Afterwards, cell lysate was collected in 1.5 ml reaction tube, sonicated for 10 sec. and centrifuged for 10 min at 14,000 rpm at 4°C. Supernatant that contains protein extract was then transferred to a new 1.5 ml reaction tube. At this point, cell lysate could be stored at -80°C, until further analysis.

Immunoprecipitation reactions were performed with CDK9 or IgG antibody-magnetic-beads conjugate using SureBeads ™ Magnetic IgG beads (section 3.1.4) according to the manufacturer's protocol. Briefly, magnetic beads were washed 3 times with wash buffer (section 3.1.8), then suspended in 1:100 of CDK9 or IgG antibody (section 3.1.3) and incubated for 3h at 4°C on rotatory shaker. Beads were then magnetized, washed 3 times with wash buffer. 400 µl of each sample were added to IgG or CDK9 magnetic-bound beads and incubated overnight at 4°C on rotatory shaker. Finally, beads were magnetized, washed 3 times with the wash buffer and eluted with 1x Laemmli buffer for 10 min at 70°C. The eluent was collected and stored at -80°C till processing by western blot.

### 3.2.13. Immunofluorescence staining

Immunofluorescence (IF) is a technique used to visualize specific proteins or antigens in cells or sections from tissue, through binding to a specific antibody that is chemically conjugated with a fluorescent dye. Eventually, a fluorescence microscope is used to examine the stained samples at the desired wave length.

**IF staining of DSB foci**

Briefly, 125,000- 150,000 cells were seeded on 15mm cover slip in 12-well plate and incubated overnight under normal growth conditions. After treatments and repair incubations, adhered cells were washed once with 1x PBS and fixed with 4% paraformaldehyde (PFA) for 15 min at RT. Then, cells were washed 3 times with PBS. For permeabilization, cells were then incubated with 0.2% TritonX-100 for 10 min at RT. This step was followed by blocking with 3% BSA/PBS for 1h at RT, before incubation with the primary antibodies (section 3.1.3) against γH2AX, 53BP1 or RAD51, diluted in Wash 1 (1.5% BSA/PBS + 0.5% Tween20) at RT for 1h in a moisturising chamber. After primary antibodies incubation, cells were washed 3 times with 0.5% Tween20/PBS, each for 5 min. Cells were next stained with the corresponding secondary antibody (section 3.1.3) for 1h at RT in dark. Nuclei were counterstained with DAPI (section 3.1.4) 1:1000 along with secondary antibodies. Cells were then 3 times washed with Wash 2 (section 3.1.8) for 10 min each.

In order to detect DSBs in cell cycle dependent manner, cells were (i) incubated with the thymidine analogue EdU for 15min, (Click-iT®EdU imaging Kit (section 3.1.4) was used to label EdU incorporation according to the manufacturer's instruction), and/or (ii) co-stained with the S/G2 specific marker CenpF; to differentiate between G1 (EdU-/CenpF-), S (EdU+/CenpF+) and G2 (EdU-/CenpF+) cells. Finally, cover slips were placed over slides, mounted with Vectashield and sealed with nail polish. Carl Zeiss Observer z1 microscope and the corresponding AxioVision software were used to capture and visualize the Z-stack images. Image J software was used for quantification.

**IF staining of R-loops**

DU145 and LNCaP cells in a cell density of 150,000 and 200,000, respectively were seeded on 15mm coverslip in 12 well plate and overnight incubated under normal growth conditions. Cells were then pre-extracted with 0.1% Triton in 1x PBS + 1:200 DTT (200mM) on ice for 10 min under gentle agitation. After cell fixation (as above

indicated), blocking was performed by overnight incubation with 3% BSA. R-loops were detected using S9.6 antibody (section 3.1.3), which detects mainly RNA-DNA hybrids. For S9.6 staining, cells were incubated overnight at 4°C with S9.6 primary antibody. Afterwards, cells were washed 2 times with 0.5% Tween20/PBS shortly, followed by another 2 times for 5 min on shaker. Cells were next stained with the secondary antibody (section 3.1.3) for 1h, together with DAPI 1:1000 at RT in dark. Eventually, cells were washed, as after the primary antibody; before mounting the cover slips on the slides using Vectashield and sealing with nail polish for visualization using microscope, as mentioned above in immunofluorescence. In order to detect R-loops in cell cycle dependent manner, cells were incubated with EdU 15 min, then EdU click kit was used as above to label EdU. Finally, cover slips were placed over slides, mounted with Vectashield and sealed with nail polish. Carl Zeiss Observer z1 microscope and the corresponding AxioVision software were used to capture and visualize the Z-stack images. Image J software was used for quantification.

### 3.2.14. DNA Fiber assay

DNA fiber assay is a method used to analyze the dynamics of the replication fork. It is based on successive incorporation of the thymidine analogues CldU (5-chloro-2'-deoxyuridine) and IdU (5-iodo-2'-deoxyuridine) into DNA during replication; which are then visualized through immunofluorescence staining.

In T25 flasks, $3x10^5$ cells were seeded under normal growth conditions till reaching ~75% confluence. Growth medium was then aspirated and cells were pulse-labeled with 0.025 mM CldU (dissolved in normal DMEM medium) and incubated for 20 min at 37°C with 5% $CO_2$. Medium was next aspirated before treatment with 0.25 mM IdU (dissolved in normal DMEM medium) for 20 min at 37°C with 5% $CO_2$. IdU medium was aspirated and cells were washed twice with ice cold 1x PBS. Cells were then scraped in 1 ml ice cold PBS. The cell suspension was adjusted to $5\times10^5$ cells/ml in ice cold PBS, using cell coulter. For DNA preparation, 3 µl of the cell suspension were spotted onto a glass slide and cells were lysed by dropping, 7 µl of the spreading buffer (section 3.1.8) directly on cell drop and mixed gently with pipet tip. Slides were incubated for 2 min at RT before being tilted with a slight angle (around 25°), allowing the drop to flow slowly down the slide. The slide was air dried and the DNA was fixed with 3:1 methanol-acetic acid for 10 min. At this point, slides could be stored at 4°C till staining. After fixation, the DNA on slides was firstly rehydrated by rinsing 2 times in dd.$H_2O$ each for 5 min. Then, slides were washed once with denaturation buffer

(section 3.1.8) and incubated in denaturation buffer for 75 min at RT. Next, slides were rinsed 2 times in 1x PBS, then 2 times (each for 5 min) in blocking solution (3% BSA, 0.1% Tween20 in 1x PBS). To detect the incorporated CldU and IdU nucleotides, slides were placed in a humid chamber and stained with the primary antibodies anti-BrdU antibodies (section 3.1.3) for 1 h at 37°C. Later, the slides were washed with 1x PBS, fixed with 4% paraformaldehyde for 10 min at RT, and washed once with PBS, followed by 3 times 5 min-washing steps with blocking solution. Thereafter, the slides were placed in a moist chamber and stained with the secondary antibodies (section 3.1.3) for 1.5 h at 37°C. Finally, the slides were rinsed 2 times in 1x PBS and once in dd.H2O and mounted with Vectashield mounting medium.

DNA fibers were photographed using fluorescence microscope (Axiovision Observer Z1) and images were then evaluated using Image J software for the lengths and structures of fibers.

DNA fiber assay allows us to determine different replication structures that represent (i) ongoing replication forks (Fiber tracks with both analogues), (ii) stalled forks (CldU only tracks), and (iii) new origin firing events (IdU only tracks). Elongation rate was assessed through measuring the lengths of DNA fibers. The length of each fiber track (CldU+ IdU) was measured, in addition to the length of the CldU track only, using the segmented lines in Image J, then IdU length was calculated by subtraction after exporting to excel sheet. Lengths were converted into µm using the conversion factor 9.8 as previously performed (Jackson and Pombo, 1998). In addition, 2.59 was used as a factor to convert µm into kb (Jackson and Pombo, 1998). Finally, CldU + IdU kb/ min was calculated.

### 3.2.15. EU incorporation

Ethynyl-labeled uridine (EU) can permeate proliferating cells and incorporate into the nascent RNA during RNA synthesis, instead of its original uridine analogue. The incorporated EU can be assessed through click chemistry Cu(I)-catalyzed reaction, which introduces fluorescent azide that can be detected by means of fluorescence detecting instruments (Jao and Salic, 2008).

In a 6-well plate, $3x10^5$ for DU145 cells or $5x10^5$ for LNCaP cells were seeded and incubated overnight under normal growth conditions. Cells were then incubated for 1h with 0.5mM EU before fixation. In case of Enzalutamide treatment, cells were treated with the different concentrations (2µM, 5µM and 20µM) on day 2 and incubated for further 24h under normal growth conditions, before proceeding with EU incorporation

for 1h and fixation. Similarly, for complementation with SPOP-wild type plasmid (section 3.1.1), cells were transfected with the transfection mixture in ratio 3:1 (Fugene-HD: plasmid) at day 2 for further 24h before proceeding with EU incorporation for 1h and fixation. For cell fixation, cells were firstly washed with 1x PBS, trypsinized, collected in 15ml falcon tubes and centrifuged for 5 min at 1200 rpm. Next, cell pellets were suspended in 1 ml PBS, then added dropwisely on 4 ml 80% cold ethanol, while vortexing. At this point, fixed cells could be stored at -20°C, till next steps.

Cells were then permeabilized by suspending in 1ml washing buffer (1x PBS + 0.2% Triton X-100 + 1% BSA). Cell pellet was then collected by centrifugation at RT for 2 min at 1200 rpm. Next, cell pellet was re-suspended in 100 µl freshly prepared reaction mixture from Click-iT®EdU imaging Kit (section 3.1.4) (75.75 µl dd.$H_20$ + 10 µl Reaction buffer + 4 µl Catalyst solution + 0.2 µl Fam azide + 10 µl Buffer additive) and incubated in dark for 30 min. Cells were centrifuged at 1200 rpm for 3 min and cell pellet was washed 2 times with 1 ml washing buffer. Cells were re-suspended in 0.5 ml washing buffer and 2 µl FxCycle™ Far Red Stain (section 3.1.4) and finally, cells were incubated for 30 min at RT, before direct analysis with Fluorescence activated cell sorting (FACS).

For FACS analysis, forward scatter (FSC) and sideward scatter (SSC) were used to give indication on the size and granularity of cells. In addition, FxCycle™ Far Red Stain for cell cycle analysis and 6- FAM azide for EU incorporation were detected using APC and FITC. The analysis was performed using FACS device MACSQuant®X and MACSQuant Analyzer 10 to set the different gates: Gate 1 (P1) shows a plot of SSC-A *vs* FSC-A with only alive cells selected. Gate 2 (P2) represents singlet cells. Eventually, a histogram for FITC-A was plotted from P2, to indicate the percentage of cells with EU intake. These values were processed and data analysis was performed using FlowLogic™Software with the same parameters and gates used during FACS measurements.

### 3.2.16. Plasmid assay for the determination of HR and EJ capacity

The efficiency of HR and NHEJ were determined using GFP-based pGC and pEJ repair substrates, respectively. These reporter substrates rely on reactivation of GFP expression upon repair of I-SceI-endonuclease induced DSBs. On one hand, pGC contains two inactive GFP genes: the first one is disturbed by insertion of I-Sce-I restriction site within the GFP gene sequence and the other gene is only a truncated copy of GFP sequence, which shares the first gene part with 520 bp homology. Upon

induction of I-SceI induced DSB within the first GFP gene copy, cells can use this homology to repair the DSB by HR, resulting in reconstitution of the GFP wild type sequence and GFP expression. On the other hand, pEJ contains two I-SceI sites that are inserted in opposite directions into the 5' untranslated region of the GFP. An artificial start codon ($ATG_{art}$) exists between the two I-SceI sites, preventing GFP translation. Upon inducing the DSBs by I-SceI endonuclease, the $ATG_{art}$ is removed and successful rejoining of the two DSB-ends results in GFP expression (Mansour et al., 2008).

To measure DSB repair efficiency using these reporters, both pGC and pEJ plasmids were firstly linearized by I-SceI endonuclease. For each reaction, 6 µg of either plasmid (pGC or pEJ) were mixed with 3µl of I-SceI (5,000 U/ml), in addition to 12.5 µl dd.H2O, then the reaction was incubated for 2 h at 37° C. Later, the restriction product was electrophoresed on 1% agarose gel for 3 h at 100 V. The band with the linearized form of the plasmid was excised and purified using Promega Kit Wizard®S Gel and PCR Clean-Up System Kit (section 3.1.4), according to the manufacturers' instructions.

For the transfection of the linearized plasmids, $1\times10^5$ cells were seeded in a 12-well plate and incubated for 24h under normal growth conditions. Cells were washed with 1x PBS before addition of 1 ml/well of antibiotic-free medium (DMEM+ 10% FCS). Afterwards, cells were transfected with the linearized form of pGC or pEJ using Fugene®HD (Promega) (section 3.1.4) in ratio 3:1 (Fugene: plasmid), according to manufacturer's protocol. pEGFP-N1 was used to determine the transfection and expression efficiency. After 48h of transfection, cell pellets were collected as previously shown (section 3.2.2). Finally, cell pellets were dissolved in 100 µl 1× PBS and GFP expression (as indication of repair efficiency) was measured using FACS.

### 3.2.17. Extraction of genomic DNA

Genomic DNA was extracted from approximately $2x\ 10^6$ cells using DNeasy Blood & Tissue Kit (section 3.1.4) according to the manufacturer's protocol. Briefly, the cell pellet was suspended in 1x PBS and proteinase K was added, followed by Buffer AL and the mixture was incubated at 56°C for 10 min, until the cells were lysed. Next, ethanol (96 – 100%) was added and mixed with the sample to obtain a homogeneous solution before transferring to a DNeasy Mini spin column placed in a collection tube. The sample was centrifuged and the collection tube was discarded with the flow throw solution. Afterwards, washing steps took place with Buffer AW1, followed by Buffer AW2. After each wash step, cells were centrifuged and the flow throw was discarded.

After wash 2, the DNeasy Mini spin column was placed in a 1.5 ml reaction tube and elution was performed using 20-30 µl nuclease free $H_2O$, instead of Buffer AE. Finally, the concentration and purity of DNA (ng/µl) were examined using NanoDrop spectrophotometer. DNA was stored at -80°C until further processing.

### 3.2.18. Polymerase chain reaction (PCR) and Sequencing

In order to ensure SPOP-KO after CRISPR/Cas9, PCR and sequencing were performed using primers that flank the Cas9-targeted site within SPOP genome (section 3.1.2).

PCR amplification reactions were performed using CfX96touch instrument (Bio-Rad) using Accupower 2X Green Star qPCR MM (section 3.1.4). The reaction included: 5 µL MasterMix 2x, 50 ng/µL DNA, 1 µL 10 pmol from each primer 'Forward: CCA GAG AGT CAA CGG GC AT', and 'Reverse: ACC AAT ACT CAT CAG ATC TGG GAA C' (section 3.1.2), with nuclease free $H_2O$ to a total volume of 10 µL**.** Samples were run in duplicates and a non-template control was used as a control. A standard program for the PCR cycle was: Pre-denaturation (95 °C for 5 min) followed by 39 cycles of denaturation (95 °C, 15 sec), annealing and extension (59 °C, 30 sec).

For the purification of the amplified PCR product, Wizard® SV Gel and PCR Clean-Up System kit (section 3.1.4) was used, according to the manufacturer's protocol. Briefly, the amplified product was mixed with an equal volume of membrane binding solution. The reaction was transferred to SV Minicolumn in a collection tube, incubated for 5 min, centrifuged, then the flow throw in the collection tube was discarded. Next, washing took place 2 times by Membrane Wash Solution with centrifugation after each time. Finally, SV Minicolumn was removed from the collection tube and transferred to 1.5 ml reaction tube and nuclease free water was added to elute the PCR product. Nanodrop spectrophotometer was used for assessing the purity and quantity of the purified DNA. DNA was stored at -20°C. Purified PCR products were sequenced at Eurofins services. Each SPOP-KO clone and parenteral cell were sent in duplicates. Sequencing alignments were performed using online tools: LAST, GeneWise, and Expat. In which, LAST was used to compare the sequences and identify the different bases between wild type and SPOP-KO cells. GeneWise was used to detect the change in amino acids and finally, Expasy translated the DNA sequences into proteins.

### 3.2.19. Assay for Transposase-Accessible Chromatin using sequencing (ATAC-seq)

ATAC-seq (Assay for Transposase-Accessible Chromatin using sequencing) is one of the most widely used techniques for the assessment of chromatin accessibility genome wide. It is based on the construction of next-generation sequencing (NGS) library, in which NGS adaptors are coupled with the transposase (Tn5). Transposase results in tagmentation to accessible fragments; where it fragments the chromatin and simultaneously integrates those adaptors into regions with open chromatin. Ultimately, the generated NGS library is sequenced and analyzed by bioinformatic tools to show the accessibility of chromatin (Fig. 9).

#### 3.2.19.1. Sample preparation and processing

Cells were harvested by trypsin, transferred to 15 ml falcon and centrifuged at 500 xg at 4 °C for 5 min and the supernatant was aspirated, then the pellet was suspended in 5 ml ice-cold PBS. Next, cells were quantified using Cell coulter. In addition, Trypanblue was used for the evaluation of cell viability, according to manufacturers' instructions using Hemocytometer; where cells were acceptable if no more than 5% are dead. Eventually, 1x $10^5$ cells were cryopreserved using 50% FCS+ 40% growth media+ 10% DMSO, placed in pre-chilled Mr.Frosty and stored at -80°C till sending to Active Motif to perform the ATAC-seq assay. At Active Motif, briefly, the cells were thawed in a 37°C water bath, pelleted, washed with cold PBS, and tagmented as previously described (Buenrostro et al., 2013), with some modifications based on (Corces et al., 2017). Briefly, cell pellets were re-suspended in lysis buffer, pelleted, and tagmented using the enzyme and buffer provided in the Nextera Library Prep Kit (Illumina). Tagmented DNA was then purified using the MinElute PCR purification kit (Qiagen), amplified with 10 cycles of PCR, and purified using Agencourt AMPure SPRI beads (Beckman Coulter). Resulting material was quantified using the KAPA Library Quantification Kit for Illumina platforms (KAPA Biosystems), and sequenced with PE42 sequencing on the NovaSeq 6000 sequencer (Illumina).

#### 3.2.19.2. Bioinformtic analysis

Data processing and analysis were conducted by Active motif. Briefly, reads were aligned using the BWA algorithm (mem mode; default settings). Duplicate reads were removed, only reads mapping as matched pairs and only uniquely mapped reads (mapping quality >= 1) were used for further analysis. Alignments were extended in silico at their 3'-ends to a length of 200 bp and assigned to 32-nt bins along the

genome. The resulting histograms (genomic “signal maps”) were stored in bigWig files. Peaks were identified using the MACS 2.1.0 algorithm at a cutoff of *p*-value 1e-7, without control file, and with the –nomodel option. Peaks that were on the ENCODE blacklist of known false ChIP-Seq peaks were removed. Signal maps and peak locations were used as input data to Active Motifs proprietary analysis program, which creates Excel tables containing detailed information on sample comparison, peak metrics, peak locations and gene annotations. For differential analysis, reads were counted in all merged peak regions (using Subread), and the replicates for each condition were compared using DESeq2.

Principal component analysis (PCA) was generated using DESeq2 plotPCA function to identify the differentiation in tags in all merged peaks regions between DU145 and LNCaP cells. The distribution of peaks relative to genomic annotations was presented using pie chart generated by R command: pie function; in which peaks were divided into different categories as: proximal promoter (TSS) (1 kb upstream to 0 kb downstream of a GENCODE transcription start site ‘TSS’), distal promoter (1-3 kb), distal intergenic (within the gene body), distal downstream (within 3 kb downstream of TSS), proximal downstream (within 1 kb downstream of TSS). Randomly located peaks were run against the same genomic database as a control. For the visualization of tags peaks distribution across different regions: transcription start sites (TSS; +/- 5 kb) or gene bodies (with 2 kb flanking regions); seqplots Bioconductor R package using the commands plotAverage and plotHeatmap was used. For heatmaps, k-means algorithm with 5 clusters, indicated by C1-C5 was used.

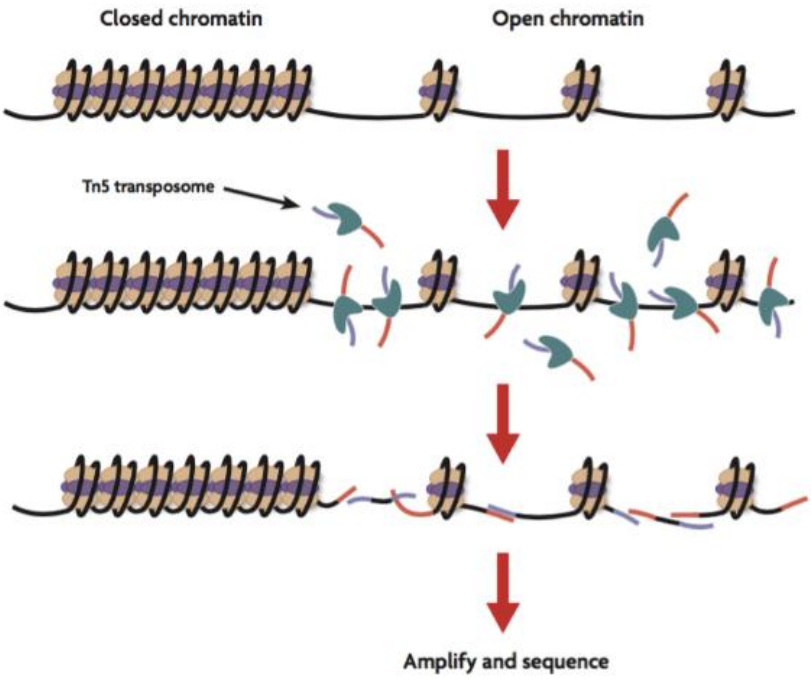

**Figure 9. Schematic illustration of ATAC-seq method.** The tn5 transposase (green) loaded with sequencing adaptors (blue and red), is incorporated only in regions with open chromatin. The loaded transposases then cut and tag the adapters to it, generating DNA fragments library, which then amplified and sequenced. https://www.activemotif.com/blog-atac-seq

### 3.2.20. MS analysis for proteomics and histones PTMs

#### 3.2.20.1. Cell pellet preparation for MS and Histone preparation

Cell pellets for proteomics analysis and histone PTMs were prepared from 7-9 $X10^6$ cells. Briefly, after seeding the cells in T125 flasks and reaching confluency, media was sucked while maintaining flasks on ice. Washing took place 5 times using ice cold 1x PBS. In the final wash step, cells were scraped using scraper and collected in 15 ml Falcon, briefly vortexed and centrifuged at 1500 rpm for 5 min at 4°C. Next, supernatant was removed and pellet was washed with ice cold 1x PBS and centrifuged, washing was repeated for 4-5 times. Before the final centrifugation, cells were transferred to 1.5 ml reaction tube. Eventually, the supernatant was sucked and the 1.5 ml reaction tube was submerged briefly in liquid N2 and stored at -80°C, till sending to Core facility for proteomics analysis at UKE or processing to histone extraction.

For histone extraction, histones were extracted from the prepared pellets using abcam histone extraction kit (section 3.1.4), according to the manufacturer's instructions. For the final step (step 7), a modification was carried out according to (Geis-Asteggiante et al., 2015; Sidoli et al., 2019), in which 50 mM ammonium bicarbonate (pH 8.0) was used instead of Balance-DDT buffer. Histone concentrations were finally measured using BCA (section 3.2.9) and stored at -80 °C, till sending to the Core facility for MS analysis.

#### 3.2.20.2. Protein extraction and tryptic digestion

At the core facility, whole protein lysates were extracted using 1% sodium deoxy cholate (SDC) in 0.1M Triethly ammonium-borate (TEAB) buffer. Purified histones were dissolved in 0.1M TEAB. Proteins were denatured for 5 Minutes at 99°C at a rotation speed of 400 rpm using a ThermoMix®C. DNA that would interfere with the MS analysis was destroyed by probe sonification with 10 pulses at 30% power. For protein concentration estimation, a BCA Protein Assay Kit (Thermo Fisher #23225) was used following the manufacturers' instructions.

A total of 20 µg of protein were used for the tryptic digestion of purified histones and whole cell lysates. Disulfide bonds were reduced using 10mM DTT for 30 minutes at

60°C. Alkylation was achieved with 20 mM iodoacetamide (IAA) for 30 minutes at 37°C in the dark. Tryptic digestion was performed at a trypsin: protein ratio of 1:100 overnight at 37°C and stopped by adding 1% formic acid (FA). The sample was dried in a vacuum concentrator (SpeedVac SC110 Savant, (Thermo Fisher Scientific, Bremen, Germany)) and stored at -80°c until further usage.

### 3.2.20.3. Spectral library generation for whole cell lysates

A spectral library was used to increase the protein identification rate for whole cell lysates trough feature mapping. Therefore, dried tryptic peptides were dissolved in 0.1 M TEAB to a final concentration of 1µg/ µl. Equal amounts of peptides from all samples were combined to generate a peptide standard. A total of 50 µg peptide standard were submitted to offline high pH revesed phase fractionation, using a monolith column (ProSwift$^{TM}$ RP-4H, 1 mm 3 250mm (Thermo Fischer Scientific)) on an Agilent 12000 series HPLC (High Performance Liquid Chromatography) system (Agilent Technologies), coupled to a fraction collector. A linear pH gradient was formed by combining defined amounts of Buffer A (Equilibration buffer): 10 mM ammonium bicarbonate (pH = 8.5) and Buffer B (Elution buffer), linearly increasing from 3-35% buffer B in 35 minutes at a flow rate of 0.2ml/min. 26 fractions, each of 0.2 ml, were collected for 35 minutes and combined to 13 fractions, that were submitted seperately to Liquid Chromatography with tandem mass spectrometry (LC-MS/MS) analysis.

### 3.2.20.4. LC-MS/MS settings

Directly prior to LC-MS analysis, samples were resolved in 0.1% FA to a final concentration of 1 µg/µl. 1 µg tryptic peptides for whole cell lysates and high-pH chromatography fractions and 0.25 µg for purified histones were injected into a UPLC (Ultra Performance Liquid Chromatography), (nano Ultra-Performance Liquid Chromatography, nanoAcquity system, Waters, Milford, MA, USA). Peptides were purified and desalted using an Acclaim PepMap 100 C18 trap (100 µm x 2 cm, 100 Å pore size,5 µm particle size) pre-column and transferred to an Acclaim PepMap 100 C18 analytical column (75 µm x 50 cm, 100 Å pore size, 2 µm particle size) for chromatographic separation. Elution was performed using a linear gradient, going from 2% to 30% Buffer B in 60 minutes (Buffer A: 0.1 % FA in H2O; Buffer B: 0.1 % FA in 90% acetonitrile (ACN)). Eluting peptides were ionized using a nano spray ion source for electrospray ionization with a spray voltage of 1800 V. Peptide ions were transferred to an orbitrap tribrid mass spectrometer (Obritrap Fusion, Thermo Fischer Scientific).

For each MS1 scanning, ions were accumulated for a maximum of 50 milliseconds or until a charge density of $2x10^5$ ions (AGC Target) was reached. Fourier-transformation based mass analysis was performed covering a mass range of 400-1200 m/z with a resolution of 120000 at m/z = 200. Isolated precursor ions were fragmented in a linear ion trap using Collision-induced dissociation (CID) at a normalized collision energy of 35. For each MS2 scan, ions were collected for a maximum ion trap fill time of 50 milliseconds or until a maximum AGC target of $5x10^4$ ions was reached and analyzed over a mass range of 400-1200 m/z. Dynamic exclusion of each precursor ions was performed for 30 seconds after first analysis.

### 3.2.20.5. Database searching

#### General settings

For whole cell lysates, as well as purified histones, LC-MS/MS data were searched with the Sequest algorithm integrated in the Proteome Discoverer software (v 2.41.15, Thermo Fisher Scientific) against a reviewed human Swissprot database, obtained in April 2020, containing 20365 entries. Carbamidomethylation was set as fixed modification for cysteine residues and the oxidation of methionine, and pyro-glutamate formation at glutamine residues at the peptide N-terminus, as well as acetylation of the protein N-terminus were allowed as variable modifications. A maximum number of 2 missing tryptic cleavages was set. Peptides between 6 and 144 amino acids were considered. A strict cutoff (false discovery rate (FDR) <0.01) was set for peptide and protein identification. Peptide and protein quantification was carried out, using the Minora algorithm, implemented in Proteome Discoverer, using a retention time matching window of 5 minutes.

#### Spectral library-based protein quantification for whole cell lysates

To increase the protein identification rate for whole cell lysates and enable the identification of low abundant proteins, a combined database searching was performed for individual samples and high pH reversed phase fractions. Each fraction and sample were handled individually. Protein abundancies for high pH fractions were removed from result files prior to statistical data analysis.

#### Identification of methylated and acetylated peptides for purified histones

To identify methylated and acetylated histones, the tri, di and mono methylation of lysins, arginine and protein N-termini, as well as, the acetylation of lysine and arginine

residues, as well as, N-termini were further considered as variable modifications. To prevent high false positive rates in protein identification due to high mass shift tolerances, database searching was performed separately for histone methylation and acetylation.

### 3.2.20.6. Statistical data analysis

For statistical analysis of whole cell lysates, protein/peptide abundance values were log2 transformed and median normalized across columns to compensate for injection amount differences. To visualize the differences and similarities between samples, hierarchical clustering (HC) and PCA were carried out, using the Perseus software (Max Plank Institute for Biochemistry, Version 1.5.8.5). For hierarchical clustering, Pearson correlation was used as a distance metric. Average linkage was applied. Pairwise complete correlation was used, to enable the consideration of missing values. As principal component (PC) cannot deal with missing data points, missing values were imputed from the normal distribution, prior to PC calculation. The first two PCs, accounting for the highest explained variance were visualized in PRISM (GraphPad, Version 8). PCA was initially performed using the whole protein matrix, including the proteins with low abundance, to test the quality of data produced. Then, another PCA was performed after applying ANOVA testing with significance of $p$-value <0.05; in order to reduce the scattering observed in the first PCA analysis that can be a result of biological and experimental differences. ANOVA testing selects for differentially abundant proteins/peptides across multiple groups. Proteins were considered significant if at least 2 testing groups had $p$-value <0.05. Students t-testing was applied (Protein level: $p$-value <0.05, Fold change difference >1.5, Peptide level: $p$-value <0.05, Fold change difference >1.5) to identify statistically significant candidates between two groups. Only proteins that were found at least 2 times in all phenotypes were included in t-testing and in the further functional analysis. T-test results were visualized as volcano plots, using an in house script in the R software environment (Version 4.2.0).

### 3.2.20.7. Functional annotation of data sets

Ontology based Gene Set Enrichment Analysis was performed by using the GSEA software (version 4.1.0, Broad Institute, San Diego, CA, USA) (Subramanian et al., 2005). GSEA analysis was based on proteins found at least 2 times in all phenotypes without t-testing. 1000 permutations were used and permutation was performed based

on gene sets. A weighted enrichment statistic was applied, using the signal-to-noise ratio as a metric for ranking genes. No additional normalization was applied within GSEA. Gene sets smaller than 15 and larger than 500 genes were excluded from analysis. For visualization of GSEA results, the EnrichmentMap (version 3.3) application within the Cytoscape environment (version 3.8.2) was used (Shannon et al., 2003). Gene sets were considered if they were identified at FDR <0.25 and *p*-value <0.1. For gene-set-similarity filtering, data set edges were set automatically. A combined Jaccard and Overlap metric was used, applying a cutoff of 0.375. For gene set clustering, AutoAnnotate (version 1.3) was used, using the Markov cluster algorithm (MCL). The gene-set-similarity coefficient was utilized for edge weighting.

### 3.2.21. Methylome

#### DNA methylation profiling

DNA was isolated from all cell lines using the Qiagen kit (section 3.1.4). Isolated DNA was then sent to the Epigenomics core facility at UKE, where all sample processing and analysis were performed. Briefly, illumina HumanMethylationEPIC BeadChip (EPIC) 450K arrays (Koelsche et al., 2021) were used for analysis of genome-wide DNA methylation patterns, using only sites covered by at least 3 reads. The percentage of methylation per site (beta value) was calculated for each sample (Maire et al., 2021).

#### Analysis

Loading, filtering, and normalization of the samples' IDAT files were done using the package limma (version 3.40.0) in R (version 3.6.0). For each sample, the mean global methylation was calculated by taking the average of all beta values.

### 3.2.22. Statistical analysis

If not mentioned, all statistical analyses were performed and graphs were produced using GraphPad Prism V9.4.1

# 4. Results

## 4.1. Generation of SPOP DU145 and LNCaP Knockout clones

In order to better understand the role of SPOP, we employed CRISPR-CAS9-based genome editing technology to establish stably SPOP-knockout (SPOP-KO) clones from (i) the castration resistant DU145 and (ii) the hormone sensitive LNCaP PCa cell lines. As illustrated in materials and methods section, All-in-one vector system, which has two main advantages: (i) Cells only need to be transfected once, as both CRISPR associated protein 9 (Cas9) and guide RNA (gRNA) are present in the same vector and expressed simultaneously and (ii) both gRNA/Cas9 expression are driven in an ideal 1:1 ratio. Briefly, cells were transfected using the all-in-one vector, which carries both SPOP-specific gRNA and Cas9 nuclease complementary DNA (cDNA). Thereafter, selected stably integrated clones were tested with western blotting for SPOP expression. A total of 38 and 40 subclones were investigated from DU145 and LNCaP, respectively. For DU145, clones #2, #16, & #18 (Fig. 10A) and clones #30, #11 & #18 in LNCaP (Fig. 10B) were chosen for further analysis. Indeed, the loss of SPOP expression was recapitulated in the aforementioned subclones using 3 different independent cell extracts. The selected clones were then analyzed for insertions-deletions mutations by PCR amplification followed by sequencing of the junction around the binding site of the gRNA within exon 5. Sequencing confirmed the insertion of an extra thymine (T) base that resulted in a frameshift mutation and generation of an early STOP codon, and properly a truncated, non-functional protein (Fig. 10C). Collectively, immunoblotting and sequencing data confirmed the generation of SPOP-KO sublines from DU145 and LNCaP cells.

Next, we checked whether there is difference in growth rate between the generated SPOP-KO subclones and their parenteral counterparts. Growth rates and doubling times (DTs) were measured using growth curves by counting cell number at different time points post seeding. Only modest decrease in the proliferation rate with a slight decrease in the DTs was observed in DU145 (WT: 1.8 d; #2: 2.0 d; #16: 2.1 d and #18: 2.0 d, Fig. 10D) and LNCaP (WT: 2.9 d; #11: 2.9 d and #18: 3.2 d, Fig. 10E) SPOP-KO clones.

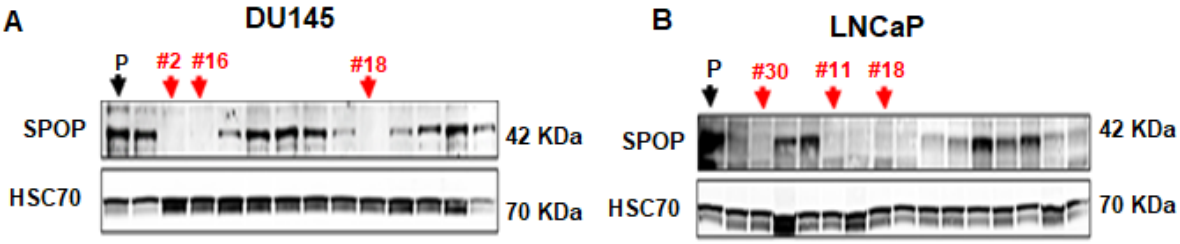


C

| Cells | Sequence | Exon | Protein translation | Mutation type |
|---|---|---|---|---|
| DU P | CCCTCTTCT-GCGAGGT | Exon 5 | TLFCEVSPCILLRLAVPRSDEYW | Wild type |
| DU 2 | CCCTCTTCTTGCGAGGT | Exon 5 | TLFLRGESLYSAETSSSQIStopStopVLV | Ins & Frameshift |
| DU16 | CCCTCTTCTTGCGAGGT | Exon 5 | TLFLRGESLYSAETSSSQIStopStopVLV | Ins & Frameshift |
| DU18 | CCCTCTTCTTGCGAGGT | Exon 5 | TLFLRGESLYSAETSSSQIStopStopVLV | Ins & Frameshift |
| LN P | CCCTCTTCT-GCGAGGT | Exon 5 | TLFCEVSPCILLRLAVPRSDEYW | Wild type |
| LN30 | CCCTCTTCTTGCGAGGT | Exon 5 | TLFLRGESLYSAETSSSQIStopStopVLV | Ins & Frameshift |
| LN18 | CCCTCTTCTTGCGAGGT | Exon 5 | TLFLRGESLYSAETSSSQIStopStopVLV | Ins & Frameshift |
| LN11 | CCCTCTTCTTGCGAGGT | Exon 5 | TLFLRGESLYSAETSSSQIStopStopVLV | Ins & Frameshift |

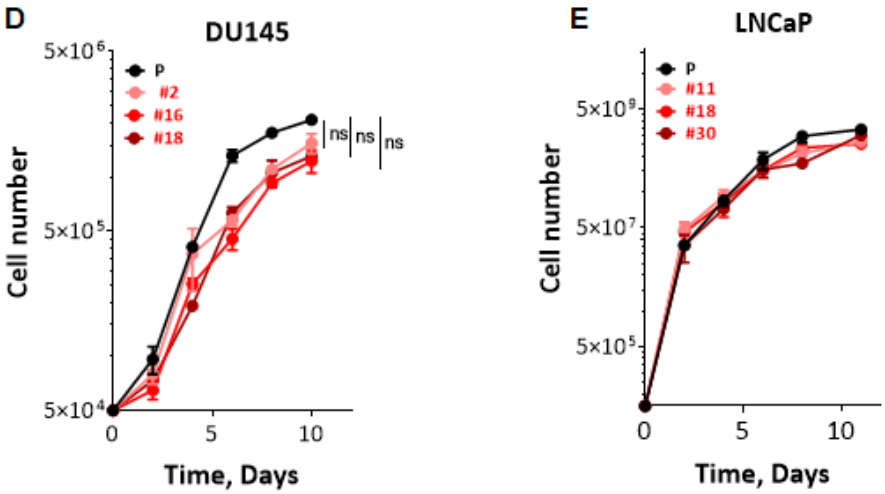


**Figure 10. Establishment of CRISPR-CAS9 mediated SPOP deficient clones.** (A&B) Western blot showing SPOP expression in some CRISPR-CAS9-treated clones from both DU145 (A) and LNCaP (B) cells. Indicated are SPOP expression in proficient wild type (P) cells (black) and SPOP-knockout (KO) subclones (red). HSC70 was used as a loading control. Molecular weights are indicated in kilo Dalton (KD). (C) Sequencing shows the indel mutation introduced after CRISPR-CAS9 transfection in the indicated subclones. Sequence change is shown in red in the DNA and protein sequences. (D) Growth curves show no significant difference in the proliferation rate between SPOP-KO DU145 (D) or LNCaP (E) cells and their parenteral counterparts. Shown are the means ±SEM of 3 different experiments. *p*-values were calculated using Mann-Whitney U test. ns: no significance.

## 4.2. Analysis of DSB repair capacity in SPOP-KO clones

### 4.2.1. γH2AX and 53BP1 foci

We sought to investigate the role of SPOP in DSB repair. Therefore, we monitored the number of γH2AX and 53BP1 foci - a well-established DSB markers - in SPOP-KO and parenteral cells at 1h and 24h post-2Gy irradiation. Results revealed a higher number of γH2AX at both 1h (WT *vs* #2: *p* =0.0002, WT *vs* #16: *p* =0.01) and 24h (*p* =0.004) post-2Gy in SPOP-KO DU145 clones compared to their parenteral wild type cells (Fig. 11A&B). Likewise, 53BP1 foci showed increase at both time points (1h: WT *vs* #2: *p* =0.01, WT *vs* #16: *p* =0.07, 24h: *p* =0.004) (Fig. 11A&C). Similar increase in the number of DSB foci at the indicated time points post-IR was demonstrated in LNCaP SPOP-KO cells compared to their wild type counterparts (Fig. 11D-F). Interestingly, both SPOP-KO DU145 and LNCaP cells showed significantly higher number of γH2AX under un-irradiated conditions (Fig. 11A&B & Fig. 11D&E), indicating accumulation of spontaneous (treatment-independent) DSBs in SPOP-KO cells.

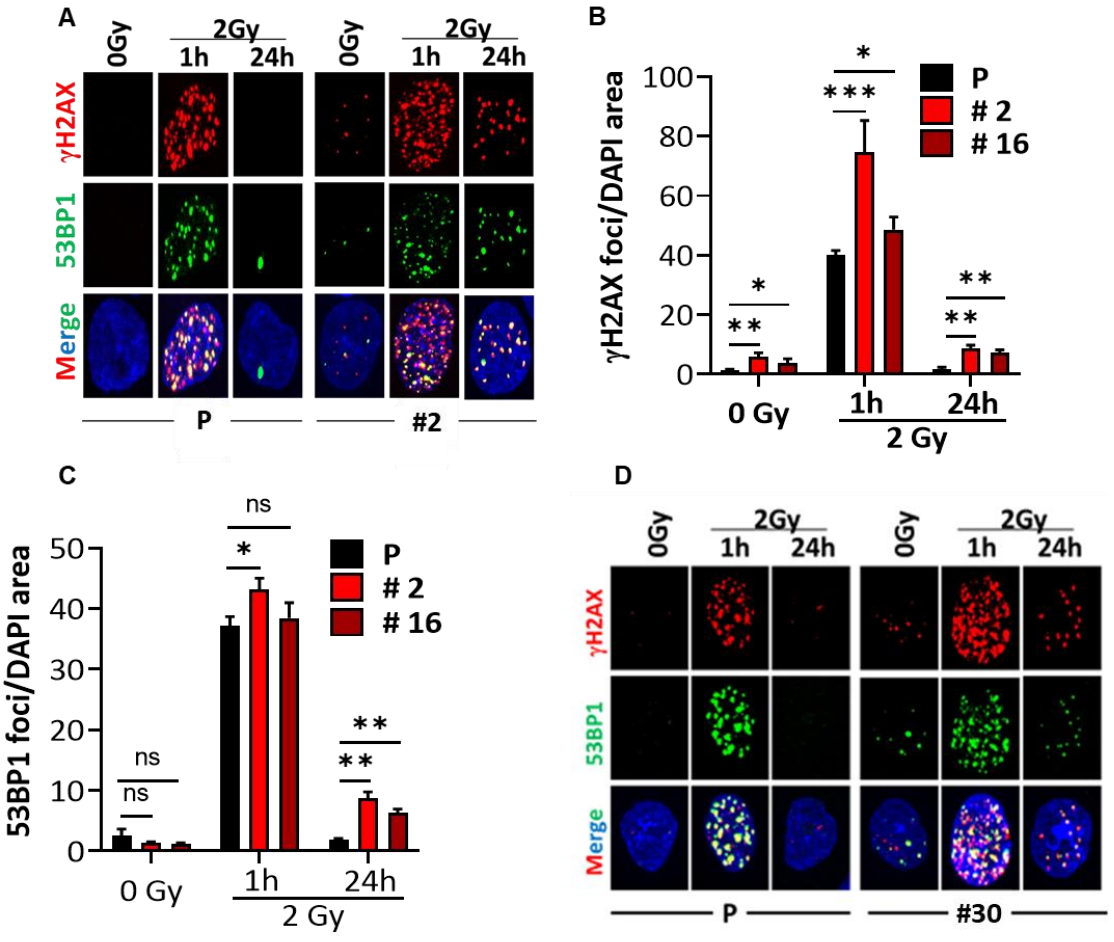

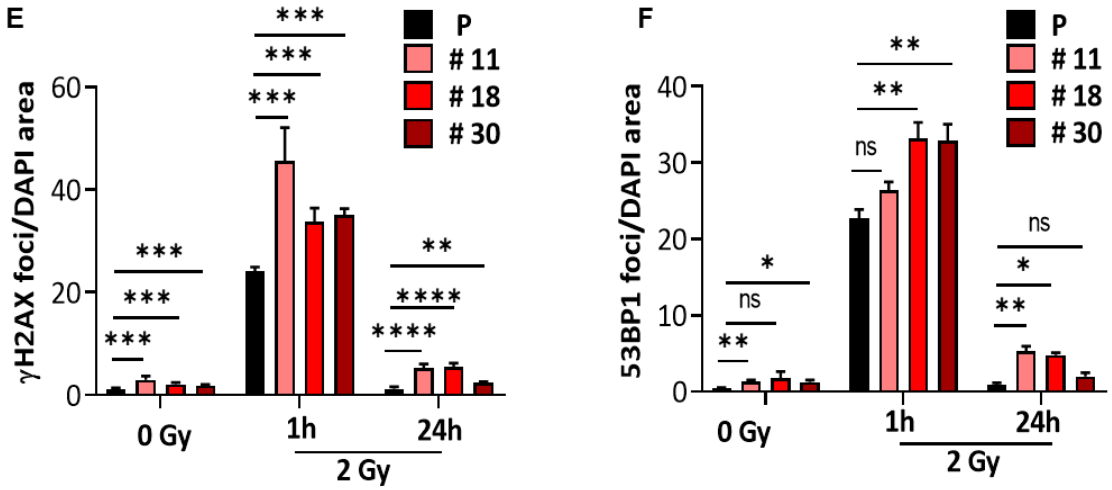


**Figure 11. Analysis of DSB repair using immunofluorescence detection of γH2AX/53BP1 foci post ionizing radiation.** (A) Representative micrographs for γH2AX/ 53BP1 foci in SPOP-KO clone #2 and their proficient (P) DU145 cells before irradiation or at 1h and 24h post-2Gy. (B&C) Quantification of the experiment presented in A. (D) Representative micrographs for γH2AX/ 53BP1 foci in SPOP-KO clone #30 and their proficient (P) LNCaP cells before irradiation or at 1h and 24h post-2Gy. (E&F) Quantification of the experiment presented in D. At least 100 cells were analyzed. DAPI (blue) was used to counterstain the nucleus. Shown are the means ±SEM from three independent experiments. *p*-values were calculated using Mann-Whitney U test: * $p$ <0.05, ** $p$ <0.01, *** $p$ <0.001, **** $p$ <0.0001 and ns: not significance.

### 4.2.2. RAD51 foci

Previously, it was reported that SPOP deficiency impairs HR repair (Boysen et al., 2015; Hjorth-Jensen et al., 2018). To investigate this issue, the recruitment of RAD51 - HR key player - at DSB sites was investigated in SPOP-KO clones. To that end, cells were irradiated with 2Gy and γH2AX and RAD51 foci were quantified at 3h and 24h post-IR. In contrary to the published data (Boysen et al., 2015; Hjorth-Jensen et al., 2018), the number of RAD51 foci was significantly higher at 3h post-2Gy in DU145 SPOP-KO cells compared to their wild type counterparts ($p$=0.01) (Fig. 12A&B), indicating even a better RAD51 loading efficiency. This number decreased significantly after 24h, indicating DSB repair via HR. However, in KO cells, the number of residual RAD51 foci (i.e. at 24h) was still profoundly higher in SPOP-KO compared to SPOP wild type DU145 cells (WT *vs* #2: $p$ =0.02, WT *vs* #16: $p$ =0.03). Consistently, LNCaP cells (Fig. 12C&D) also showed more RAD51 foci loading and more residual in SPOP-KO clones in comparison to parenteral cells. Thus, this data indicate that HR is not impaired in SPOP-KO cells.

Notably, number of spontaneous γH2AX foci was significantly higher in DU145 SPOP-KO cells compared to their wild type cells (WT *vs* #2: $p$ =0.002, WT *vs* #16: $p$ =0.03),

Fig. 12A&E). Likewise, these data were recapitulated in LNCaP cells, showing accumulation of spontaneous γH2AX foci in SPOP-KO cells compared to SPOP wild type ones (Fig. 12C&F). Consistently, no difference in RAD51 protein expression was observed between deficient clones of SPOP and their proficient counterparts (Fig. 12G).

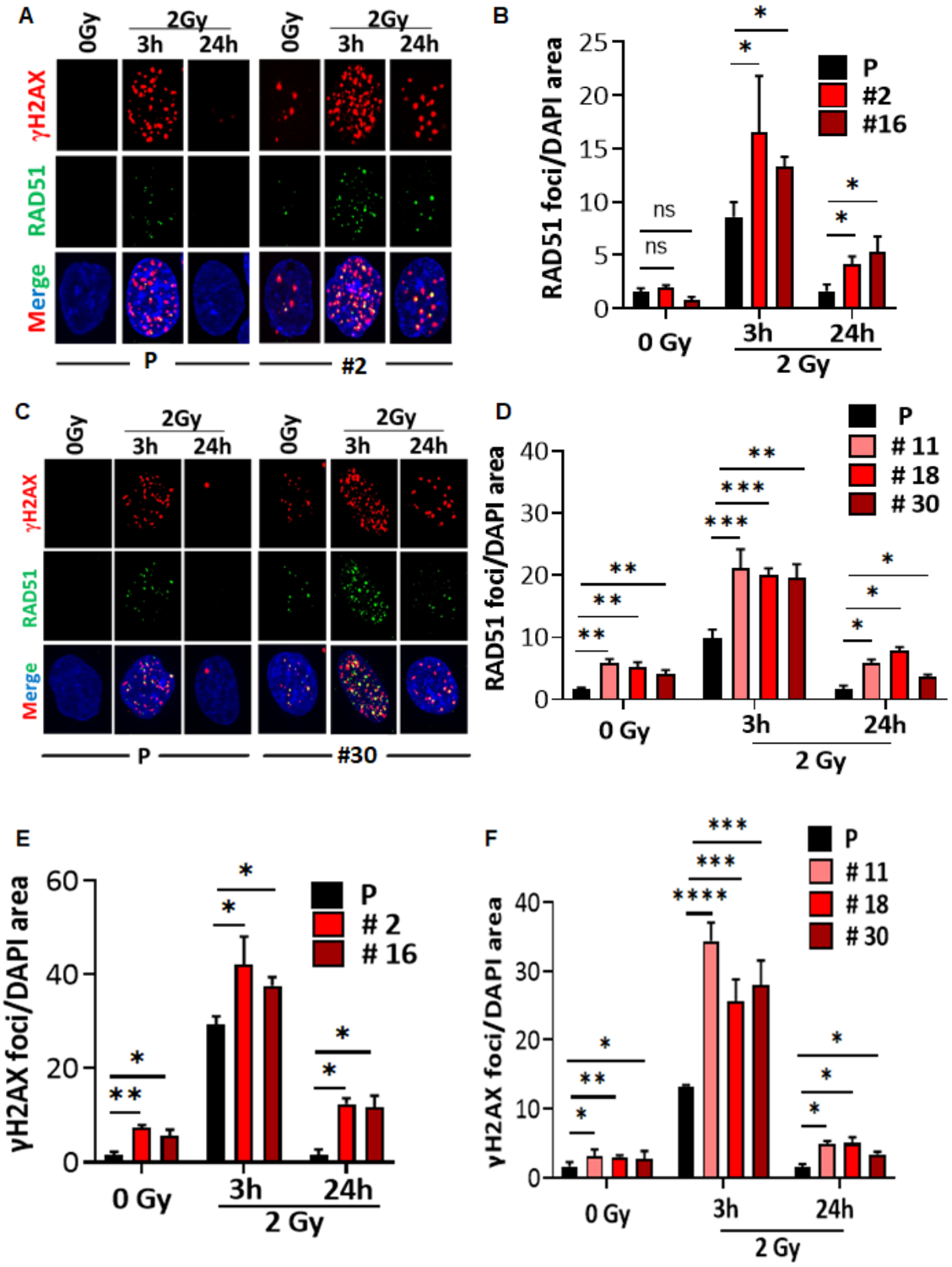

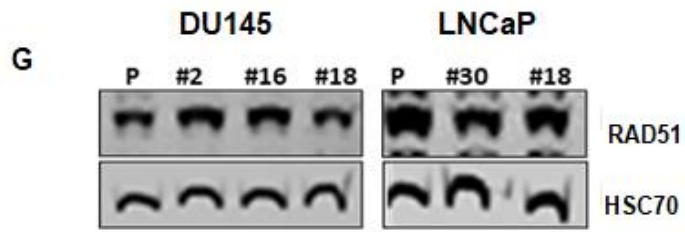


**Figure 12. Analysis of HR repair in SPOP-KO cells.** (A) Representative micrographs for γH2AX/ RAD51 foci in SPOP-KO clone #2 and their proficient (P) DU145 cells before irradiation or at 3h and 24h post-2Gy. (B&E) Quantification of the experiment presented in A. (C) Representative micrographs for γH2AX/ RAD51 foci in SPOP-KO clone #30 and their proficient (P) LNCaP cells before irradiation or at 3h and 24h post-2Gy. (D&F) Quantification of the experiment presented in C. At least 100 cells were analyzed. DAPI (blue) was used to counterstain the nucleus. Shown are the means ±SEM from three independent experiments. *p*-values were calculated using Mann-Whitney U test: * $p$ <0.05, ** $p$ <0.01, *** $p$ <0.001, **** $p$ <0.0001 and ns: not significance. (G) Western blot showing RAD51 protein expression in parenteral SPOP proficient (P) and the indicated SPOP-KO subclones of DU145 (left-panel) or LNCaP (right panel) cells. HSC70 was used as a loading control.

### 4.3. Direct measurement of NHEJ and HR using plasmid assay

The above results reflect in contrast to previously published data that cells can proficiently conduct HR in the absence of SPOP. In order to further address this, we directly measured HR efficiency using the previously reported HR-substrate pGC (Fig. 13A) (Mansour et al., 2008). Briefly, I-SceI-linearized pGC was transfected into SPOP-KO and wild type cells, and the percentage of GFP-positive ($GFP^+$) cells – as indication of HR efficiency - was monitored using FACs. As illustrated in Fig. 13B, no changes in the percentage of $GFP^+$ cells were demonstrated in SPOP-KO *vs* wild type DU145 (0.32 ±0.08 *vs* 0.28 ±0.03, $p$ =0.15) or LNCaP (2.12 ±0.2 *vs* 2.1 ±0.18, $p$ =0.5). In addition, to directly measure NHEJ efficiency, cells were transfected with the I-Sce-I-linearized form of the EJ-substrate pEJ (Fig. 13C) plasmid and the percentage of GFP+ cells was measured by FACS as an indication for EJ efficiency. Compared to SPOP wild type cells, we demonstrated a slight increase in the EJ % in SPOP-KO DU145 (1.2-fold, $p$ =0.2667) and LNCaP (1.2-fold, $p$ =0.2667) cells (Fig. 13D). Collectively, these data revealed that SPOP is not directly involved in either NHEJ or HR, however, SPOP-KO cells accumulate DSBs.

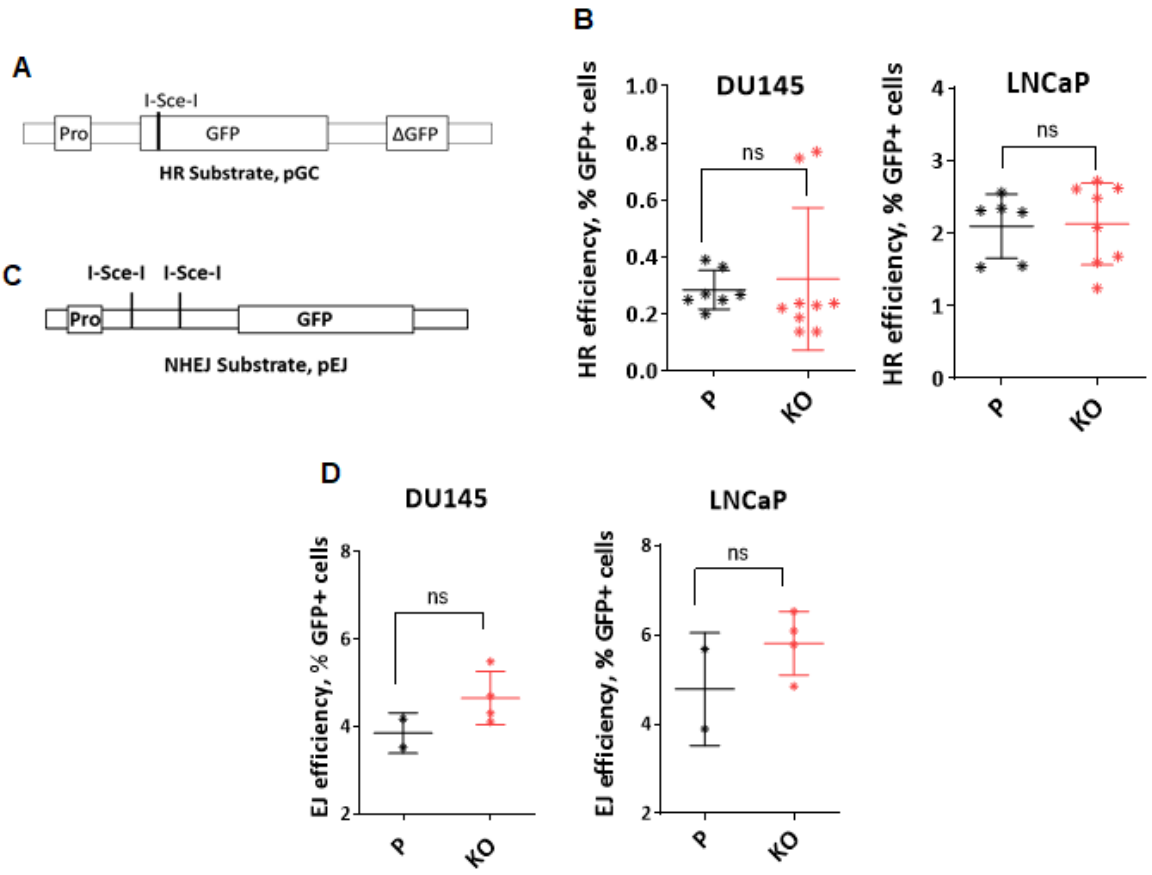


**Figure 13. Direct measurement of HR and NHEJ efficiencies using repair substrates.** (A) Schematic illustration for the HR substrate pGC. (B) SPOP proficient or KO subclones (pooled) of either DU145 (#2, #16, #18) (left panel) or LNCaP (#30, #11, #18) (right panel) were transfected with 1 µg I-SceI-linearized pGC and the percentage of GFP-positive cells, as an indication for HR efficiency was monitored using flow cytometer 48h-post transfection. (C) Schematic demonstration for the NHEJ repair substrate pEJ. (D) SPOP proficient or the pooled KO subclones of either DU145 (left panel) or LNCaP (right panel) were transfected with 1 µg I-SceI-linearized pEJ and the percentage of GFP-positive cells, as an indication for NHEJ efficiency, was monitored using flow cytometer 48h-post transfection. Repair efficiency was normalized to the transcription efficiency measured by pEGFP-N1. Means ±SEM are shown for two independent experiments. *p*-values were calculated using Mann-Whitney U test. ns: not significant.

## 4.4. DNA damage checkpoints in SPOP-KO cells

Since SPOP-KO cells accumulate higher number of spontaneous, as well as, induced DSBs, we then determined whether SPOP loss impairs the DDR. Therefore, ATM-ChK2 and ATR-ChK1 signaling were analyzed upon induction of DSBs by IR in SPOP-KO *vs* wild type cells. Cells were irradiated with 10 Gy and phosphorylation of ATM, ChK2, ATR and ChK1 were monitored after 1.5 post-IR. As shown in Fig. 14A, ATM, ChK2 and ATR were efficiently phosphorylated upon irradiation in both SPOP-KO and wild type DU145 cells. On the other hand, ChK1 phosphorylation was

reduced in SPOP-KO compared to wild type DU145 cells. These data were recapitulated in LNCaP cells, showing efficient ATM-ChK2 checkpoint but impaired ATR-ChK1 in SPOP-KO cells (Fig. 14B). Indeed, no difference in the expression of the un-phosphorylated forms of the aforementioned DDR proteins was observed in any of cell strains.

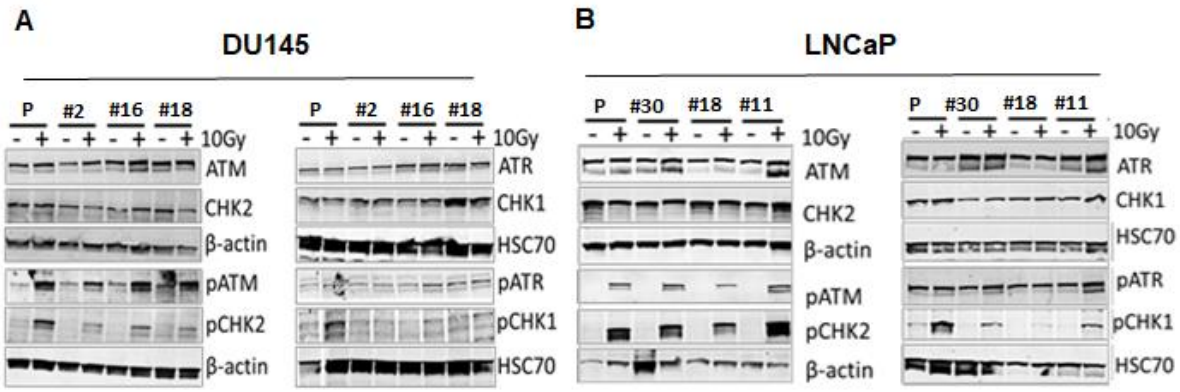


**Figure 14. Western blot demonstrating the expression of DDR factors in SPOP-KO clones.** The indicated SPOP-KO subclones and their proficient counterparts from DU145 (A) or LNCaP (B) cells were irradiated or not with 10Gy and total proteins were isolated after 1.5h. Expression and phosphorylation of the indicated DDR factors were investigated using western blot. β-actin and HSC70 were used as loading controls.

### 4.5. SPOP deficiency causes replication stress

Next, we sought to elucidate the source of the increased number of spontaneous DSBs accumulated in SPOP-KO cells. Given, the inefficient Chk1 phosphorylation and hence, intra-S/S-G2 checkpoints, it is thus reasonable to speculate that these spontaneous DSBs can be accumulated as a consequence of replication stress (RS). Several studies including our own reported a γH2AX pattern that suggested widespread uniform phosphorylation of H2AX (pan-nuclear γH2AX signal) in the nucleus upon genotoxic treatment. Such pan-nuclear γH2AX signals were observed under several RS conditions, and were proportional to the intensity of the induced RS (Köcher et al., 2012; Meyer et al., 2013; Parsels et al., 2018; Moeglin et al., 2019; Meyer et al., 2020). As shown in Fig. 15A, we observed elevated percentage of spontaneous pan-nuclear γH2AX signal in SPOP-KO clones (8.1 ±1.8 %, 7.8 ±1.9 %, and 8.5 ±2.8 % in clones #2, #16, and #18, respectively) compared to parenteral wild type cells (2.7 ±0.93 %). In addition, higher number of pan-nuclear staining was demonstrated in SPOP-KO cells 24h post-2Gy (Fig. 15A). This data implies a role for SPOP in preventing RS accumulation. To address this issue in more details, we

visualized replication tracts and measured fork speed and structures using the DNA fiber method (see materials and methods). Briefly, cells were pulse-labeled with thymidine analogues CldU and IdU and lysed, then DNA fibers were spread and immuno-detected with specific antibodies against CldU and IdU, sequentially for 20 min each (Fig. 15B). First, we assessed the fork speed of fiber tracts in the three SPOP-KO DU145 clones and their wild type cells (Fig. 15C). The distribution of replication tract lengths was consistent with a slowing in fork progression in SPOP-KO DU145 cells (Fig. 15C). Similarly, LNCaP SPOP-KO clones showed slower replication rate than their wild type cells (Fig. 15D). Next, we counted fibers that retained only the first label (CldU) indicating fork stalling (Fig. 15E). We found all SPOP-KO DU145 (Fig. 15E) and LNCaP (Fig. 15F) cells having more fork stalling compared to their wild type cells (1.4-fold, 1.7-fold and 1.3-fold, for SPOP-KO DU145 clones #2, #16 and #18, respectively and 2.6-fold, 2.7-fold, and 3.4-fold for SPOP-KO LNCaP clones #11, #18 and #30, respectively). In addition to fork slowing and stalling, we counted fibers with only second label (IdU) as indication for the new origin firing rate (Fig. 15G). SPOP-KO DU145 (Fig. 15G) and LNCaP (Fig. 15H) clones exhibited higher number of newly fired origins (1.3-fold, 1.5-fold and 1.2-fold, for SPOP-KO DU145 clones #2, #16 and #18, respectively and 1.8-fold, 1.8-fold, and 2-fold for SPOP-KO LNCaP clones #11, #18 and #30, respectively). Altogether, these data suggest that the increased replication stresses might explain the increased accumulation of spontaneous DSBs in SPOP-KO clones.

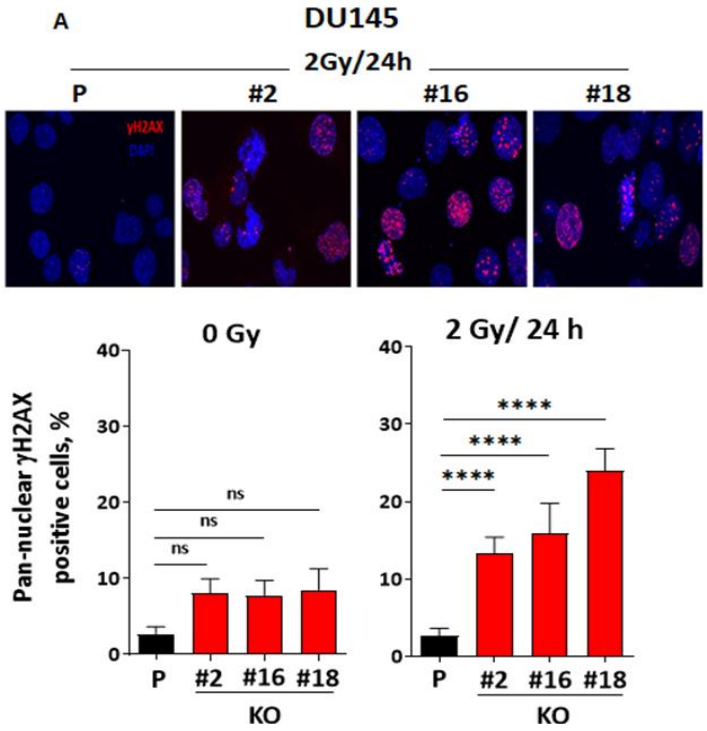

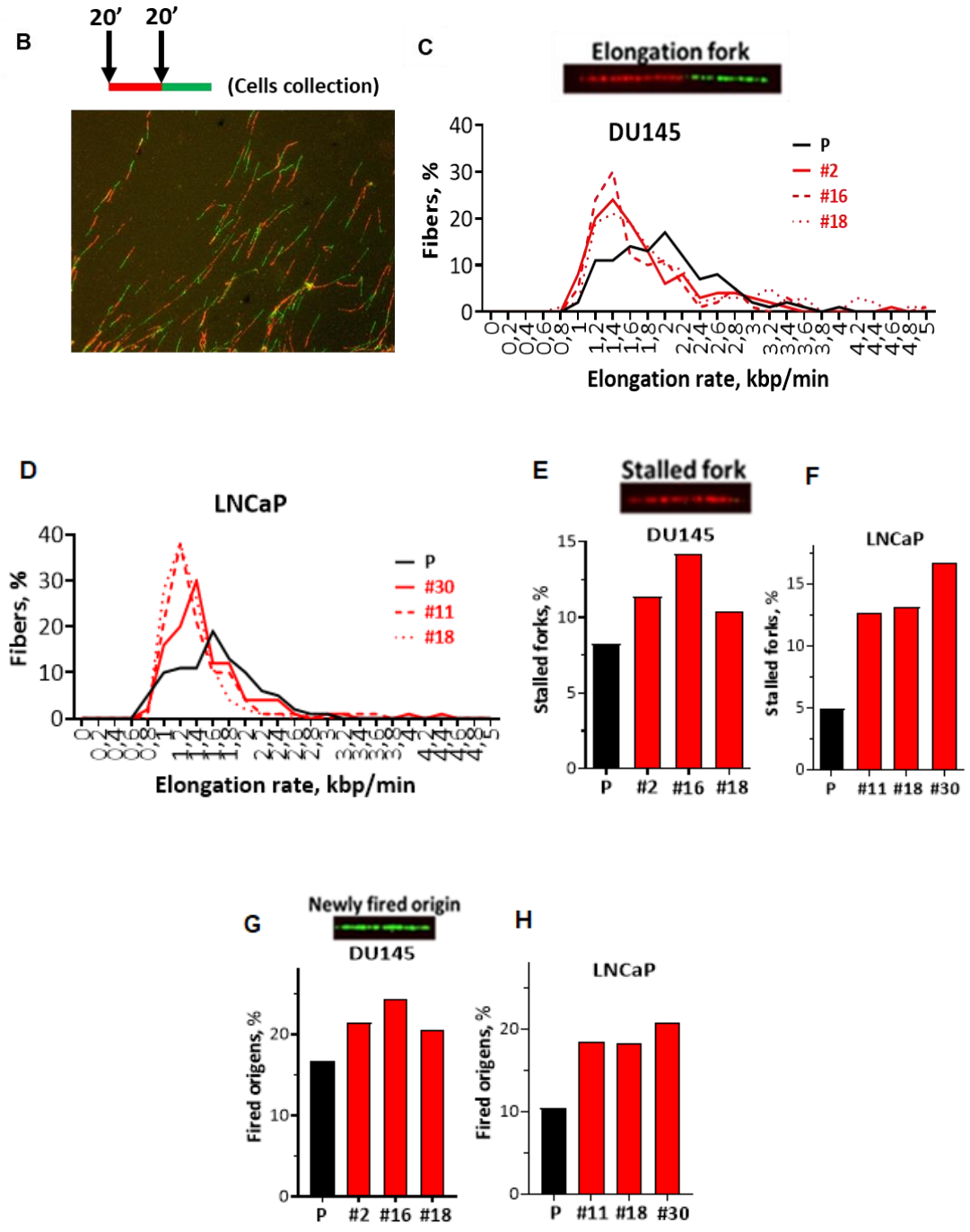


**Figure 15. Analysis of DNA replication using DNA fiber assay.** (A) Upper panel: Representative micrographs of pan nuclear staining of γH2AX generated at 24h post-2Gy in DU145 parenteral cells and SPOP-KO clones (#2, #16, #18). Lower panel: Quantification of pan nuclear γH2AX in DU145 SPOP proficient (P) and KO sublines (#2, #16, #18), generated spontaneously at 0 Gy and 24h post-2 Gy. DAPI (blue) was used to counterstain the nucleus. Shown are means ±SEM of at least 3 independent experiments. *p*-values were calculated using Mann-Whitney U test: **** $p$ <0.0001 and ns: not significance. (B) Upper panel: Scheme of the DNA fiber assay. Cells were pulse-labelled with CldU (red tract) for 20 min, followed by incubation with IdU (green tract) for 20 min before being collected by scraping. Lower panel: Representative microscopic images of DNA fibers after spreading. Both thymidine analogues (CldU and IdU) were visualized via

immunofluorescence. Scale bar: 10 µm. (C) Upper panel: A micrograph represents a replication fork elongation fiber tract. Lower panel: Quantification of elongation rates of parenteral SPOP proficient (P) and the indicated SPOP-KO DU145 cells (#2, #16, #18). (D) Quantification of elongation rates in the indicated LNCaP SPOP-KO clones (#30, #11, #18) *vs* their proficient counterparts (P). (E&F) Upper panel: A micrograph representing a stalled replication fork. Lower panel: Quantification of the percentage of stalled replication forks in SPOP-KO and proficient DU145 (E) and LNCaP (F) cells. (G&H) Upper panel: A microscopic image represents a newly fired origin. Lower panel: Quantification of the percentage of newly fired origins in SPOP-KO *vs* proficient DU145 (G) and LNCaP (H) cells. All experiments were performed in triplicates and at least 250 fibers were measured for each experiment.

### 4.6. SPOP accumulates cell cycle independent DSBs

Next, we reasoned that if only replication stresses attribute for the accumulation of DSBs in SPOP-KO cells, then spontaneous DSBs should be generated exclusively in S-phase during replication. To analyze this issue, unsynchronized SPOP-KO clone #16, as well as, wild type DU145 cells were pulse-labeled for 15 min with EdU to mark S-phase cells. Then γH2AX foci were co-stained along with S/G2 phase marker CenpF to subsequently monitor DSBs generated in either S-phase (EdU+/CenpF+) or G2-phase (EdU-/CenpF+) cells as previously described (Beucher et al., 2009; Köcher et al., 2012; Bakr et al., 2015). As shown in Fig. 16, in SPOP wild type cells, number of γH2AX foci was expectedly higher in G2-phase (2.67 ±0.66 foci/cell) than S- and G1 phases (1.38 ±0.19 and 0.78 ±0.2 foci/cell, respectively). Interestingly, SPOP-KO cells exhibited significantly higher number of spontaneous γH2AX foci in all cell cycle phases (G1: 4.62 ±0.9 foci/ cell, $p$ <0.0001; S: 6.49 ±0.78 foci/cell, $p$ <0.0001 and G2: 8.2±1.2 foci/ cell, $p$ =0.004). This implies the presence of other mechanism that causes replication stress and DSBs in SPOP-KO cells.

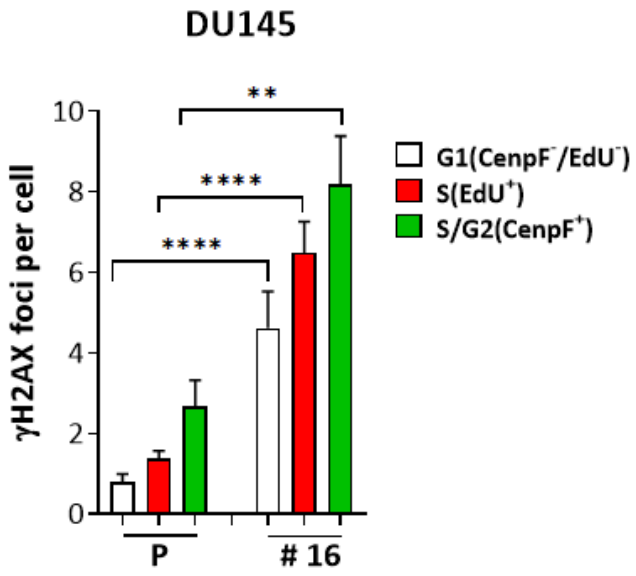


**Figure 16. Cell cycle dependent analysis of DSBs.** Asynchronized cells were firstly pulsed-labelled with EdU for 15 min to mark S-phase cells and nuclei were stained for γH2AX and additionally co-stained with CenpF to mark S/G2 phase cells. Shown are the quantifications of the number of γH2AX foci in G1 (CenpF-/EdU-), S (cenpF-/EdU+) and S/G2 (CenpF+/EdU+) cells in DU145 parenteral and SPOP-KO clone #16. At least 100 cells were analysed. Results are presented as means ±SEM of three independent experiments. $p$-values were calculated using Mann-Whitney U test: ** $p$ <0.01, **** $p$ <0.0001.

### 4.7. SPOP loss accumulates R-loops in all cell cycle phases

Previously, it was shown that R-loops can accumulate in all cell cycle phases, which in turn might result in the generation of DSBs and replication stress (Allison and Wang, 2019). Aiming at deciphering the mechanisms by which SPOP-KO cells accumulate spontaneous DSBs in cell cycle-independent manner, we assessed the accumulation of R-loops in SPOP-KO cells. To that end, IF staining using the S9.6 antibody was performed to recognize R-loops in the nuclei of SPOP-KO DU145 clone #16 and LNCaP clone #30, as well as in their wild type cells. Results revealed a significant upregulation of R-loops in the nuclei of both SPOP-KO DU145 (9.7-fold, $p$ <0.0001) (Fig. 17A&B) and LNCaP (3.6-fold, $p$ <0.0001) clones (Fig. 17C&D).

In order to elucidate whether the accumulation of R-loops in SPOP-KO cells is cell cycle-specific, we pulse labelled the cells with EdU for 15 min to mark S-phase cells and R-loops were stained using S9.6 antibody. Regardless of SPOP status, we observed a clear increase in the signal of R-loops in S-phase compared to non-S-phase cells, supporting the previously published data that these structures are stabilized specifically in S phase (Struve et al., 2022). Importantly, R-loops signals were significantly higher in S-phase (3.9-fold, $p$ =0.001) and non-S-phase (6.9-fold, $p$ <0.0001) of SPOP-KO DU145 cells (Fig. 17E&F). Similar results were demonstrated in SPOP-KO LNCaP cells with a 2.9-fold and 4.3-fold increases in S-phase ($p$ <0.0001) and non-S-phase ($p$ <0.0001) cells, respectively (Fig. 17G&H). Altogether, these results indicate that SPOP exerts a direct role in preventing R-loop accumulation, which explains the generation of DSBs in all cell cycle phases in the absence of SPOP.

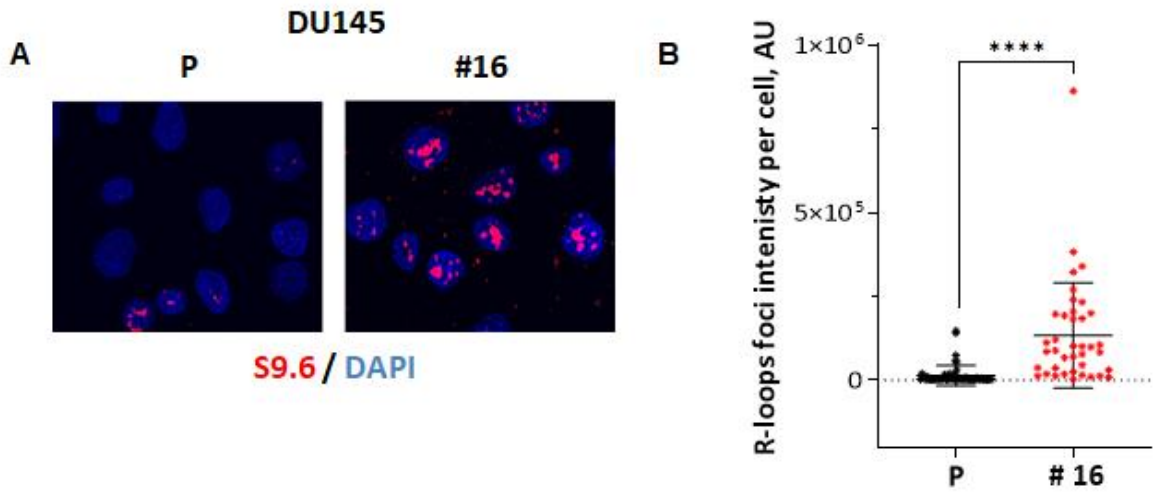

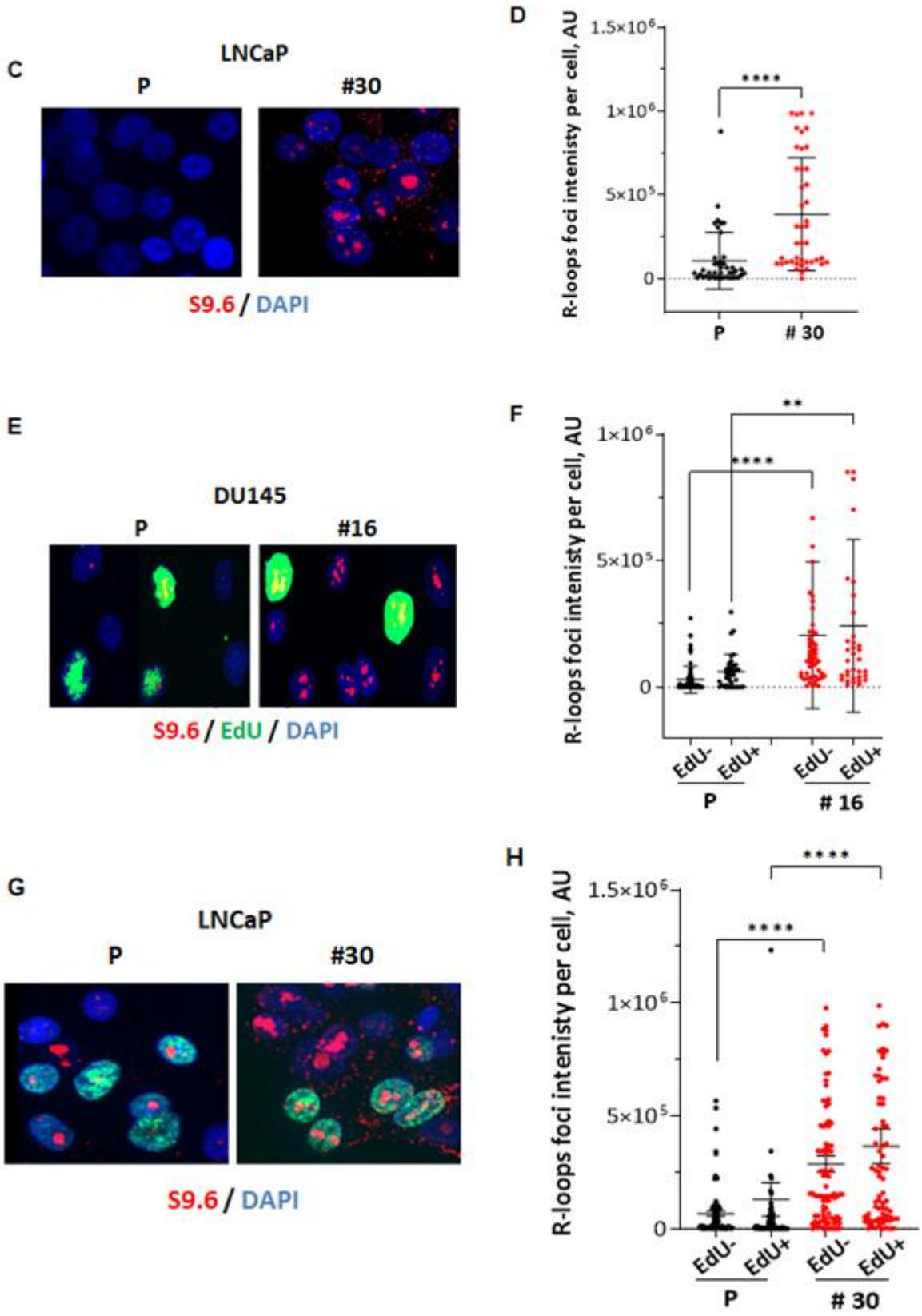


**Figure 17. Analysis of R-loops in cell cycle dependent manner.** (A) Representative microscopic immunofluorescence images of R-loops detected by S9.6 antibody in SPOP-KO DU145 clone #16 and its proficient counterpart (P). (B) Quantification of R-loops foci intensity per cell. (C) Representative images for R-loops in LNCaP SPOP proficient (P)

and KO (#30) cells. (D) Quantification of the experiment presented in C. (E) Representative micrographs of R-loops in S-phase (EdU+, green) *vs* G1/G2 (EdU-) cells (SPOP proficient *vs.* KO DU145 cells). (F) Quantification of the experiment presented in E. (G) Representative microscopic images of R-loops in S-phase (EdU+, green) *vs* G1/G2 (EdU-) cells (SPOP proficient *vs*. KO LNCaP cells). (H) Quantification of the experiment presented in G. About 100 cells were analyzed. DAPI was used to visualize the nuclei. Shown are means ±SEM, of three independent experiments. *p*-values were calculated using Mann-Whitney U test: ** $p$ <0.01, and **** $p$ <0.0001.

## 4.8. R-loops resolution

To ensure that R-loops are properly regulated and avoid genomic instability, several proteins act in concert to prevent aberrant R-loop formation and remove excessive R-loops. Since R-loops were accumulated in the absence of SPOP, it is hence reasonable to test whether R-loops resolution is efficiently working in SPOP-KO cells. To address this, we next investigated in SPOP-KO *vs* wild type cells the expression of different proteins involved in R-loops resolution such as XPG, XPF, and RNase H1. As depicted in Fig. 18A (DU145) and Fig. 18B (LNCaP), SPOP deficient and proficient cells revealed similar expression of XPG, XPF and RNase H1, indicating proficient R-loops resolution in SPOP deficient cells. Together, these data suggest that the accumulation of R-loops in all cell cycle phases is not attributed to inefficient R-loops resolution.

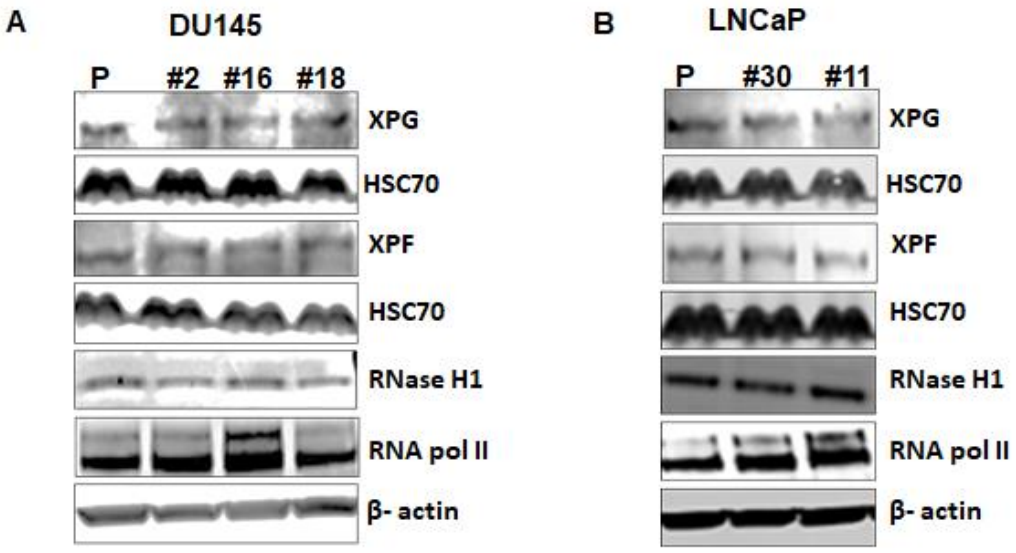


**Figure 18. Analysis of the expression of R-loops resolving proteins**. Representative western blots showing the expression of RNA pol II and different proteins involved in R-loops resolution (XPG, XPF and RNase H1) in SPOP-KO subclones of (A) DU145 (#2, #16, #18) and LNCaP (#30, #11) *vs* their parenteral wild type counterparts (P). HSC70 or β-actin were used as loading controls.

## 4.9. SPOP deficiency causes transcription deregulation

Since R-loops are formed during transcription, thus, transcription deregulation can lead to the accumulation of R-loops, as previous studies showed. Therefore, we next investigated transcription activity by quantifying EU incorporation into nascent RNA as previously described (Jao and Salic, 2008). Briefly, cells were incubated with EU for 1h and its incorporation during RNA synthesis as an indication for transcription activity was measured using FACS. In comparison with SPOP wild type cells that showed an EU incorporation percent of 42.1 ±3 %, a significantly reduced percentage of cells with incorporated EU was demonstrated in SPOP-KO clones #2 (9-fold, $p$ =0.004) and #16 (13.8-fold, $p$ =0.004), indicating an impaired transcription activity in SPOP-KO DU145 cells (Fig. 19A&B). In order to confirm that this effect is attributed to SPOP loss, clone #16 was transfected by SPOP-expressing vector for 24h before EU labelling. As illustrated in Fig. 19B, re-expression of SPOP in this clone partially rescued the transcription activity as evidenced by a significantly increased number of cells with EU uptake in complemented SPOP-KO clone (#16+SPOP:19.41 ±3.51 % *vs* #16: 3.04 ±1.5, 6.4-fold, $p$ =0.006). Investigating the EU uptake kinetics showed a time-dependent increase in EU incorporation in DU145 SPOP-KO cells, however, the overall EU uptake remained lower in these cells compared to their SPOP wild type counterparts (Fig. 19A). Intriguingly, the opposite has been observed in SPOP-KO LNCaP cells, where profound increase in cells with EU incorporation was reported in SPOP-KO clones #11 (1.3-fold, ns.), #18 (2.3-fold, $p$ =0.02) and #30 (1.8-fold, $p$ =0.02). Re-introducing SPOP gene in clone #30 decreased cells with EU incorporation to reach comparable level observed in wild type LNCaP cells (Fig. 19C).

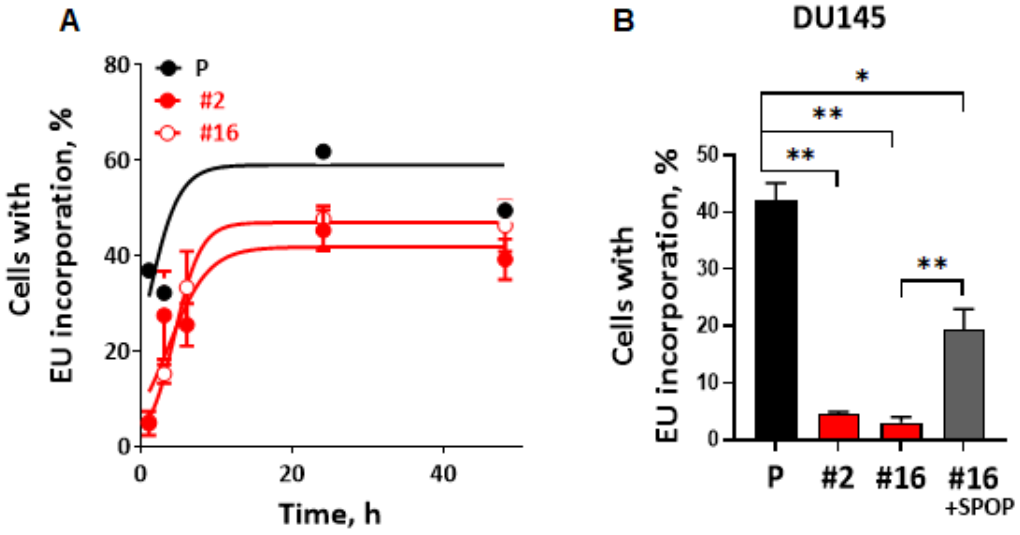

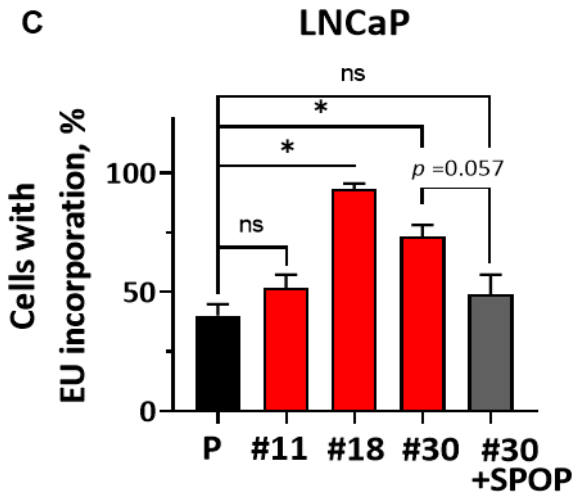


**Figure 19. Analysis of transcription in DU145 and LNCaP SPOP-KO sublines.** (A) Transcription activity was measured by the investigation of EU incorporation kinetics after the indicated time points using flow cytometry. Cells were incubated with 0.5 mM EU for the indicated time points and the percentage of cells incorporated EU was analyzed using FACS. (B&C) Quantification of EU incorporation after 1h incubation with EU in SPOP proficient (P) *vs* the indicated SPOP-KO clones of DU145 (B) and LNCaP (C) cells. SPOP-KO clones #16 (DU145) and #30 (LNCaP) were transfected with SPOP wild type expression vector for complementation and EU incorporation was measured 48h-post transfection. *p*-values were calculated using Mann-Whitney U test from at least 3 independent experiments. Significance: * $p < 0.05$, ** $p < 0.01$ and ns: not significant.

## 4.10. Investigating the mechanism behind opposing transcription deregulations in DU145 and LNCaP SPOP-KO cells

The above data reveal a contrarily deregulation of transcription in DU145 and LNCaP cells. These two cell lines differ in their status of the transcription factor AR. While LNCaP cells are AR-positive, DU145 cells lack AR expression due to strong DNA methylation of the AR gene (Jarrard et al., 1998; Fialova et al., 2016). AR is known to act as a transcription factor that positively regulates transcription (Tan et al., 2015). Since AR is described to be a substrate of SPOP (Geng et al., 2014), we therefore hypothesized that AR signaling might be stimulated in LNCaP SPOP-KO cells, which in turn enhanced the transcription activity. As anticipated, the loss of SPOP in LNCaP cells increased AR protein expression, as well as, the expression of its downstream target PSA (Fig. 20A). In order to verify the role of AR in enhanced transcription activity in LNCaP SPOP deficient cells, we inhibited AR signaling by treating LNCaP SPOP-KO clone #30 and its wild type cells with different concentrations of Enzalutamide (2 µM, 5 µM or 20 µM) for 24h then analyzed EU incorporation as above. Our results demonstrated an Enzalutamide dose-dependent inhibition of the transcription activity. Interestingly, after 2µM Enzalutamide treatment, transcription decreased in SPOP-KO

cells, reaching the transcription levels in LNCaP SPOP wild type cells (Fig. 20B). In addition, treating SPOP-KO LNCaP cells with 20 μM Enzalutamide further lowered transcription to almost half the normal levels of their parenteral cells (Fig. 20B).

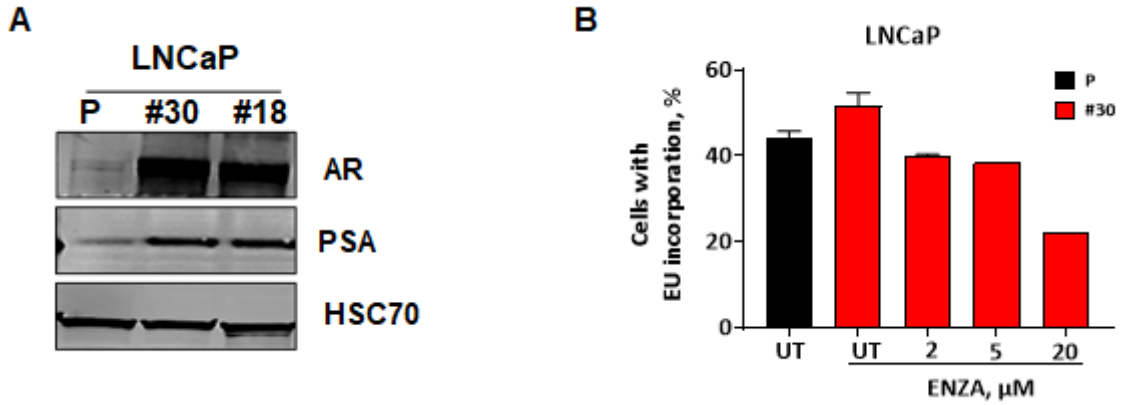


**Figure 20. Role of AR signaling in SPOP-mediated transcription regulation.** (A) Western blot showing protein expression of AR and its downstream target PSA in LNCaP SPOP-KO clones (#30, #18). HSC70 was used as a loading control. (B) Cells were treated with DMSO (UT) or the indicated concentrations of the AR blocker enzalutamide (ENZA) for 24h and the percentage of EU-positive cells was thereafter quantified, as an indication for transcription activity. Shown are means ±SD of triplicates for each condition.

We next reasoned that, if AR upregulation in SPOP-KO LNCaP cells stimulates transcription that leads to the accumulation of R-loops and DSBs; then reducing transcription levels in SPOP-KO cells to comparable levels of SPOP wild type cells, would prevent R-loops and DSBs accumulation. In line with this assumption, treatment of SPOP-KO LNCaP cells with 2 μM Enzalutamide decreased significantly the number of R-loops ($p$ =0.001) (Fig. 21A&B), as well as, spontaneous γH2AX ($p$ <0.001) and 53BP1 ($p$ <0.001) foci (Fig. 21C&D). Although the higher concentration of Enzalutamide (20 μM) decreased the transcription beyond the untreated SPOP proficient cells; it remarkably only slightly decreased the number of R-loops (Fig. 21A&B, $p$ =0.06) and failed to prevent the accumulation of spontaneous DSBs (Fig. 21C&D). This indicates that R-loops and eventually DSBs are accumulated when transcription hemostasis is deviated from normal.

Altogether, our data reveal that both DU145 and LNCaP SPOP-KO sublines accumulate R-loops and DSBs through different mechanisms. While, transcription is inhibited in the AR-negative DU145 SPOP-KO cells, it is upregulated in the AR-positive LNCaP SPOP-KO cells due to upregulation of AR signaling. In both cases, this leads to the accumulation of R-loops that eventually increase the number of spontaneous DSBs in all cell cycle phases.

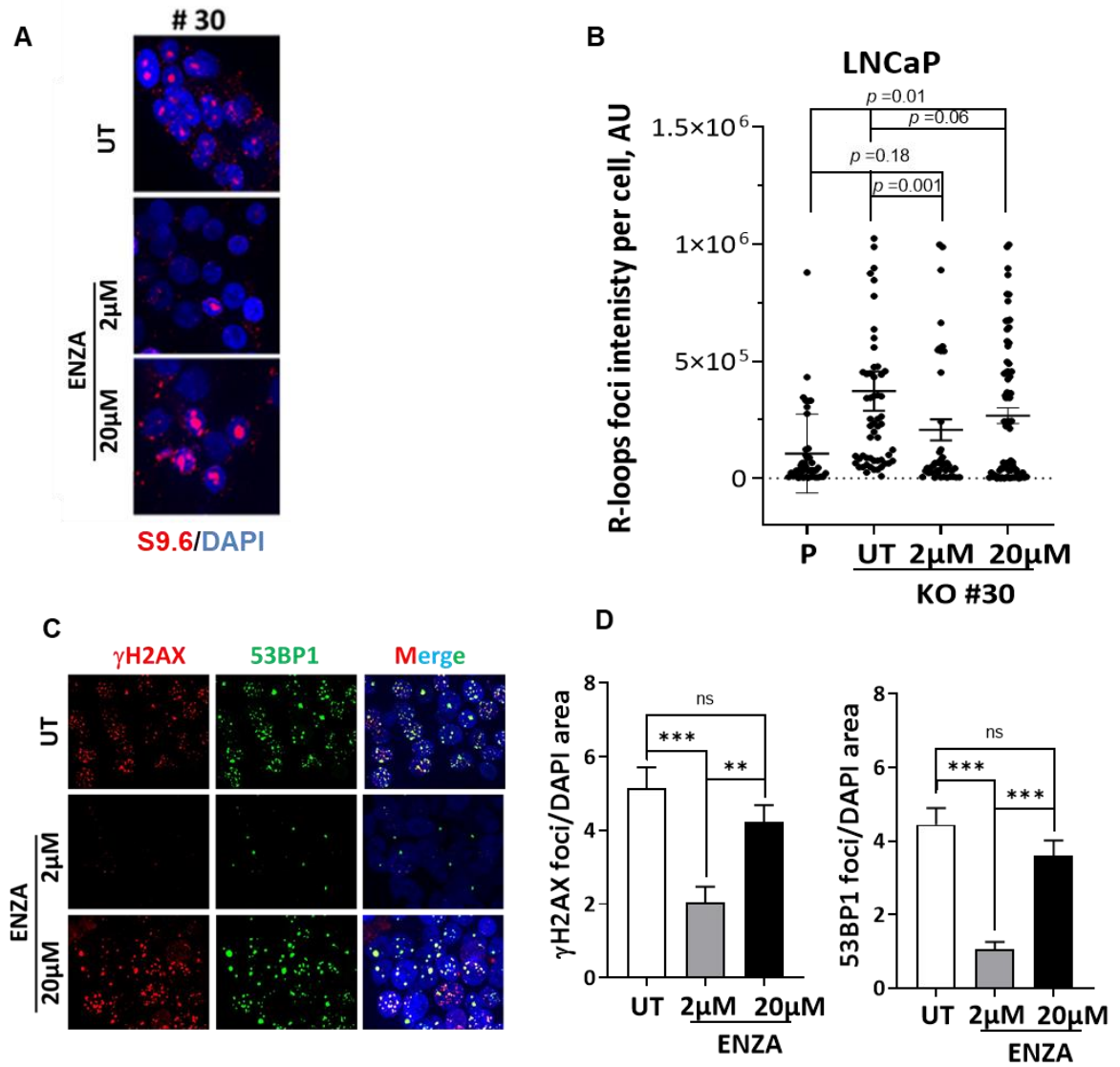


**Figure 21. Effect of AR blocking on R-loops and DSBs.** LNCaP SPOP-KO cells (clone #30) were treated with either DMSO (UT) or the indicated concentrations of the AR blocker enzalutamide (ENZA) for 24h before analysis of R-loops and DSBs. (A) Representative micrographs of R-loops visualized using S9.6 antibody in LNCaP SPOP-KO clone #30 after the indicated treatments. (B) Quantification of the experiment presented in A, (P) indicates parenteral UT cells. (C) Representative microscopic images of γH2AX/ 53BP1 foci 24h post the indicated treatments. (D) Quantification of the experiment presented in C. DAPI was used to counterstain the nuclei. At least 100 cells were used in the quantification. Data are shown as means ±SEM, of 2 independent experiments. Mann-Whitney U test was used to calculate *p*-values. Significance: ** $p$ <0.01, *** $p$<0.001 and ns: not significant.

## 4.11. SPOP loss impairs transcription elongation

The above data indicate a role for SPOP in regulating transcription. Next, we sought to mechanistically get insights on this role. Previous data reported that RNA pol II is present in the SPOP wild type interactome, which might explain a regulatory role of

SPOP in RNA pol II function (Hjorth-Jensen et al., 2018). To address this possibility, RNA pol II expression and loading onto chromatin were analyzed in SPOP-KO *vs* wild type cells using subcellular fractionation and western blotting. Results revealed increased RNA pol II protein levels in SPOP-KO DU145 (1.3-fold) and LNCaP (1.2-fold) clones compared to their wild type counterparts (Fig. 22A&B). While, RNA pol II chromatin enrichment was similar in SPOP-KO *vs* wild type DU145 cells, it was enhanced in SPOP-KO LNCaP cells compared to their wild type counterparts (Fig. 22C). This is in fact consistent with the reported enhanced EU incorporation in LNCaP SPOP-KO cells (Fig. 19C).

Transcription is a complicated process at each step from initiation through elongation to termination, which is characterized by differential phosphorylation of the C-terminal of RNA pol II at the ser5 and ser2 positions (Hsin and Manley, 2012). Initiation step starts by loading of RNA pol II at the beginning of genes followed by phosphorylation of its C-terminal domain at ser5. Subcellular fractionation followed by immunoblotting revealed increased phosphorylation at this position in the chromatin fractions of SPOP-KO DU145 cells (Fig. 22C), indicating an enhanced initiation step. Interestingly, chromatin-bound fraction of ser2 phosphorylated RNA pol II was profoundly reduced in SPOP-KO DU145 clones compared to their wild type cells (Fig. 22C), indicating an impaired elongation step in SPOP deficient DU145 cells. This explains the impaired transcription activity observed in these cells (Fig. 19A&B). On the other hand, both ser5 and ser2 phosphorylation of RNA pol II were increased in LNCaP SPOP-KO cells (Fig. 22C), which together with the increased RNA pol II chromatin fraction explain the enhanced transcription activity in these cells (Fig. 19C), caused by stimulation of AR signaling. Collectively, this data suggests that transcription initiation is even more promoted in DU145 SPOP-KO cells than in parenteral cells, however, the elongation is impaired.

### 4.12. Analysis of CDK9 mediated transcription signaling

CDK9, the kinase component of p-TEFb, is essential for transcription elongation by RNA pol II. pCDK9 phosphorylates RNA pol II at ser2 to stimulate productive elongation through releasing promoter-proximal paused RNA pol II into gene bodies (Peterlin and Price, 2006; Bacon and D'Orso, 2019). To be active, CDK9 needs not only to be associated with a Cyclin T, but also to be phosphorylated on the threonine

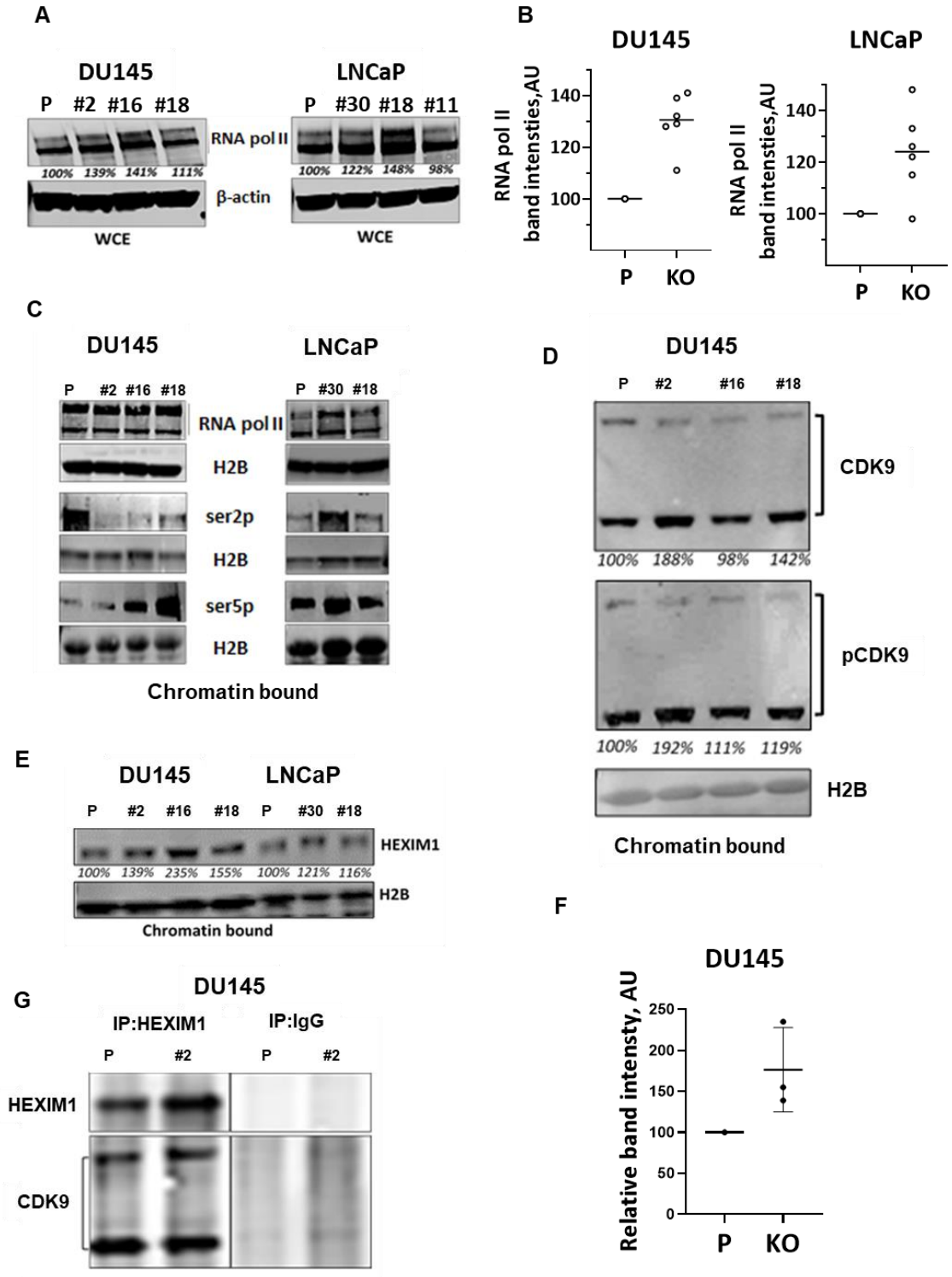


**Figure 22. Investigation of the expression and chromatin fractions of transcription factors in SPOP deficient cells.** (A) Western blot showing the expression of RNA pol II in the whole cell lysate (WCL) in the indicated SPOP-KO DU145 (Left panel) and LNCaP (left panel) *vs* their wild type counterparts (P). Relative band intensities are indicated. β-actin was used as a loading control. (B) Quantification of the experiment presented in A. (C) Western blot demonstrating the chromatin bound fractions of RNA pol II, and its phosphorylated forms at serine 5 (ser5p) and serine 2 (ser2p) residues in the indicated SPOP deficient DU145 (left panel) and LNCaP (right panel) clones and their proficient cells. H2B was used as a loading control. (D&E) Western blots indicating the chromatin bound fractions of (D) CDK9, pCDK9, and (E) HEXIM1, in DU145 SPOP-KO clones (#2, #16, #18)

*vs*. their parenteral cells (P). HEXIM1 chromatin fractions in LNCaP SPOP-KO clones (#30, #18) and parenteral (P) cells were shown in E. H2B was used as a loading control. (F) Quantification of relative band intensities of HEXIM1 in DU145 SPOP proficient and pooled KO cells. (G) Co-immunoprecipitation (CoIP) analysis showing the interaction between HEXIM1 and CDK9. CoIP was performed using an anti-CDK9 antibody and membrane was screened by western blot for HEXIM1 and CDK9 in DU145 SPOP-KO (#2) clone and its parenteral counterpart (P). IgG was used as a control for CoIP efficiency and specifity.

186 residue (Malumbres, 2014). Since RNA poll II is less phosphorylated at ser2, we sought to test whether this can be attributed to impaired CDK9-dependent transcriptional signaling. To that end, we analyzed the chromatin enrichment levels of CDK9 and pCDK9 in SPOP-KO *vs* wild type DU145 cells. Subcellular fractionation combined with immunoblotting analysis revealed even higher loading of both CDK9 (except for clone #16) and pCDK9 (in all clones) in the chromatin bound fractions of SPOP-KO cells compared to their wild type cells (Fig. 22D).

Previous studies demonstrated that in order to phosphorylate RNA pol II on ser2, pCDK9 should be freed from its inactive complex with HEXIM1 (Bacon and D'Orso, 2019). In order to test the possibility that pCDK9 might be present more in its inactive complex with HEXIM1 in SPOP-KO cells, which then would explain the impaired pol II ser2 phosphorylation in these cells. We observed enhanced chromatin-bound levels of HEXIM1 in SPOP-KO DU145 (Fig. 22E&F) and LNCaP (Fig. 22E) cells compared to their SPOP wild type counterparts. In addition, using CoIP, we found that more CDK9 was present in a complex with HEXIM1 in DU145 SPOP-KO clone #2 compared to SPOP wild type cells (Fig. 22G). This modest increase in the level of CDK9-HEXIM1 complex in SPOP deficient cells might partially explain the impaired transcription elongation in these cells.

## 4.13. Proteomic analysis reveals deregulation in genes related to chromatin structure and histones post-translational modifications

To gain insight into the mechanism underlying transcription deregulation in SPOP deficient cells, we sought to compare the proteomic profile of SPOP-KO *vs* wild type cells. To that end, total protein was isolated from both SPOP-KO DU145 and LNCaP sublines, as well as, their wild type counterparts and subjected to MS analysis.

### Proteomics of DU145 SPOP-KO *vs* wild type cells

SPOP-KO (#2, #16, #18) clones, each was tested in duplicates in MS, and triplicates for parenteral cells. A total of 4821 proteins were detected and used in PCA analysis (data not shown). In order to decrease the biological and experimental variabilities

observed, another PCA analysis was performed after applying ANOVA testing (*p*-value <0.05). This resulted in a clear separation of the SPOP-KO sublines #2, #16 and in #18 (to a less extent) from their wild type cells, with principal component (PC2) of 45.8% and (PC1) of 24.8% (Fig. 23A).

Next, we sought to identify significantly differential proteins between SPOP deficient and proficient cells. Out of the included 4821 proteins, 2623 proteins were detected in all replicates of each subline and therefore, were included in the subsequent analysis. 289 proteins were found to be significantly differentially expressed between DU145 parenteral and SPOP-KO cells (*p*-value <0.05; fold change difference >1.5). Consistent with reported lower transcription efficiency (Fig. 19A&B), SPOP-KO DU145 cells showed 185 differential downregulated proteins and 104 upregulated proteins (Fig. 23B) compared to their parenteral counterparts. A volcano plot (Fig. 23C) shows the upregulated proteins in either DU145 SPOP-KO or wild type cells. Next, we set out to perform ontology gene set enrichment analysis (GSEA) on the detected proteins to detect which pathways are significantly deregulated. GSEA revealed 325 gene sets to be significantly upregulated in SPOP deficient phenotype with false discovery rate (FDR) < 25%. To gain insight into which pathways are enriched, MCL cytoscape analysis for the pathways enrichment visualization was performed with specified cutoff values (FDR q-value 0.25, *p*-value 0.1). SPOP-KO cells showed upregulation in pathways related to transcription, RNA splicing and replication. Interestingly, among significantly upregulated pathways in SPOP-KO DU145 cells were chromatin structure related pathways, such as chromatin remodeling and histone post-translational modification (HPTMs) pathways (Fig. 23D). Furthermore, GSEA demonstrated the enrichment of gene sets related to condensed chromosome (Fig. 23E) and methylated histones (Fig. 23F), with FDR values of 0.05 and 0.13, respectively. Heatmaps of differentially expressed genes of condensed chromosome are depicted in Fig. 23G, while, Fig. 23H shows the histone methylation genes. This highlights the possibility that the transcription stress and impaired transcription elongation reported in SPOP-KO DU145 cells can be attributed to altered chromatin structure.

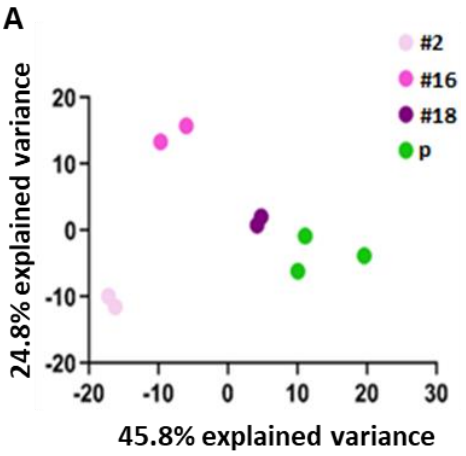
A
#2
#16
#18
p
24.8% explained variance
45.8% explained variance

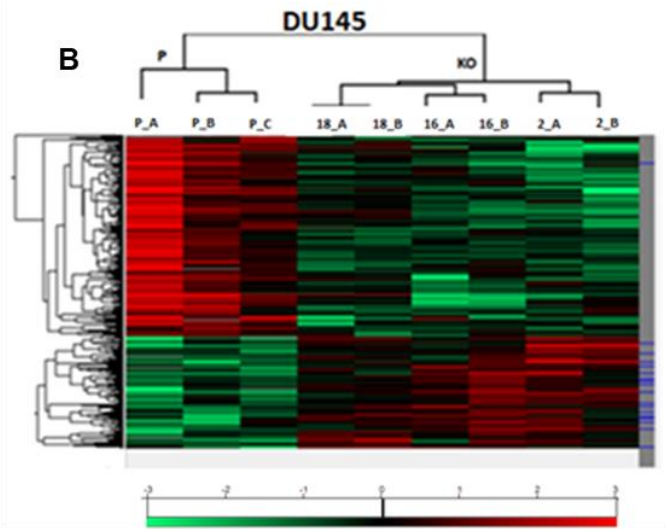
B
DU145
P
KO
P_A
P_B
P_C
18_A
18_B
16_A
16_B
2_A
2_B

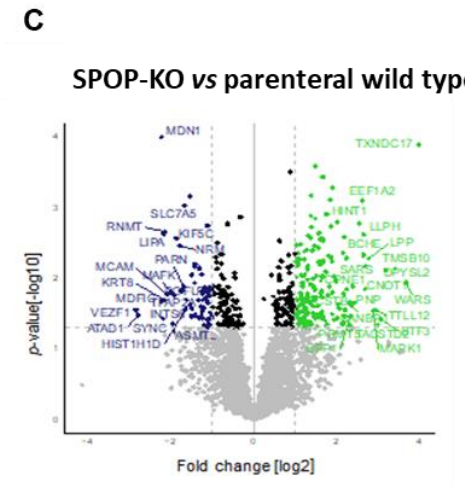
C
SPOP-KO vs parenteral wild type
p-value[-log10]
Fold change [log2]

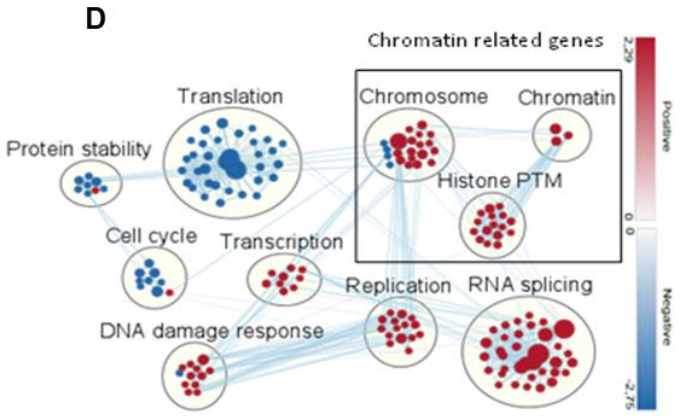
D
Chromatin related genes
Translation
Chromosome
Chromatin
Protein stability
Histone PTM
Cell cycle
Transcription
Replication
RNA splicing
DNA damage response
Positive
Negative

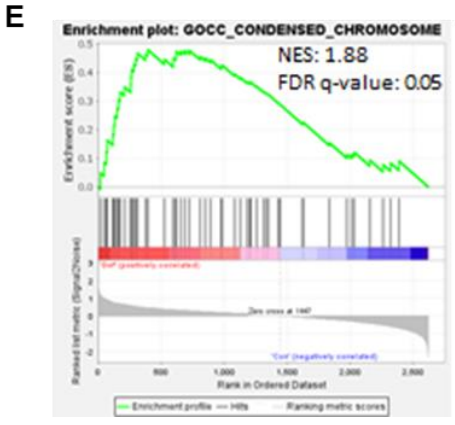
E
Enrichment plot: GOCC_CONDENSED_CHROMOSOME
NES: 1.88
FDR q-value: 0.05

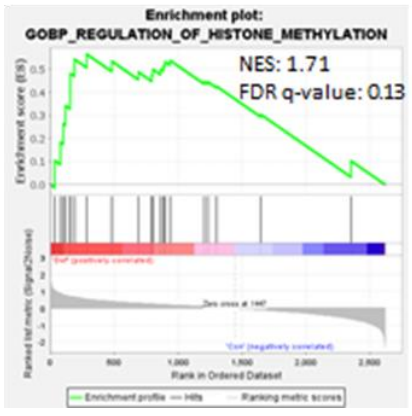
F
Enrichment plot:
GOBP_REGULATION_OF_HISTONE_METHYLATION
NES: 1.71
FDR q-value: 0.13

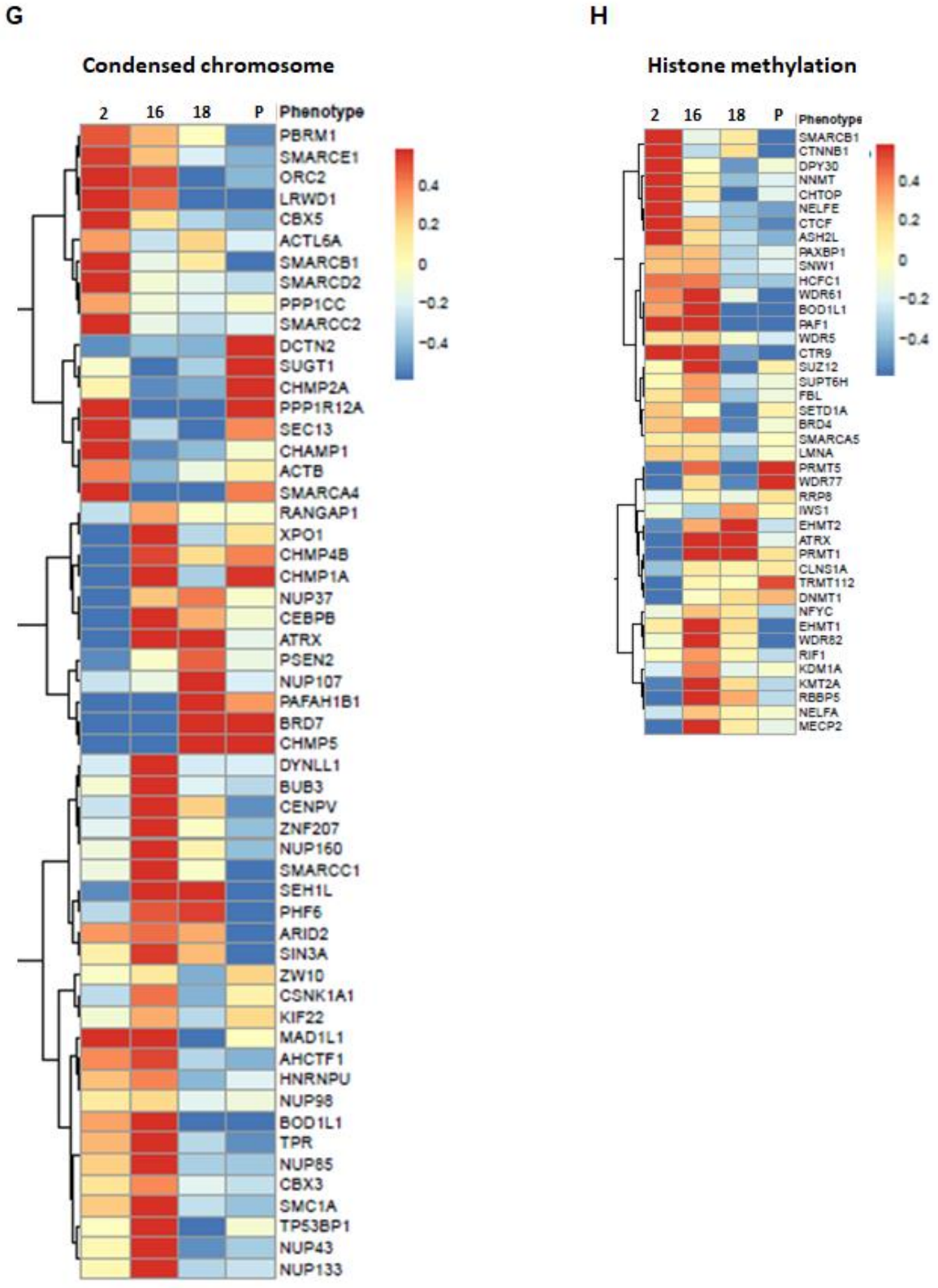


**Figure 23. Differential quantitative proteome analysis in SPOP-KO *vs* proficient DU145 cells.** SPOP proficient and deficient cells (#2, #16, #18) were used in the analysis. (A) Scatter plot visualization of the first 2 principal components (PCs). Y-axis represents 24.8% and x-axis represents 45.8% of total variation in the data, accounting for the highest amount of explained variance, based on 416 proteins ANOVA significant between all groups (*p*-value <0.05). Missing values were imputed from the normal distribution prior to

visualization. (B) Heatmap visualisation using pearson correlation based hierarchical clustering with average linkage based on 289 statistically differential abundant proteins (*p*-value <0.05; Fold change difference >1.5) between SPOP proficient and deficient DU145 cells. (C) Volcano plot showing *p*-values of significantly (*p*-value <0.05; Fold change difference <2) upregulated proteins between DU145 wild type cells (green) and SPOP-KO clones (blue). (D) A visualization of MCL (Markov Clustering algorithm) clustered enrichment map of gene ontology-based GSEA results, showing upregulated and downregulated pathways in SPOP deficient clones compared to their parenteral counterparts (FDR <0.25, *p*-value <0.1). (E&F) Enrichment plots of (E) condensed chromosome or (F) histone methylation gene sets enriched in DU145 SPOP-KO clones generated from gene ontology based GSEA. Normalized enrichment score (NER) and false discovery rate (FDR) obtained from GSEA are indicated on each plot. (G&H) Heatmaps genes list included in enriched gene sets from E&F, respectively.

### Proteomics of LNCaP SPOP-KO *vs* wild type cells

Duplicates of each of LNCaP SPOP-KO sublines (#30, #11) and their proficient counterparts were tested in MS. Analysis of the whole protein matrix quantified a total of 4821 proteins that were used to investigate the differences and similarities between SPOP proficient and deficient cells using PCA (data not shown). PCA (Fig. 24A) performed after ANOVA testing (*p*-value < 0.05) showed clear separation of SPOP-KO sublines #30, #11 from their wild type counterparts with PC2 of 76.8% and PC1 of 14.2%.

2352 proteins were quantified at least 2 times in each cell line; of which 593 statistically significant differentially expressed proteins were identified between LNCaP SPOP proficient and deficient cells (*p*-value <0.05; fold change difference >1.5), (Fig. 24B). In line with the data presented in (Fig. 19C), LNCaP SPOP deficient cells revealed 523 differentially upregulated proteins compared to proficient cells, while only 68 proteins were downregulated (Fig. 24B). Fig. 24C shows a volcano plot of upregulated proteins in either LNCaP SPOP deficient or proficient cells. In addition, performing gene ontology enrichment analysis using the 2352 proteins demonstrated significant upregulation in 148 gene sets in the SPOP deficient phenotype with False discovery rate (FDR) < 25%. MCL Enrichment visualization in cytoscape (FDR q-value 0.25, *p*-value 0.1) showed the upregulation of pathways as translation in LNCaP SPOP-KO cells (Fig. 24D). Additionally, GSEA showed enrichment of gene sets related to translation initiation (Fig. 24E), and positive regulation of translation (Fig. 24F), with FDR values of 0.000 and 0.027 respectively. Heatmap of the positive regulation of translation gene set is shown in (Fig. 24G). This data is consistent with transcription upregulation observed earlier in LNCaP SPOP-KO cells (Fig. 19C).

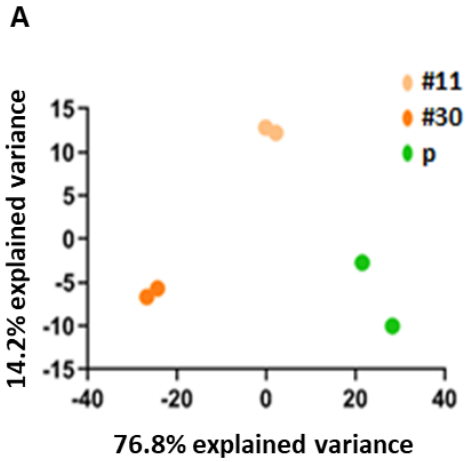
A
#11
#30
p
14.2% explained variance
76.8% explained variance

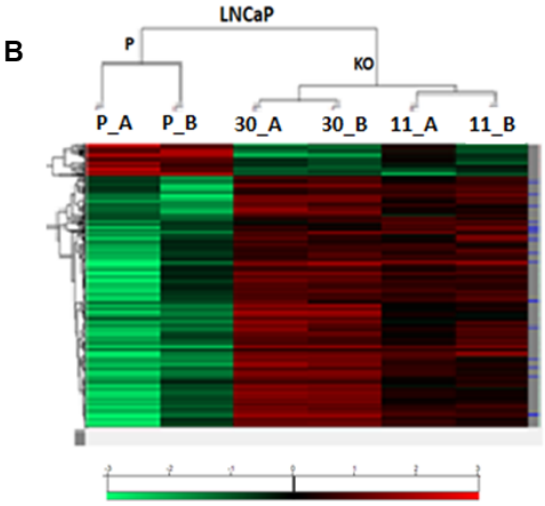
B
LNCaP
P
KO
P_A
P_B
30_A
30_B
11_A
11_B

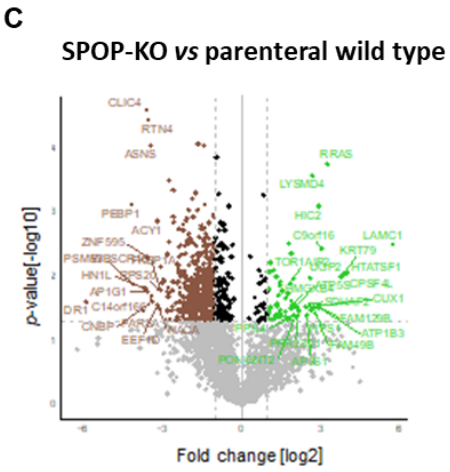
C
SPOP-KO vs parenteral wild type
p-value[-log10]
Fold change [log2]

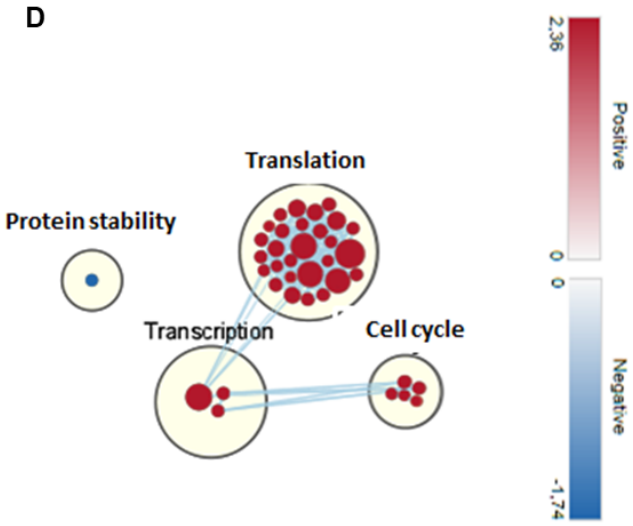
D
Translation
Protein stability
Transcription
Cell cycle
2.36
Positive
0
0
Negative
-1.74

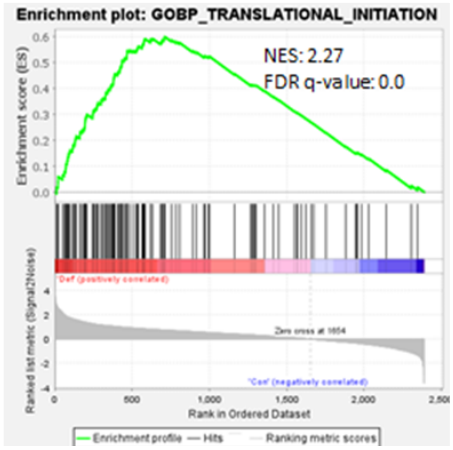
E
Enrichment plot: GOBP_TRANSLATIONAL_INITIATION
NES: 2.27
FDR q-value: 0.0
Enrichment score (ES)
Ranked list metric (Signal2Noise)
Rank in Ordered Dataset
Enrichment profile
Hits
Ranking metric scores

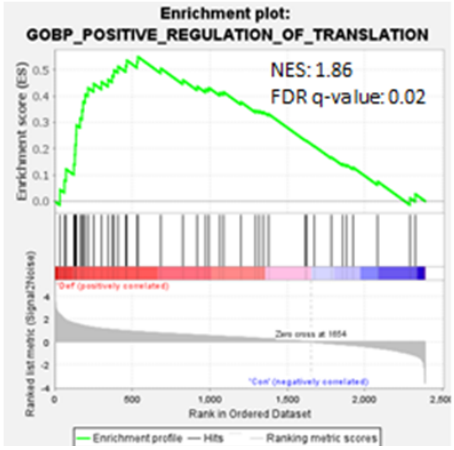
F
Enrichment plot:
GOBP_POSITIVE_REGULATION_OF_TRANSLATION
NES: 1.86
FDR q-value: 0.02
Enrichment score (ES)
Ranked list metric (Signal2Noise)
Rank in Ordered Dataset
Enrichment profile
Hits
Ranking metric scores

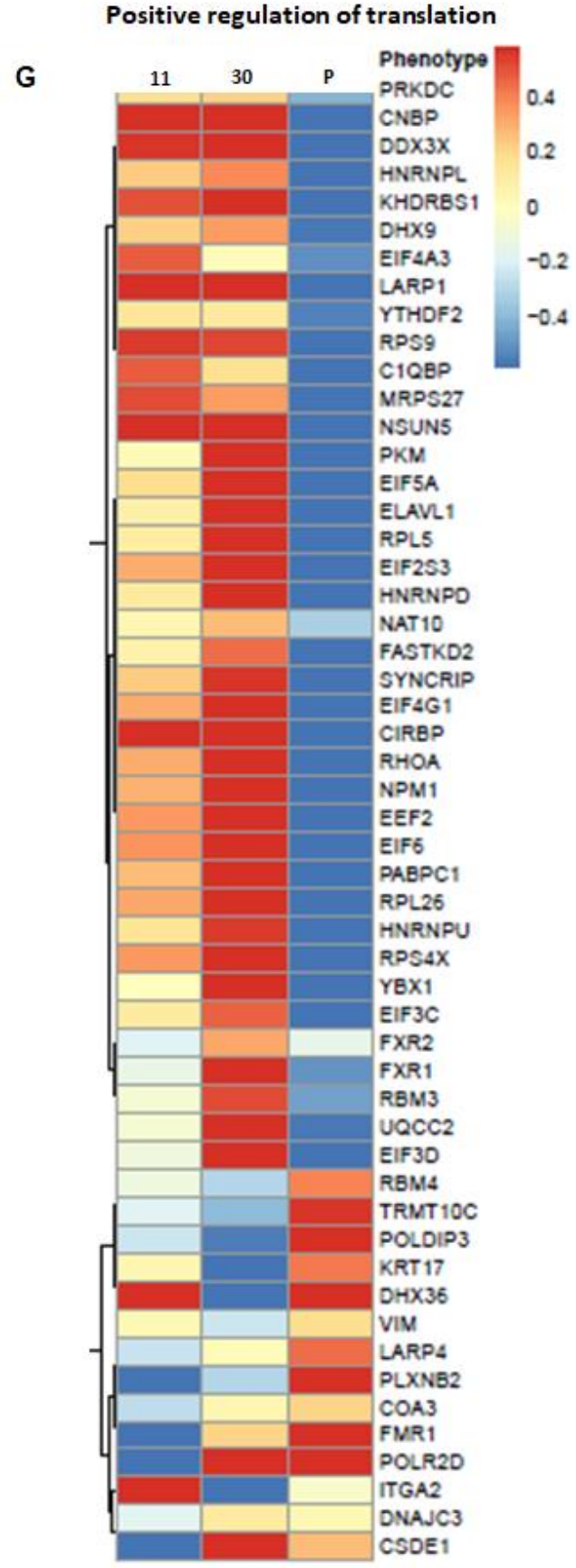


**Figure 24. Differential quantitative proteome analysis in SPOP-KO *vs* proficient LNCaP cells.** LNCaP wild type cells and KO (#30, #11) are included in the analysis. (A)

Scatter plot visualization of the first 2 PCs. Y-axis represents 14.2% and x-axis represents 76.8% of total variation in the data, accounting for the highest amount of explained variance, based on ANOVA proteins significant between all groups (*p*-value <0.05). Missing values were imputed from the normal distribution prior to visualization. (B) Heatmap visualisation using pearson correlation based hierarchical clustering with average linkage based on 593 statistically differential abundant proteins (*p*-value <0.05; Fold change difference >1.5) between SPOP proficient and deficient cells. (C) Volcano plot visualization of *p*-values of significantly upregulated (*p*-value <0.05; Fold change difference <2) proteins in LNCaP parenteral (green) and KO (brown) cells. (D) MCL clustered enrichment map visualisation of gene ontology-based GSEA results, showing upregulated and downregulated pathways in SPOP deficient cells compared to proficient cells (FDR <0.25, *p*-value <0.1). (E&F) Enrichment plots of (E) translational initiation and (F) positive regulation of translation gene sets enriched in LNCaP SPOP-KO clones, generated from gene ontology based GSEA. Normalized enrichment score (NER) and false discovery rate (FDR) obtained from GSEA are indicated on each plot. (G) Heatmap of the gene list of positive regulation of translation.

The absence of any changes in the chromatin modification and HPTMs gene sets in LNCaP SPOP-KO cells that were identified in DU145 SPOP-KO clones, suggests different mechanisms by which SPOP regulates the transcription dynamics in LNCaP and DU145 cells. Where, SPOP loss in the AR-negative DU145 cells probably leads to chromatin and histone modifications that result in compact chromatin structure, hence, slows down elongation step during transcription (Fig. 19A&B). Contrarily, the upregulated AR signaling in LNCaP SPOP-KO cells (Fig. 19C) bypasses the effect of SPOP loss on chromatin structure.

### 4.14. Analysis of chromatin accessibility in SPOP-KO cells

Based on the above data, we sought to validate if chromatin is compact in DU145 SPOP-KO cells. Therefore, the chromatin accessibility was analyzed in both SPOP-KO and wild type DU145 or LNCaP cells using ATAC-seq. ATAC-seq was performed on tagmented DNA isolated from SPOP-KO DU145 clone #16 or LNCaP SPOP-KO clone #30 *vs* their parenteral counterparts, each in duplicate. PCA analysis of read counts of all merged peaks was used to evaluate the variation between and within groups. As shown in Fig. 25, parenteral cells of DU145 or LNCaP were clearly clustered and separated from their SPOP-KO counterparts. Furthermore, DU145 SPOP proficient and deficient cells were clearly distinguished from LNCaP cells.

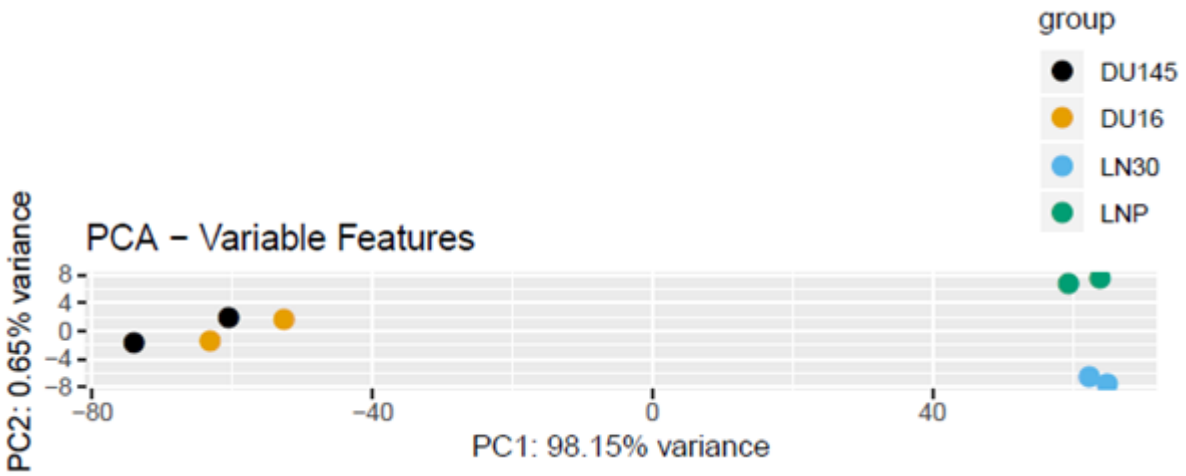


**Figure 25. Principle component analysis (PCA) of ATAC-seq data.** Shown is the PCA of read counts of all merged ATAC-seq peaks in the indicated SPOP-KO and wild type DU145 and LNCaP cells.

In line with our hypothesis that transcription downregulation in SPOP-KO DU145 cells is attributed to increased chromatin compaction, a reduced chromatin accessibility was reported in SPOP-KO DU145 cells compared to their wild type counterparts (Fig. 26A&B). This was evidenced by the lower peak signal of tag distributions observed in the average plots in both the promoter regions (Fig. 26A) and gene bodies (Fig.26B). Moreover, differential read counts of all merged peak regions confirmed the condensed chromatin structure in SPOP-KO DU145 cells, as manifested by the more number of downregulated regions than compared to SPOP wild type counterparts (Fig. 26C).
On the other hand, in accordance with the enhanced transcription activity in SPOP-KO LNCaP sublines, higher peaks intensities of tag distributions were demonstrated across both the promoter (Fig. 26D) and gene bodies (Fig. 26E). Furthermore, differential analysis of merged peak regions read counts showed more upregulated regions in LNCaP SPOP-KO cells than in parenteral cells (Fig. 26C). Altogether, this data shows that SPOP loss impairs the chromatin accessibility as observed in the AR-negative DU145 cells. However, when AR is present, it acts as a transcription factor to rescue the effect of SPOP loss on the chromatin structure.

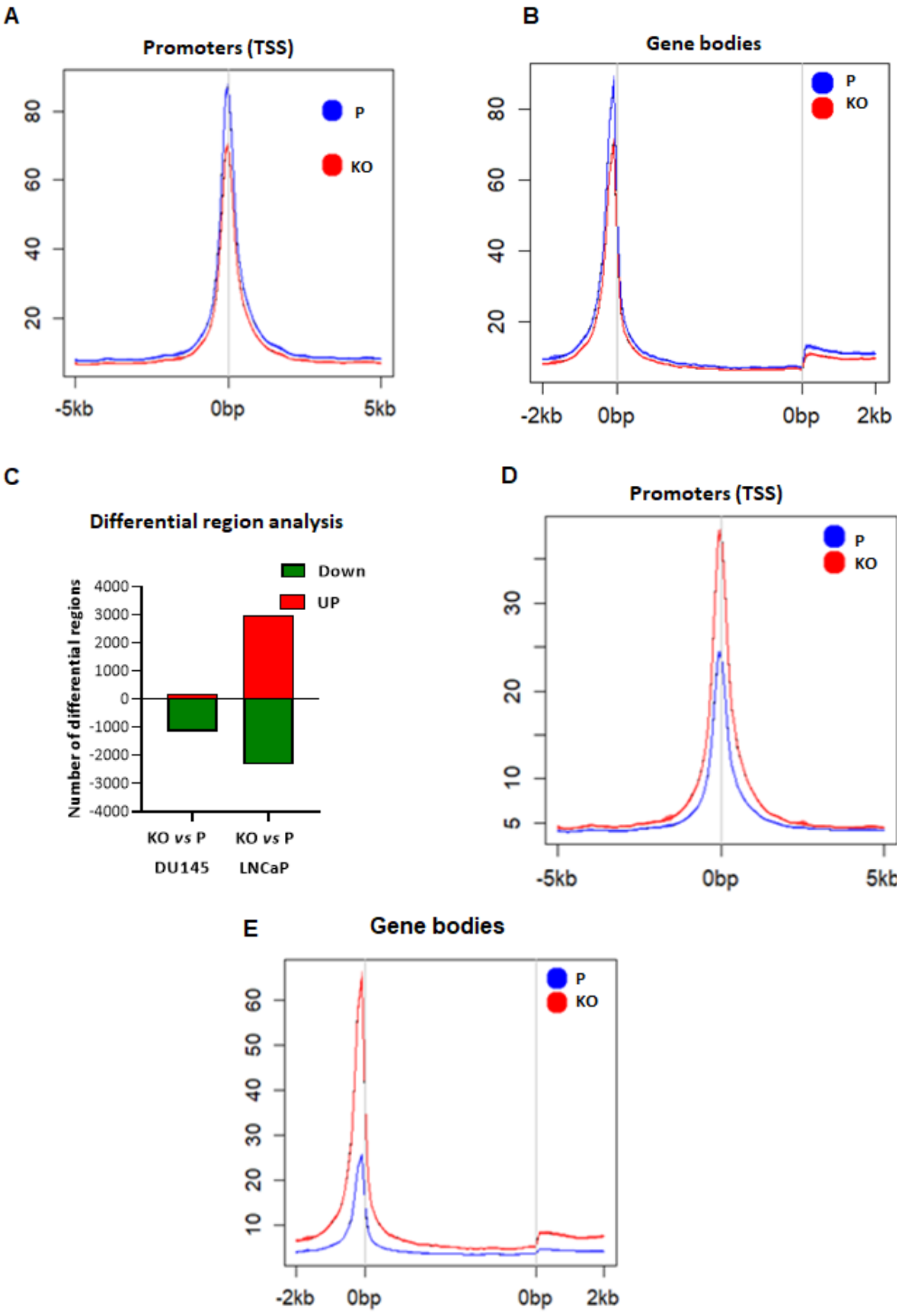


**Figure 26. Analysis of chromatin accessibility using ATAC-seq.** (A&B) Comparisons in DU145 wild type *vs* KO (#16) cells of tag distributions in (A) the promoter region within

the transcription start sites (TSS; +/- 5 kb), and (B) in the gene bodies within 2 kb flanking regions. DU145 SPOP proficient cells (P) are shown in blue and SPOP-KO clone #16 in red. (C) Shown are the numbers of differential regions using DESeq2 with padj <0.1. Comparison was represented for the number of differential regions in SPOP proficient (P) of either DU145 or LNCaP in reference to their SPOP-KO subclones. (D&E) Comparisons in LNCaP wild type *vs* KO (#30) cells of tag distributions in (D) the promoter region within the transcription start sites (TSS; +/- 5 kb), as well as, in (E) the gene bodies within 2 kb flanking regions. LNCaP SPOP proficient cells (P) are shown in blue and SPOP-KO clone #30 in red.

### 4.15. Investigation of histone post-translational modifications using MS

Since proteomic analysis showed upregulation of histone methylation gene set (Fig. 23H), it was reasonable to test whether the compact chromatin structure observed in SPOP-KO DU145 cells is attributed to abnormal epigenetic changes that mediate chromatin compaction such as increased methylated histones and/or decreased histone acetylation. Therefore, we established a modified MS-based assay to study global histone post-translational modifications in SPOP-KO cells.

In DU145 cells a total of 172 methylated and 620 acetylated histone peptides were detected. PCA analysis revealed a clear separation of KO sublines from wild type cells in methylated (Fig. 27A) and acetylated histones (Fig. 27B). 20 out of the 172 methylated histones were found at least in 2 replicates of each phenotype. Likewise, 35 out of the 620 acetylated histones were detected.

DU145 SPOP-KO cells showed 4 out of 20 significantly differentially upregulated methylated histones compared their wild type counterparts. (*p*-value <0.05; Fold change difference <1.5) (Fig. 27C). Interestingly, H3K27me3 was among the upregulated methylated histones detected in SPOP-KO DU145 cells. H3K27me3 is known to be a heterochromatin marker that associates with chromatin compaction (Saksouk et al., 2015). On the other hand, no difference in histone acetylation was reported between SPOP-KO DU145 cells and their wild type counterparts (Fig. 27D). known to be a heterochromatin marker that associates with chromatin compaction (Saksouk et al., 2015). On the other hand, no difference in histone acetylation was reported between SPOP-KO DU145 cells and their wild type counterparts (Fig. 27D)

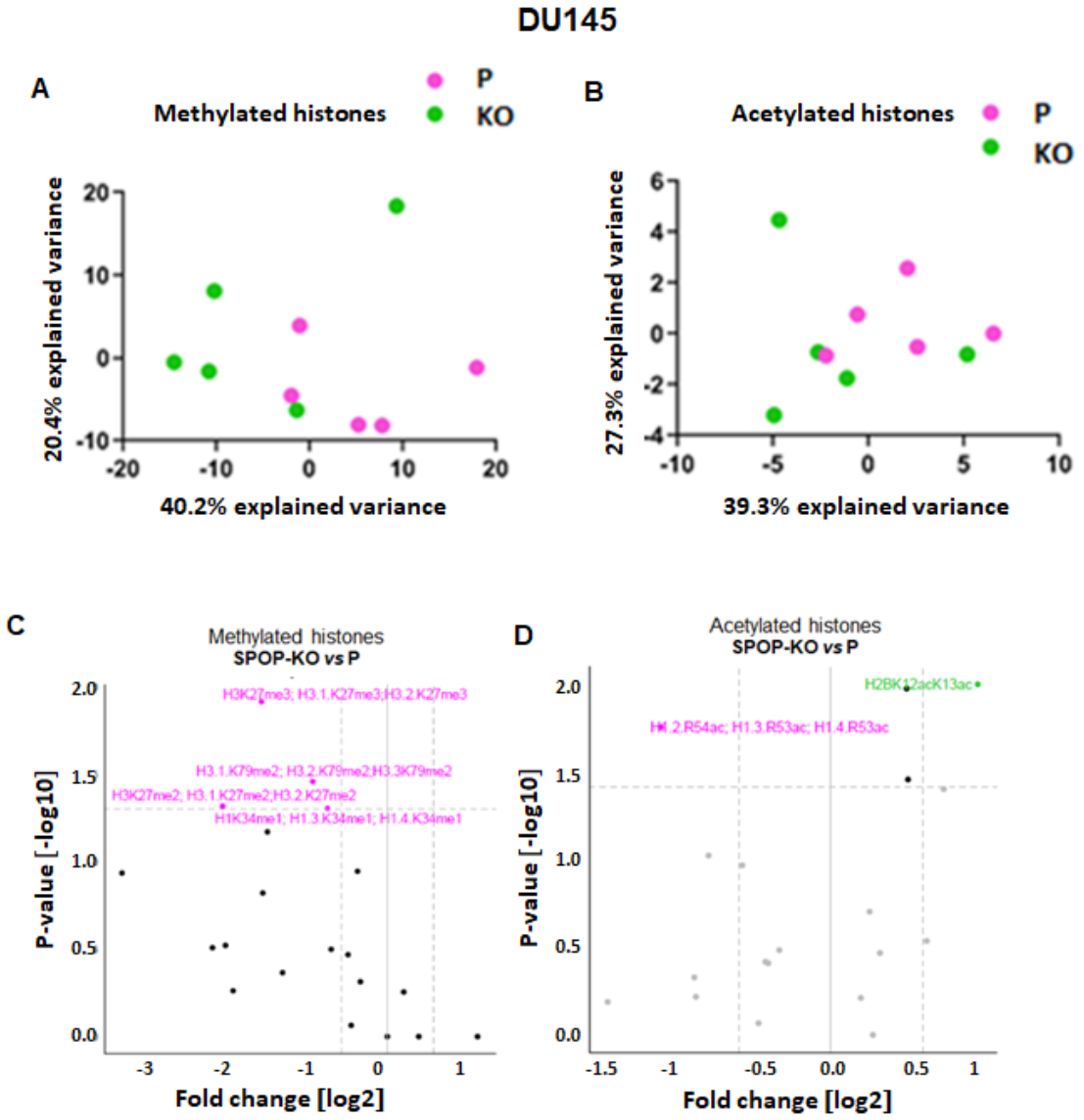


**Figure 27. Global histone methylation and acetylation in DU145 SPOP deficient cells.** (A) Scatter plot visualization of the first 2 PCs, accounting for the highest amount of explained variance, based on the quantification of 172 methylated and unmodified histones. Missing values were imputed from the normal distribution prior to visualization. (B) Scatter plot visualization of the first 2 PCs, accounting for the highest amount of explained variance, based on 620 acetylated and unmodified histones. Missing values were imputed from the normal distribution prior to visualization. (C&D) Volcano plots visualization of t-testing results between DU145 SPOP-KO clone #16 and DU145 parenteral (P) cells, comparing the abundance of (C) methylated or (D) acetylated histones peptides. Peptides were considered significantly differential abundant, if they were identified with a *p*-value <0.05, in addition to passing 1.5-fold change cutoff. Respective histones of significantly differential peptides are annotated.

In LNCaP cells, a total of 316 methylated or 231 acetylated histone modifications were quantified and used in PCA analysis (Fig. 28A&B). 64 out of the 316 methylated and 40 out of the 231 acetylated histones were detected at least 2 times in the replicates

of each phenotype. In line with the absence of histone PTMs pathways in MCL analysis of LNCaP SPOP-KO cells (Fig. 24D), no upregulated methylated histones were detected in SPOP-KO cells (Fig. 28C). Additionally, no change in the acetylated histones was detected in SPOP deficient cells as compared to their parenteral counterparts (Fig. 28D).

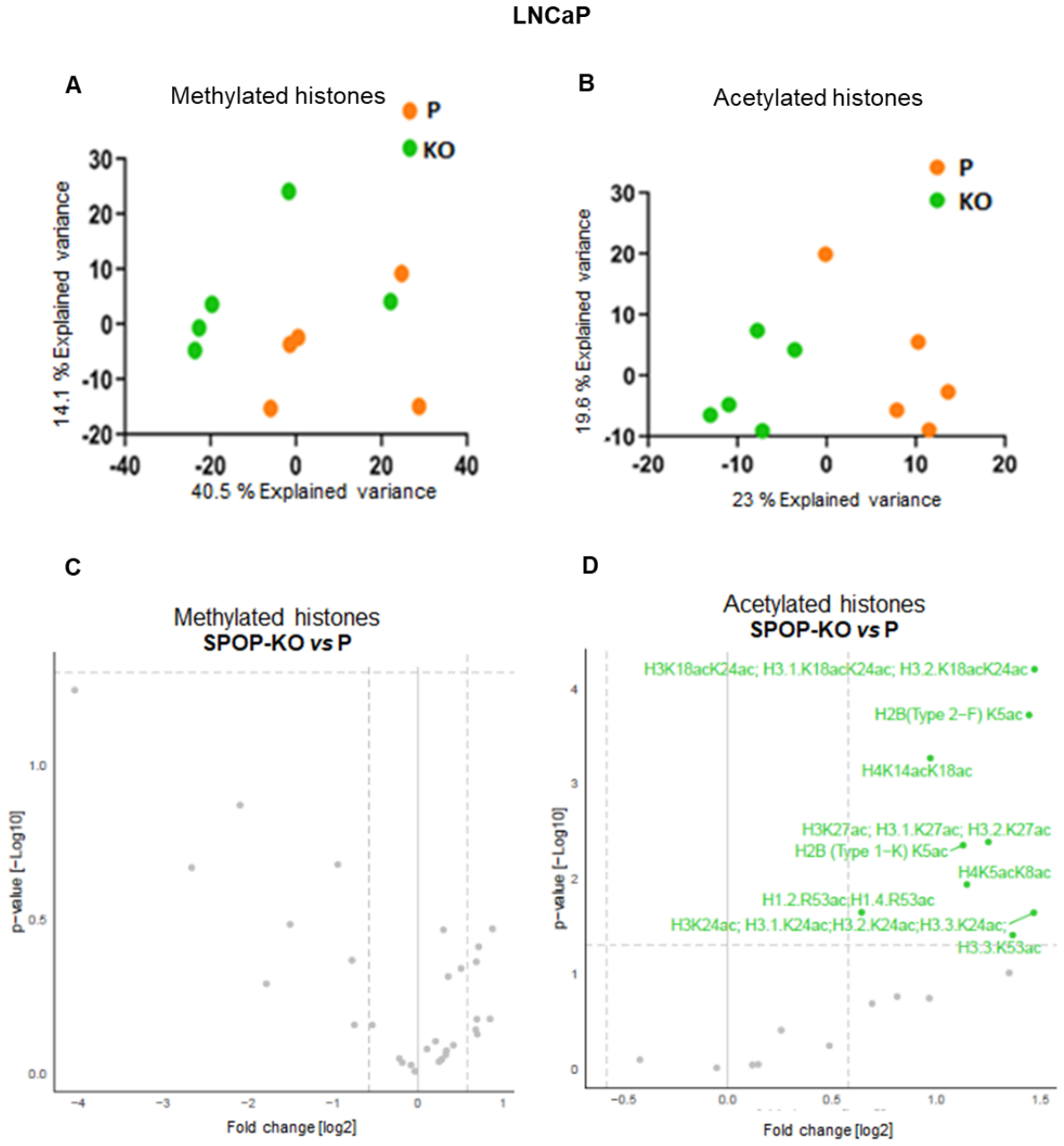


**Figure 28. Histone post-translational modifications in SPOP LNCaP deficient cells.** (A) Scatter plot visualization of the first 2 PCs, accounting for the highest amount of explained variance, based on 316 methylated and unmodified histone peptides. Missing values were imputed from the normal distribution prior to visualization. (B) Scatter plot visualization of the

first 2 PCs, accounting for the highest amount of explained variance, based on 231 acetylated and unmodified histones. Missing values were imputed from the normal distribution prior to visualization. (C&D) Volcano plots visualization of t-testing results between LNCaP SPOP-KO clone #30 and LNCaP parenteral (P) cells, comparing the abundance of (C) methylated histone peptides or (B) acetylated histones peptides. Peptides were considered significantly differential abundant, if they were identified with a *p*-value <0.05, in addition to passing 1.5 Fold change cutoff. Respective histones of significantly differential peptides are annotated.

### 4.16. DNA methylome analysis in SPOP-KO clones

DNA methylation has been shown to be an epigenetic modification that results in compact chromatin structure. Additionally, an interplay has been discovered between histones and DNA methylation (Rose and Klose, 2014). Noteworthy, our MS analysis revealed an upregulation of several DNA and histone methyl transferases (Fig. 23H). Therefore, we sought to analyze if the global DNA methylation is another factor that results in compact chromatin structure in SPOP-KO cells of DU145. To that end, total DNA was isolated from SPOP-KO sublines, as well as, their parenteral wild type cells and the global DNA methylation was investigated using illumina Human Methylation 450 Bead Chip (450K) arrays. As shown in Fig. 29, pooled DU145 SPOP-KO clones (#2, #16, #18) demonstrated 15% increase in global DNA methylation compared to parenteral cells (mean ±SD: 0.5432 ±0.04654 *vs* 0.4764 ±0.000). On the other hand, LNCaP SPOP proficient and pooled deficient clones (#30, #18) showed no difference (0.6244 ±0.0097 in SPOP-KO cells *vs* 0.6184 ±0.000).

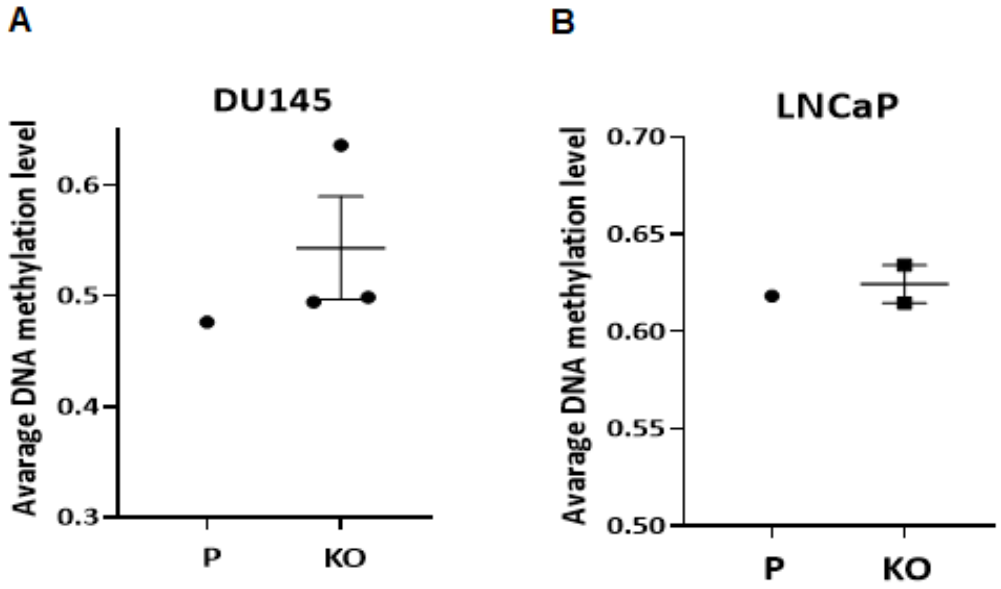


**Figure 29. Global DNA methylation analysis in SPOP-KO cells.** Illumina Human Methylation 450 Bead Chip (450K) arrays were used to investigate the average global methylation levels in (A) SPOP deficient clone #16 *vs* proficient SPOP (P) DU145 cells or (B) SPOP-KO clone #30 *vs* parenteral LNCaP cells.

Altogether, our results show that the enhanced methylation of DNA and histones result in compact chromatin structure in SPOP-KO cells of DU145 leading to transcription stress by decreased transcription. However, LNCaP SPOP-KO cells show no change in the methylated DNA and histones, yet still, predisposed to transcription stress through transcription upregulation and more accessible chromatin, as a result of the enhanced AR signaling.

## 5. Discussion

DNA damage response and repair are potent barriers to prevent cancer development and progression (Jackson and Bartek, 2009). Therefore, these pathways are repetitively reported to be deregulated in several cancer types including PCa (Mateo et al., 2017). PCa is the most common male cancer in Germany and the second leading cause of male cancer deaths (Globocan, 2020); yet, the mechanisms behind its initiation and progression are still not entirely clear. Unlike other tumors, structural genomic rearrangements are the most common with ERG fusion present in around 50% of the patients (Tomlins et al., 2005; Abeshouse et al., 2015). Although PCa is rarely characterized by the presence of somatic point mutations; studies revealed that SPOP missense mutations are the most common in PCa (10-15%) (Barbieri et al., 2012; Frank et al., 2018). Interestingly, SPOP mutations are mutual exclusive with ERG fusion and occur in the primary localized disease, not just the metastatic (Barbieri et al., 2012). Therefore, understanding SPOP role in PCa can identify a cluster of the ERG negative patients that could benefit from targeted therapy. SPOP is working as a tumor suppressor in PCa through its ability to bind and degrade different substrate proteins such as AR (Geng et al., 2014), SRC-3 (Geng et al., 2013), DEK (Theurillat et al., 2014) , TRIM24 (Groner et al., 2016), and ERG (Gan et al., 2015), thus controlling the proliferation and invasion of PCa. Moreover, SPOP was found to inhibit the stem-like characteristics of PCa through degradation of NANOG (Zhang et al., 2019). SPOP mutations have been reported to be associated with an unusually high frequency of genomic rearrangements and poor prognosis in PCa (García-Flores et al., 2014; Boysen et al., 2015), however, the mechanisms by which SPOP promotes genome stability is yet so far not fully discovered.

The main aim of the current study is to investigate the mechanism underlying the accumulation of DSBs and genomic instabilities in SPOP deficient PCa cells. In order to better address this, we employed the CRISPR-CAS9 technology to establish stable SPOP-KO sublines from both the AR-negative ($AR^-$) DU145 (Fig. 10A) and AR-positive ($AR^+$) LNCaP (Fig. 10B) cells. SPOP-KO was confirmed using WB and sequencing. Surprisingly, an insertion of a ‘’T’’ base was detected in all SPOP-KO sublines (Fig. 10C). This insertion led to a frameshift mutation and possibly a truncated SPOP protein. A possible explanation for the finding that all KO sublines share the same insertion mutation could be that they have been subjected to the same selection procedures, starting with immunoblotting to detect clones with no detectable SPOP

protein expression and then sequencing. Indeed, no difference in the proliferation rate was observed between SPOP-KO cells of neither DU145 (Fig. 10D) nor LNCaP (Fig. 10E) cells compared to their wild type counterparts, indicating that any difference observed in SPOP-KO clones in our study is not related to variation in the proliferation rate, however, is dependent on SPOP itself.

### 5.1. SPOP deficiency accumulates secondary DSBs

Using DSB-foci assay, we reported increased numbers of γH2AX and 53BP1 foci (global DSBs markers) at 24h post-2Gy in SPOP-KO DU145 and LNCaP cells compared to their wild type counterparts (Fig. 11A-C and Fig. 11D-F). Intriguingly, the number of DSBs at earlier time points i.e. 1 and 3 h post 2Gy was also increased in the SPOP-KO sublines of both strains (Fig. 11A-C and Fig. 11D-F). Similarly, we demonstrated a higher number of RAD51 foci at 3 and 24 h post-2Gy in SPOP-KO sublines established from both DU145 and LNCaP cells than in their parenteral cells (Fig. 12A&B and Fig. 12C&D). This data indicates that the reported increase in the number of residual DSBs (γH2AX, 53BP1 and RAD51 foci) are not due to repair deficiency, but rather due to the accumulation of secondary DSBs in SPOP-KO cells. Efficient DSB repair was further validated in SPOP-KO cells, using repair substrates to specifically investigate HR or NHEJ efficiency, showing no significant difference in either HR or NHEJ efficiency between SPOP-KO and wild type cells in both strains (Fig. 13B and Fig. 13D), indicating the presence of other mechanism underlying the accumulation of DSBs in SPOP deficient cells. Noteworthy, we detected more spontaneous DBSs (γH2AX and RAD51 foci) i.e. generated without external stimulus in SPOP-KO cells of DU145 (Fig. 12A, B&E) and LNCaP (Fig. 12C, D&F), compared to their wild type cells. Previous studies showed that SPOP knockdown has no effect on sensing DSBs, however, more residual DSBs were accumulated post-IR or after the induction of RS using campothecin or hydroxyurea (Boysen et al., 2015; Hjorth-Jensen et al., 2018; El Bezawy et al., 2020; Maekawa and Higashiyama, 2020). However, contrarily to our data, they attributed the accumulation of residual DSBs to HR repair impairment in SPOP deficient cells, as depicted by reduced RAD51 foci formation post 2Gy (Boysen et al., 2015).

The inconsistency between our data and the aforementioned studies can be attributed to the difference in the applied analysis and biological systems used. In which, the analysis used in Boysen et al., relied on the percentage of cells with more than 20 RAD51 foci at 30 min post 2Gy as an indication for HR, which indeed may have missed

and underestimated the real number of RAD51 foci. In addition, in the same study, Boysen and co-workers demonstrated less HR repair efficiency using reporter assay, which contradicts with our finding here (Fig. 13B). However, it is important to note that they used SPOP-KD cells transfected with SPOP wild type expressing plasmid as a control. Ectopic expression represents in fact an overexpression status that indeed differs from the wild type status as in our case here. SPOP overexpression was previously associated with an oncogenic effect in kidney cancer (Li et al., 2014). Therefore, it is tempting to assume that SPOP expression is tightly controlled to avoid oncogenic activity. The expression of several DDR and DNA repair factors have also been shown to be tightly regulated to avoid accumulation of genomic instabilities. For instance, lower RAD51 expression impairs DSB repair via HR, leading to the accumulation of several genomic alterations/rearrangements and correlates with poor prognosis in different cancer (Bindra et al., 2004). On the other hand, overexpression of RAD51 promotes genomic instabilities and poor prognosis in colorectal cancer (Tennstedt et al., 2013).

Altogether, this data indicated that SPOP deficient cells accumulate spontaneous, as well as, IR-induced DSBs, despite efficient HR and NHEJ repair capacity and intact cell cycle checkpoints.

### 5.2. SPOP loss causes replication stress

Previously, it was demonstrated that siRNA-mediated SPOP-KD causes replication stress that is associated with reduced expression (at both the transcription and protein levels) of several key DNA repair and replication factors including ATR, ChK1, BRCA2 and RAD51 (Hjorth-Jensen et al., 2018). In the current study however, we reported efficient expression (at the protein level) of the canonical DDR factors such as ATM, ChK2, RAD51 and ATR in SPOP-KO DU145 and LNCaP cells. This is in fact in line with Boysen et al., who reported unchanged levels or activated forms of the aforementioned DDR factors (Boysen et al., 2015). Of note, we detected a lower ChK1 phosphorylation in SPOP-KO cells that explains the finding of Jensen et al., who demonstrated, after 48h and 72h post-SPOP depletion, a spontaneous reduction in the number of S-Phase cells and an increase in G1 population (Hjorth-Jensen et al., 2018). This indicates indeed the presence of RS in SPOP deficient cells, which was further validated by reporting an increased number of pan-nuclear γH2AX (pan-γH2AX) - a previously reported indicator of RS (Köcher et al., 2012; Meyer et al., 2013, Parsels et al., 2018; Moeglin et al., 2019; Meyer et al., 2020) - both spontaneously and 24 h (Fig.

15A) post 2Gy in SPOP-KO sublines compared to their wild type cells. Consistently, it was not surprising to observe using DNA fiber assay that SPOP-KO DU145 and LNCaP cells accumulate RS as evident by the (i) decreased replication rate, (ii) prolonged replication fork stalling and (iii) increased new origin firing.

Indeed, the ATR-ChK1 axis is crucial in the control of replication (Petermann and Caldecott, 2006), however, the observed decrease in ChK1 phosphorylation in SPOP-KO cells can not entirely explain the profound effect on RS. Therefore, we do think that the inability of SPOP deficient cells to protect their replication forks is likely multi-facetted, since efficient HR and DDR were reported in SPOP-KO cells. Noteworthy, it is unlikely that aberrant androgen signaling underlies the RS observed in SPOP-KO cells, since the RS was observed in both AR-negative (DU145), as well as, AR-positive (LNCaP) cells.

### 5.3. SPOP deficiency results in transcription stress and accumulation of R-loops

The above indicated data might reveal that the accumulation of RS is the cause of increased genomic instability in SPOP deficient PCa. If this is true, we should expect the accumulation of DSBs exclusively in S-Phase cells. However, we interestingly reported that spontaneously generated DSBs are accumulated in all cell cycle phases in SPOP-KO sublines (Fig. 16) revealing the involvement of other mechanism(s), other than RS in the accumulation of DSBs and genomic instability in SPOP-KO cells.

Faithful and timely expression of genes is essential for cell survival. On one hand, the integrity of DNA template is crucial for accurate transcription, which explains the accumulation of transcription stress upon damaging the DNA (Steurer et al., 2022). On the other hand, the spatiotemporal control of the multiple transcriptional steps is necessary to prevent any genomic instability caused by, for example, collisions with the replication machinery, the formation of co-transcriptional R-loops and the formation of non-B DNA structures. Since transcription and replication share the same template (Sebastian and Oberdoerffer, 2017; Crossley et al., 2019), we hypothesized that transcription could be the predisposing mechanism for DSBs and RS associated with SPOP deficiency. In line with our hypothesis, we reported transcription deregulations in both DU145 and LNCaP SPOP-KO cells, yet, by different mechanisms. In the AR-negative DU145 cells, SPOP loss was associated with transcription downregulation (Fig. 19A&B). Surprisingly, SPOP deficiency in the AR-positive LNCaP cells was accompanied with transcription upregulation (Fig. 19C). This paradoxical effect was

attributed to AR signaling (explained in details in section 5.5.). Previously, it was shown that transcription stress due to transcription upregulation or downregulation predisposes to R-loops accumulation, RS, and DSBs (Sebastian and Oberdoerffer, 2017). On one hand, reduced transcription – as in DU145 cells – might be resulting from RNA pol II stalling or increased pausing at proximal promoter sites, which leads to enhanced formation of R-loops (Core and Adelman, 2019; Crossley et al., 2019). Stalled RNA pol II can result from - for example - transcription complex arrest and backtracking. The transcription elongation factor (TFIIS) stimulates the endonuclease activity of RNA pol II to rescue transcription complexes that have arrested and backtracked (Zatreanu et al., 2019). Mutations in backtracking sites of TFIIS indeed inhibit RNA cleavage and stabilizes backtracked complexes, leading to transcription stress and accumulation of R-loops and DSBs (Sheridan et al., 2019; Zatreanu et al., 2019). Further, deregulated transcription following the loss of the transcription regulator BRD4 in cancer cells results in R-loops accumulation, RS and DNA damage (Swami et al., 2020). On the other hand, transcription upregulation – as in LNCaP cells- due to stimulation of transcription factors such as AR and ER, in turn enhances transcription rate. This consequently, increases co-transcriptional R-loops formation, probably to an extent more than their resolving rate, thereby accumulating R-loops (Kotsantis et al., 2016; Stork et al., 2016; Nicholas et al., 2021).

In the current study, it was not surprising to observe an accumulation of the transcription intermediates R-loops - marker for transcription stress, in all cell cycle phases in SPOP deficient clones of both DU145 (Fig. 17E&F) and LNCaP (Fig. 17G&H) cells; with no change in protein levels of the R-loops resolving proteins RNase H1, XPG, XPF, DHX9, TOP1, TOP2A, and SRSF (Fig. 18A&B & data not shown). The association between R-loops accumulation on one hand and RS, and DSBs on the other hand, have been previously reported in several studies (Aguilera and García-Muse, 2012; Sollier and Cimprich, 2015; Allison and Wang, 2019). R-loops accumulation results in RS upon collision with replication fork. This generates ssDNA breaks (SSBs) that are then converted to DSBs (García-Muse and Aguilera, 2016; Hamperl et al., 2017). Moreover, R-loops can directly cause DSBs, while being processed by the transcription coupled nucleotide excision repair proteins, XPG and XPF (Sollier et al., 2014). Therefore, it was expected to detect R-loops and DSBs in all cell cycle phases in SPOP-KO clones of DU145 (Fig. 17E&F, Fig. 16) and LNCaP (Fig. 17G&H).

Previously, it has been emphasized the role of the transcription machinery in promoting genome stability (Jonkers and Lis, 2015). Therefore, interference with core processes such as transcriptional elongation will cause genomic instabilities. Interestingly, the protein networks associated with SPOP were found previously to be highly enriched for components of the general mRNA transcription and its related processes such as RNA splicing and processing (Hjorth-Jensen et al., 2018). In line with this, we revealed in the current study that SPOP loss impairs the elongation step as evidenced by declined chromatin bound fractions of RNA pol II ser2p in SPOP-KO DU145 cells (Fig. 22C). The hypo-phosphorylation of RNA pol II ser2 and with that impaired elongation step, was expectedly associated with a feedback increase in the initiation step as indicated by an increase in the phosphorylation level of RNA pol II ser5 (Fig. 22C) and increased protein expression level of RNA pol II (Fig. 22A&B). The SPOP loss mediated impairment of the elongation step appears therefore, to be more probably genome-wide but not gene-specific, confirming our findings, which showed no change in the expression levels of several DDR factors.

In line with its currently described role in transcription regulation, SPOP was previously reported to be located in nuclear speckles (Nagai et al., 1997; Groner et al., 2016). Nuclear speckles are present in nucleus harboring several transcription factors that play crucial role in transcription and RNA processing (Galganski et al., 2017; Ha, 2020; Faber et al., 2022). Interestingly, interactome analysis revealed an association between SPOP and transcription, mRNA splicing and export complexes (Hjorth-Jensen et al., 2018). Although Jensen et al, demonstrated a binding between SPOP and RNA pol II, they did not reveal the impact of this binding on the regulation of transcription process (Hjorth-Jensen et al., 2018). Here, we interestingly revealed mechanistically that SPOP loss does not reduce pol II expression, chromatin loading or its initial activation (Fig. 22C).

### 5.4. SPOP regulates chromatin accessibility by controlling global histone and DNA methylation

Our proteomics data indicated significant increase in the enrichment of chromatin-structure related pathways in SPOP-KO DU145 cells. Among them are proteins involved in histone and DNA methylation.

Several histone PTMs are shown to influence the chromatin accessibility, hence, play role in transcription. Methylation and acetylation are the most important HPTMs that regulate transcription. While acetylation is associated mainly with transcription

activation, histone methylation triggers mainly transcriptional repression (Gates et al., 2017; Millán-Zambrano et al., 2022). Using MS analysis for Histone PTMs, we detected upregulation of methylated histones in DU145 SPOP deficient cells compared to their wild type counterparts. Some of these upregulated methylated histones are known to result in transcription repression such as di and tri methyl H3K27 (Fig. 27C). It is hence tempting to hypothesize a direct role for SPOP in regulating the global histone methylation that might explain its above described role in transcription. In consistence with this role, the histone methyltransferase SETD2 was found to be a substrate for SPOP-mediated protein degradation. Biochemical experiments demonstrated that modulation of SPOP expression confers differential H3K36me3 on SETD2 target genes, and induce H3K36me3-coupled alternative splicing events (Zhu et al., 2017).

Notably, the low number of significantly upregulated methylated histones in our MS analysis, in addition to, detecting DNA methyltransferases in our proteomic data, revealed the involvement of other factors that are involved in SPOP-mediated regulation of chromatin structure. Another regulatory factor of chromatin structure is the DNA methylation (Moore et al., 2013; Lakshminarasimhan and Liang, 2016). Interestingly, mutations in SPOP gene are reportedly associated with genome-wide DNA hypermethylation in PCa (Abeshouse et al., 2015; Zhang et al., 2021).

Here, we reported an increased DNA methylation in DU145 SPOP-KO cells compared to their wild type counterparts (Fig. 29), indicating a condensed chromatin in SPOP deficient cells. Previously, Zhang et al., presented the DNA methyltransferase GLP as SPOP degradation substrate (Zhang et al., 2021). Therefore, SPOP deficient cells showed higher levels of GLP. GLP forms a complex with another DNA methyltransferase, called G9a to stimulate DNA methylation through recruiting the DNA methyltransferase gene (DNMT) (Zhang et al., 2021). This data was additionally in line with our proteomics data revealing the upregulation of DNA methytransferases as EHTM1 and EHTM2 (Fig. 23H) that were previously described to encode GLP and G9a, respectively and results in hypermethylation of DNA, in addition to, H3K9 methylation (Tachibana et al., 2005). Interestingly, in the same study they reported that GLP-G9a complex causes gene silencing also by working as histone methyltransferase, promoting the mono and dimethylation of H3K9. This indeed indicates that both DNA and histone methylation are working in concert together to regulate the accessibility of the chromatin, and hence transcription activity; and SPOP is playing a critical role in both DNA and histone methylation.

Consistent with this, our ATAC-seq analysis revealed a compact chromatin and less chromatin accessibility in DU145 SPOP-KO cells. The reported less chromatin accessibility in SPOP deficient cells was interestingly demonstrated both at the promoter regions (Fig. 26A) and gene bodies (Fig. 26B), implying a genome-wide rather than site specific role for SPOP in regulating the chromatin structure, accessibility and with that the transcription.

### 5.5. A Crosstalk between SPOP and AR-signaling regulates chromatin structure and transcription

In the current study, we demonstrated DSBs, R-loops accumulation and RS in SPOP deficient clones of both DU145 and LNCaP, as a result of transcription stress. Interestingly, contrarily to DU145 SPOP-KO sublines, we reported an upregulation of transcription in LNCaP SPOP-KO cells, as manifested by increased number of cells with incorporated EU (Fig. 19C). This was expectedly associated with enhanced RNA pol II protein expression (Fig. 22A&B), as well as its loading to chromatin (Fig. 22C); in addition to an increased phosphorylation and chromatin loading of RNA pol II on ser5 (Fig. 22C) and ser2 (Fig. 22C), which are markers of transcription initiation and active elongation, respectively. Ectopic expression of SPOP wild type plasmid in LNCaP SPOP-KO clones further confirmed that the increased transcription is SPOP dependent (Fig. 19C).

Since, AR - the transcription factor - is considered one of the main differences between DU145 ($AR^-$) and LNCaP cells ($AR^+$); we indeed hypothesized its involvement in the different transcription stress mechanisms observed in the SPOP deficient cells of DU145 and LNCaP cells. Using WB, we reported higher AR protein expression in LNCaP SPOP-KO clones than in their parenteral counterparts that expectedly, upregulated its downstream target PSA (Fig. 20A). Our data is in line with Geng et al., who reported the AR as SPOP substrate that accumulated with SPOP deficiency (Geng et al., 2014). Consistent with our hypothesis, treating the cells with the AR blocker ‘enzalutamide’ confirmed the AR dependent transcription upregulation in LNCaP SPOP-KO cells. where, we detected a dose dependent transcription reduction in LNCaP SPOP deficient cells (Fig. 20B). In line with our hypothesis, other studies showed the role of AR in transcription. AR is a member of the steroid hormone receptor family, in which its signaling plays role in the normal function of prostate, as well as in the development and progression of PCa. It acts as a transcription factor that upon activation by androgens translocate to nucleus (Davey and Grossmann, 2016). It

activates transcription through chromatin remodeling that allows euchromatin, the recruitment of different transcription factors, mediator complex and the activation of transcription machinery factors as RNA pol II. Altogether, eventually upregulates transcription (Özturan et al., 2022). With the role of AR in transcription upregulation and chromatin modification, we indeed detected neither upregulation of methylated histones, using MS for histone PTMs (Fig. 28C), nor methylated global DNA (Fig. 29). That consequently, clarified the absence of enriched compact chromatin and methylated histone pathways in the proteomic analysis (Fig. 24D), contrarily to DU145 SPOP-KO clones. Additionally, this data explained the more chromatin accessibility we demonstrated in the promoter (Fig. 26D) and gene bodies (Fig. 26E) regions in LNCaP SPOP deficient sublines than in their proficient counterparts. Hence, the enhanced AR signal in SPOP deficient LNCaP cells, reverses the upregulated methylation of histones and DNA, caused by SPOP loss in DU145 cells, thereby, resulting in more accessible chromatin, and consequently, upregulated transcription.

Consistent with our results, AR has been previously shown to result in more open chromatin through different factors and proteins that modify the chromatin structure. Euchromatin occurs through histone PTMs as (i) histone acetyltransferases that acetylate different histones resulting in open chromatin, (ii) histone methylases that methylate histones on lysine residues, which allow for chromatin opening, as the mono and dimethylation of H3K4, and (iii) histone demethylases that demethylates histones associated with heterochromatin, as the methylated forms of H3K9 and H3K27 (Grbesa et al., 2021).

The enhanced AR signal in SPOP-KO LNCaP cells, which resulted in upregulated transcription (Fig. 19C) and its deviation from hemostasis, can explain the accumulation of R-loops (Fig. 17G&H) in cell cycle independent manner and DSBs. Indeed, treating the cells with Enzalutamide further confirmed that maintaining transcription in hemostasis is pivotal, otherwise, accumulates DSBs and R-loops. Where, the reduction in transcription to a level comparable to LNCaP parenteral cells with the 2 µM Enza, rescued LNCaP SPOP-KO clones and reduced the number of DSBs (Fig. 21C&D) and R-loops (Fig. 21A&B). Contrarily, it was no surprise to detect re-accumulation of R-loops (Fig. 21A&B) and DSBs (Fig. 21C&D), after the higher concertation of Enzalutamide (20 µM), which decreased the transcription below the normal level of LNCaP parenteral cells, imitating what happened in DU145 SPOP-KO cells.

In line with our results, previous studies have shown that AR upregulates R-loops and accumulates DSBs. Nicholas et al., previously demonstrated an upregulation of R-loops in Ewing sarcoma breakpoint region 1 (EWSR1) gene, by AR signaling as a result of its activity as transcription factor. This resulted in chromosomal breaks and rearrangements in Ewing Sarcoma (Nicholas et al., 2021). Additionally, another study reported that SPOP depletion by knockdown in LNCaP ($AR^+$) cells, resulted in increased DSBs as demonstrated by the accumulation of yH2AX foci spontaneously, but contrarily to us, they have not shown this accumulation in DU145 ($AR^-$). DSBs accumulation in $AR^+$ cells were attributed to Topoisomerase 2A (TOP2A), where they reported that AR mediated DSBs through TOP2. The depletion of SPOP, reduced Tyrosyl-DNA phosphodiestrases (TDPs) and endo/exonucleases Meiotic recombination 11(MRE11) that are essential for releasing TOP2A from its inactive complex with DNA. Therefore, the inactive TOP2A failed to complete DNA repair. In fact, Watanabe et al., contradicted their results, by reporting accumulation of spontaneous DSBs in $AR^+$ SPOP-KD cells only (Watanabe et al., 2020). Since, in this case, different DDR should have been revealed, however, they reported no change in DDR as indicated by pATM and pChK2, that indicate the absence of any damage. However, in our data we reported no change in DDR, yet, we still have accumulation in DSBs irrespective from AR status.

### 5.6. Proposed model for the mechanism of genomic instabilities in SPOP deficient PCa

Collectively, our study proposes a model for SPOP role in regulating genomic stability through controlling the transcription dynamics and chromatin accessibility. Therefore, SPOP loss affects the aforementioned processes, however depending on AR-status. On one hand, in AR-negative cells, SPOP loss decreases the chromatin accessibility due to increased DNA and histone methylation, leading to decreased/delayed transcription. On the other hand, in AR-positive cells, SPOP loss stimulates the activity of AR signaling, which in turn as a transcription factor stimulates the transcription activity. In both cases, unscheduled R-loops will be accumulated, which in turn lead to RS and DSBs accumulation in cell cycle-independent manner (Fig. 30). This indeed explains the worse prognosis of PCa patients with SPOP mutations (García-Flores et al., 2014).

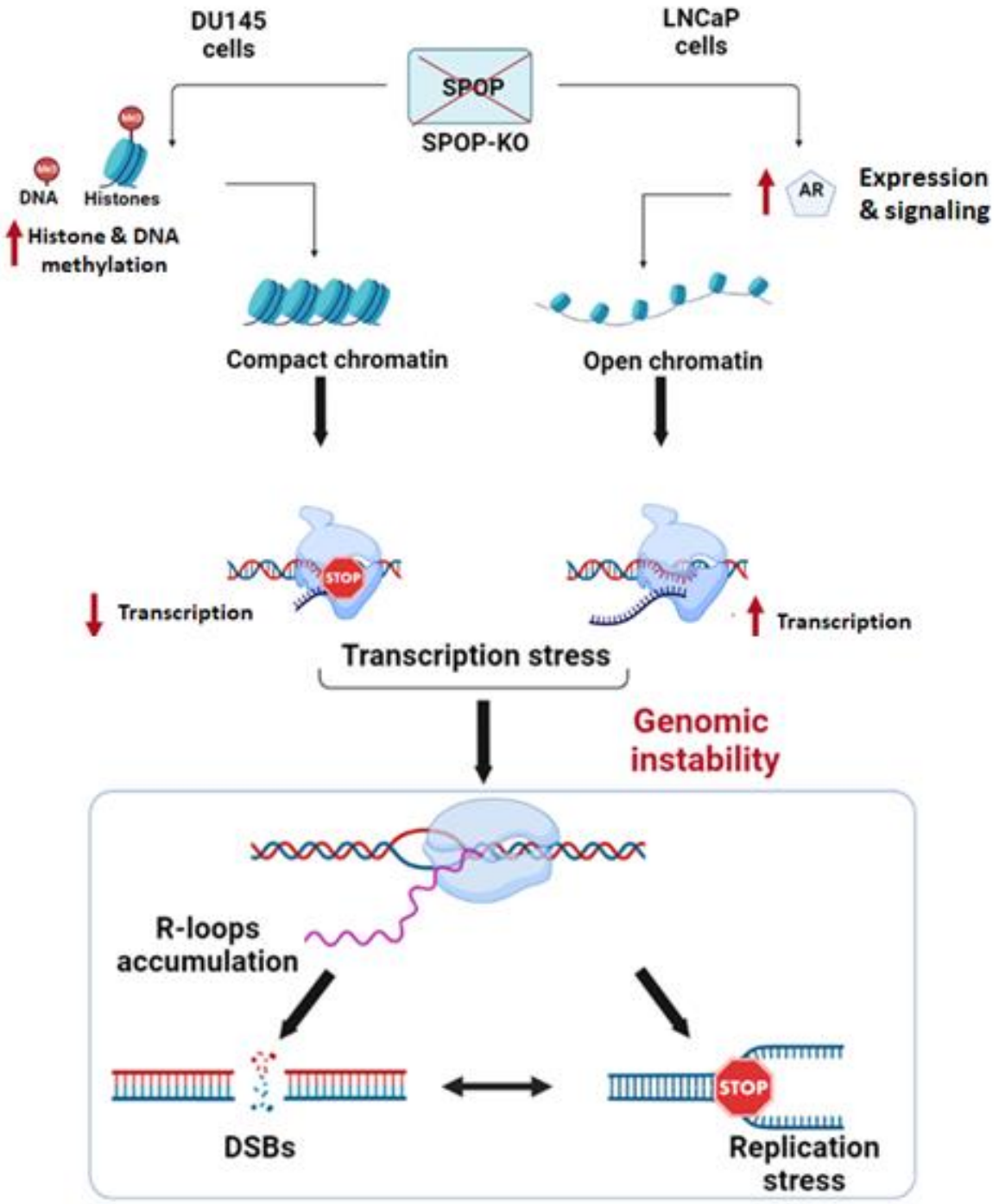


**Figure 30. Proposed model of the mechanism of genomic instabilities in SPOP-deficient PCa.** SPOP regulates the dynamics of transcription machinery through regulating the chromatin accessibility and hence, prevents the accumulation of R-loops and DSBs. Therefore, SPOP loss leads to the accumulation of both R-loops and DSBs, however, using different mechanisms according to the AR status. In AR-negative DU145 cells, SPOP loss results in increased DNA and histone methylation and with that decreased chromatin accessibility, leading to decreased/delayed transcription. In AR-positive cells, SPOP loss stimulates the activity of AR signaling, thereby, upregulates the transcription activity. In both cases, unscheduled R-loops, RS and DSBs will be

accumulated that eventually lead to genomic instability. This Figure was created in Biorender.com

## 5.7. Outlook

This study has elucidated a new mechanism for genomic instabilities in SPOP deficient cells of PCa, which can have profound implications on the discovery of new targeted medications to personalize the treatment and improve the survival. Therefore, as future directions:

**On the bench side**, we recommend further high throughput analysis that includes transcriptome analysis. This aims to identify whether SPOP affects different methyltransferases and demethylases that result in upregulation of DNA and histones methylation. Moreover, since our study revealed accumulation of spontaneous DSBs, whole genome sequencing can identify which genomic instabilities are associated with SPOP loss. Next, we are hoping to transfer this study from the **bench to bed side**, by unveiling new targeted therapy for SPOP mutated PCa patients. Where, we are aiming to use a specific library that targets the identified altered methyltransferases or demethylases. Thereby, identifying new therapies for testing in preclinical and clinical practice.

Additionally, SPOP has been described to be the most common mutated in prostate cancer and is associated with genomic instabilities (Boysen et al., 2015). Therefore, it is probably associated with high tumor mutational burden. Hence, patients with SPOP mutations can benefit from immune targeted therapy as programmed cell death 1 and its ligand checkpoint inhibitors (PDL-1 and PD1), in addition to cytotoxic T-lymphocyte antigen-4 (CTLA-4). Tumor mutational burden is defined as the number of somatic non synonymous mutations, which results in neo-antigens that stimulate immune response. Consequently, a defense mechanism is also triggered that involves checkpoints as PDL-1, thus protect against the immune response by stimulating self-tolerance. These checkpoints are expressed on the surface of tumors, thereby, tumors can escape immune response. Therefore, PDL-1 antagonists acts against these checkpoints to trigger immune response against tumors (Allgäuer et al., 2018; Wang et al., 2021). In addition, PDL-1 has previously been reported to be a substrate of SPOP, therefore, SPOP deficient cells may benefit from PDL-1 antagonists. As a result, different patients with SPOP deficient status through mutations can benefit from various new treatment options.

# 6. Summary and Zusammenfassung

## 6.1. Summary

PCa is the most common male cancer in Germany and the second leading cause of male cancer deaths. Genomic instability and DNA repair defects are considered hallmarks of PCa. PCa is mainly characterized by the presence of structural genomic rearrangements with the ERG fusion being the most common, in around 50% of the patients. However, unlike other cancers, point mutations are less common in PCa. Importantly, SPOP point mutations have been revealed in around 10-15 % of PCa, being the most frequent point mutated tumor suppressor gene in PCa. SPOP mutations have been associated with the highest frequency of genomic instabilities and worse prognosis in PCa. However, the mechanism is yet not fully characterized.

In this study, we aimed to unveil the mechanism underlying increased genomic instabilities associated with SPOP loss of function. To that end, we established SPOP-KO sublines from LNCaP ($AR^+$) and DU145 ($AR^-$) cells. The results of the current study can be summarized as follows:

I. In the AR-negative DU145 cells:

1. SPOP loss results in upregulated global DNA and histone methylation (measured by illumina HumanMethylation array and MS-based proteomics, respectively).
2. This leads to increased chromatin compaction and reduced chromatin accessibility (measured by ATAC-seq).
3. The reduced chromatin accessibility in DU145 SPOP-KO cells results in transcription stress and decreased transcription activity (measured by EU incorporation), due to decreased transcription dynamics, as revealed by profound reduction in RNA pol II phosphorylation at ser2p (a marker of active elongation).
4. Stalled transcription leads to accumulation of the RNA-DNA hybrid transcription intermediates R-loops (measured by IF).
5. The accumulation of unscheduled R-loops and slowed transcription activity result in replication stress (RS) upon colliding with the replication machinery (monitored by DNA fiber assay), leading to DSBs in S-phase (investigated by IF detection of γH2AX in EdU+ cells) and chromosomal aberrations.

6. Furthermore, DSBs are generated in G1 and G2 phases upon accumulation of unscheduled R-loops (measured by IF detection of γH2AX in EdU-/CenpF- and EdU-/CenpF+ cells, respectively).

II. In AR-positive (LNCaP) cells:

1. As, a substrate of SPOP, AR transcription signaling is enhanced, as illustrated by increased expression of AR and its downstream target PSA.
2. Given that AR is a transcription factor, its signal stimulation leads to enhanced transcription activity (as measured by increased EU incorporation), which masked the effect of SPOP loss on transcription.
3. Furthermore, no increase in global histone or DNA methylation was observed in these cells.
4. The unscheduled increase in transcription activity leads to accumulation of R-loops, RS and DSBs similar to SPOP-KO DU145 cells.

In conclusion, the current study unveils the role of SPOP in maintaining genomic stability through regulating chromatin accessibility and transcription dynamics to prevent transcription stress, accumulation of R-loops, RS and DSBs.

## 6.2. Zusammenfassung

Das Prostatakarzinom (PCa) ist die häufigste maligne Tumorerkrankung bei Männern in Deutschland und die zweithäufigste krebsbedingte krebsbedingte Todesursache. Genomische Instabilität und DNA Reparatur-Defekte sind typische Charakteristika des PCa, die sich oft in strukturellen genomischen Rearrangements äußern. Von diesen sind *ERG* Genfusionen die häufigste, die sich bei ca. 50% der Patienten findet. Anders als bei anderen Tumorerkrankungen sind Punktmutationen indes selten beim PCa. Eine häufige Punktmutation betrifft das *SPOP* Tumorsuppressor-Gen, welche bei 10-15% der Patienten meist früh zu Beginn der Erkrankung auftritt. *SPOP* Mutationen sind mit erhöhter genomischer Instabilität und einer schlechteren Prognose assoziiert. Die molekularen Auswkirkungen der Mutationen sind jedoch bisher unzureichen untersucht.

In diesem Projekt wurden die Mechanismen der genomischen Instabilität auf dem Boden der *SPOP*-Mutation mit Verlust der SPOP-Funktion weitergehend untersucht. Hierfür wurden *SPOP knockout* (KO) Zellen der hormonsensitiven, Androgenrezeptor-positiven ($AR^+$) PCa-Zelllinie LNCaP und der AR-negativen Zelllinie DU145 generiert. Die Ergebnisse des Projekts sind wiefolgt:

I. <u>$AR^-$ DU145 Zellen</u>

1. SPOP Verlust resultiert in einer globalen Zunahme der DNA und Histonmethylierung (bestimmt durch illumina HumanMethylation array und Massenspektrometrie-basierte Proteomanalyse).
2. Dies führt zu einer Verdichtung des Chromatins und vermindert Zugänglichkeit des Chromatins für regulatorische Proteine (analysiert durch ATAC-seq).
3. Die verminderte Zugänglichkeit des Chromatins in *SPOP*-KO DU145-Zellen resultiert in transkriptionalem Stress und verminderter transkriptionaler Aktivität (gemessen durch EU-Inkorporation) durch eine Verminderung der Transkriptionsdynamik, die sich in einer eindeutigen Reduktion der RNA pol II Phosphorylierung des ser2-Restes äußert (als Marker aktiver Elongation).
4. Eine unterbrochene Transkription führt zur Akkumulation von sog. R-loops als hybride RNA-DNA-Transkriptions-Zwischenstufe (bestimmt per IF).
5. Die Akkumulation außerplanmäßiger R-loops und verlangsamter transkriptionaler Aktivität induziert Replikationsstress (RS) bei Kollision mit der Replikationsgabel (analysiert mittels DNA Fiber Assay), was zu DNA-Doppelstrangbrüchen (DSB)

während der S-Phase führt (analysiert mittels IF-Messung von γH2AX in $EdU^+$ Zellen) und chromosomalen Aberrationen.

6. Darüber hinaus entstehen auch DSBs in der G1 und G2 Phase des Zellzyklus durch Akkumulation ungeplanter R-loops (analysiert mittels IF-Messung von γH2AX in EdU-/CenpF- und EdU-/CenpF+ Zellen).

II. $AR^+$ LNCaP Zellen

1. Die Transkription des AR, einem Substrat von SPOP, ist gesteigert in $AR^+$, SPOP-mutierten LNCaP-Zellen, was eine Überexpression des Prostata-spezifischen Antigens (PSA) als AR-Effektor führt.
2. Da AR ein Transkriptionsfaktor ist, führt dessen vermehrte Stimulation zu vermehrter transkriptionaler Aktivität (gemessen durch EU Inkorporation), was den Einfluss des SPOP-Verlusts auf die Transkription maskiert.
3. In diesen Zellen zeigte sich keine Veränderung des globalen DNA und Histonmethylierungsmusters in SPOP-KO Zellen.
4. Die induzierte Zunahme der AR-assoziierten Transkription führt zur Akkumulation von R-loops, RS und DSB ähnlich wie bei den AR- DU145-Zellen

Zusammenfassend illustriert das vorgestellte Projekt die Rolle von SPOP in der Erhaltung der genomischen Stabilität durch Regulation der Zugänglichkeit des Chromatins und der Dynamik der Transkription zur Verhinderung von Transkriptionsstress, der Akkumulation von R-loops, RS und DSBs.

## 7. List of abbreviations

| | |
|---|---|
| 3’-ssDNA | 3’ single stranded DNA |
| 53BP1 | p53-binding protein 1 |
| CAN | Acetonitrile |
| AQR | Aquarius |
| AR | Androgen receptor |
| ATAC-seq | Assay for Transposase-Accessible Chromatin using sequencing |
| ATF2 | Activating Transcription Factor 2 |
| $ATG_{art}$ | Artificial start codon |
| ATM | Ataxia-telangiectasia mutated |
| ATR | Ataxia telangiectasia and RAD3 related |
| BACK | BTB and C-terminal Kelch |
| BCL2 | B-cell lymphoma 2 |
| BER | Base excision repair |
| BRCA1 | Breast cancer gene 1 |
| BRCA2 | Breast cancer gene 2 |
| BRD4 | Bromodomain-containing protein 4 |
| BrdU | Bromodeoxyuridine |
| BTB | Broad-complex, tramtrack and bric-a-brac |
| Cas9 | CRISPR associated protein 9 |
| CRPC | castration resistant Prostate cancer |
| CD | Co-directional |
| Cdc20 | Cell Division Cycle 20 |
| CDC25 | Cell division cycle 25 A |
| CDK | Cyclin dependent kinase |
| CDK2 | Cyclin-dependent kinase 2 |
| CDK7 | Cyclin-dependent kinase 7 |
| CDK9 | Cyclin dependent kinase 9 |
| cDNA | Complementary DNA |
| CenpF | Centromere protein F |
| CHD1 | Chromatin remodeler chromodomain helicase DNA-binding protein 1 |
| ChK2 and ChK1 | Serine–threonine checkpoint effector protein kinases 2 and 1 |

| | |
|---|---|
| CID | Collision-induced dissociation |
| CldU | 5-Chloro-2'-deoxyuridine |
| CRISPR | Clustered regularly interspaced short palindromic repeats |
| CRPC | Castration resistant Prostate cancer |
| CTD | C-terminal domain |
| CtIP | Carboxy-terminal binding protein |
| CTLA-4 | cytotoxic T-lymphocyte antigen-4 |
| CUL3 | Cullin-3 |
| Cyc T | Cyclin T |
| Cyto-SPOP | Cytoplasmic SPOP |
| DAPI | 4′,6-Diamidin-2-phenylindol |
| Daxx | Death-associated protein 6 |
| dd.$H_2O$ | Distilled water |
| DDR | DNA damage response |
| DEK | DEK Proto-Oncogene |
| DHX9 | ATP-dependent nucleic acid helicase |
| D-loop | Displacement loop structure |
| DMEM | Dulbecco`s Modified Eagle Medium |
| DMSO | Dimethylsulfoxide |
| DNA-PK | DNA-dependent protein kinase |
| DNA-PKcs | DNA-dependent protein kinase complex |
| DNMT | DNA methyltransferase gene |
| DSBs | Double strand breaks |
| DSIF | DRB-sensitivity-inducing factor |
| DTs | Doubling times |
| DTT | Dithiothreitol |
| DUSP7 | Dual specificity protein phosphatase 7 |
| EDTA | Ethylenediamine tetraacetic acid |
| EdU | 5-ethynyl-2’-deoxyuridine |
| EglN2 | Egl-9 Family Hypoxia Inducible Factor 2 |
| EHTM1/2 | Euchromatic Histone Lysine Methyltransferase 1/2 |
| ERG | ETS related gene |
| ETS | E-26 transformation- specific |
| EU | 5-Ethynyl-uridine |

| | |
|---|---|
| EXO1 | Exonuclease 1 |
| FA | Formic acid |
| FACS | Fluorescence activated cell sorting |
| FANCD2 | FA complementation group D2 |
| FCS | Fetal Calf Serum |
| FDR | False discovery rate |
| FOXA1 | Forkhead box protein A1 |
| FSC | Forward scatter |
| Gli2 | GLI Family Zinc Finger 2 |
| GLP | G9a-like protein euchromatic methyltransferases |
| gRNA | Guide RNA |
| GSEA | Gene set enrichment analysis |
| GTF | General transcription factors |
| HC | Hierarchical clustering |
| HEXIM1 | Hexamethylene Bis- acetamide-inducible Protein 1 |
| HR | Homologous recombination |
| HPLC | High Performance Liquid Chromatography |
| IAA | Iodoacetamide |
| IDH1 | Isocitrate dehydrogenase 1 |
| IdU | 5-Iodo-2´-deoxyuridine |
| IF | Immunofluorescence |
| Indel | Insertion-deletions |
| IR | Ionizing radiation |
| Kb | Kilobase |
| KD | Knockdown |
| KO | Knockout |
| LARP7 | La-related Protein 7 |
| LC-MS/MS | Liquid Chromatography with tandem mass spectrometry |
| MATH | Meprin and TRAF-C homology |
| Mb | Megabase |
| MCL | Markov cluster algorithm |
| MDC1 | DNA damage checkpoint protein 1 |
| MePCE | 7SK snRNA Methyl phosphate Capping Enzyme |
| MLH1 | MutL homolog 1 |

| | |
|---|---|
| MMR | Mismatch repair |
| MRE11 | Meiotic recombination 11 |
| MSH2/6 | MutS homolog 2/6 |
| MYC | MYC Proto-Oncogene |
| NaCl | Sodium Chloride |
| NaOH | Sodium Hydroxide |
| NELF | Negative elongation factor |
| NER | Nucleotide excision repair |
| NGS | Next generation sequencing |
| NH4C03 | Ammonium bicarbonate |
| NHEJ | Non homologous end joining |
| NLS | Nuclear localization sequence |
| nt | Nucleotide |
| P | Parenteral cells |
| p53 | p53 tumor suppressor protein |
| PAM | Protospacer adjacent motif |
| PAM | protospacer adjacent motif |
| PARP1 | Poly [ADP-ribose] polymerase 1 |
| pATM/pATR | Phosphorylated ATM/ATR |
| PBS | Phosphate buffer solution |
| PC 1 or 2 | Principal component 1 or 2 |
| PCA | Principal component analysis |
| PCa | Prostate cancer |
| pCDK9 | Phosphorylated cyclin dependent kinase 9 |
| pChK2 and pChK1 | Phosphorylated ChK2 and ChK1 |
| PCNA | Proliferating cell nuclear antigen |
| PCR | Polymerase chain reaction |
| PDL-1 | programmed cell death 1 and its ligand |
| PFA | Paraformaldehyde |
| PI3K/AKT | Phosphoinositide-3-kinase–protein kinase B/Akt |
| PIKKs | Phosphatidyleinositol 3-kinase-like protein kinase |
| PMS2 | PMS1 Homolog 2 |
| PMSF | Phenylmethylsulfonyl fluoride |

| | |
|---|---|
| PS | Penicillin/Streptomycin |
| PSA | Prostate specific antigen |
| p-TEFb | Positive transcription elongation factor b |
| PTEN | Phosphatase and Tensin Homolog |
| PTMs | Histone post translational modifications |
| RAD51 | RAD51 Recombinase |
| RAD54L | RAD54 Like |
| RCC | Renal cell carcinoma |
| RIF1 | RAP1-interacting factor 1 |
| R-loops | RNA-DNA hybrids |
| RMI2 | RecQ Mediated Genome Instability 2 |
| RNA pol II | RNA polymerase II |
| RNA pol II ser2p | RNA pol II phosphorylated on serine 2 |
| RNA pol II ser5p | RNA pol II phosphorylated on serine 5 |
| RNase H1 and 2 | Ribonucleases H1 and 2 |
| ROS | Reactive oxygen species |
| RPA | Replication protein A |
| RS | Replication stress |
| SDC | Sodium deoxy cholate |
| SDS | Sodiumdodecylsulfat |
| SDS-PAGE | Sodium dodecyl sulfate–polyacrylamide gel electrophoresis |
| SENP7 | SUMO Specific Peptidase 7 |
| ser | Serine |
| SETX | Senataxin |
| snRNP | 7SK small nuclear ribonucleo-protein |
| SPOP | Speckle-type POZ protein |
| SRC3 | Steroid receptor coactivator-3 |
| SSC | Sideward scatter |
| ssDNA | Single stranded DNA |
| sgRNA | Single guide RNA |
| T186 | Threonine 186 |
| TC-NER | Transcription associated NER |
| TDPs | Tyrosyl-DNA phosphodiestrases |
| TEAB | Triethly ammonium-borate |

| | |
|---|---|
| TF | Transcription factors |
| TFIIH | Transcription factor II Human |
| TG | Tris/Glycin buffer |
| TMPRSS | Transmembrane Serine Protease 2 |
| Tn5 | Transposase |
| TOP2A | Topoisomerase 2A |
| TDPs | Tyrosyl-DNA phosphodiestrases |
| TRIM24 | Tripartite Motif Containing 24 |
| TSS | Transcription start site |
| UPLC | Ultra Performance Liquid Chromatography |
| UV | Ultraviolet light |
| WB | Western Blot |
| WT | Wild type cells |
| XLF | XRCC4-like factor |
| XPC | Xeroderma pigmentosum complementation group C |
| XPF | Xeroderma pigmentosum type F |
| XPG | Xeroderma pigmentosum type G |
| XRCC4 | X-ray cross complementation |
| γH2AX | Phosphorylated histone variant ‘H2AX’ |

## 8. References

Abeshouse, A., Ahn, J., Akbani, R., Ally, A., Amin, S., Andry, C. D., Annala, M., Aprikian, A., Armenia, J., Arora, A., Auman, J. T., Balasundaram, M., Balu, S., Barbieri, C. E., Bauer, T., Benz, C. C., Bergeron, A., Beroukhim, R., Berrios, M., Zmuda, E. (2015). The Molecular Taxonomy of Primary Prostate Cancer. Cell, 163(4), 1011–1025.

Adamo, P., & Ladomery, M. R. (2016). The oncogene ERG: A key factor in prostate cancer. In Oncogene (Vol. 35, Issue 4, pp. 403–414).

Adelman, K., & Lis, J. T. (2012). Promoter-proximal pausing of RNA polymerase II: emerging roles in metazoans. In Nature reviews. Genetics (Vol. 13, Issue 10, pp. 720–731).

Aguilera, A., & García-Muse, T. (2012). R Loops: From Transcription Byproducts to Threats to Genome Stability. In Molecular Cell (Vol. 46, Issue 2, pp. 115–124).

Al-Ubaidi, F. L. T., Schultz, N., Loseva, O., Egevad, L., Granfors, T., & Helleday, T. (2013). Castration therapy results in decreased Ku70 levels in prostate cancer. Clinical Cancer Research, 19(6), 1547–1556.

Allgäuer, M., Budczies, J., Christopoulos, P., Endris, V., Lier, A., Rempel, E., Volckmar, A. L., Kirchner, M., von Winterfeld, M., Leichsenring, J., Neumann, O., Fröhling, S., Penzel, R., Thomas, M., Schirmacher, P., & Stenzinger, A. (2018). Implementing tumor mutational burden (TMB) analysis in routine diagnostics—a primer for molecular pathologists and clinicians. In Translational Lung Cancer Research (Vol. 7, Issue 6, pp. 703–715).

Allison, D. F., & Wang, G. G. (2019). R-loops: Formation, function, and relevance to cell stress. In Cell Stress (Vol. 3, Issue 2, pp. 38–46).

Angeles, A., Bauer, S., Ratz, L., Klauck, S., & Sültmann, H. (2018). Genome-Based Classification and Therapy of Prostate Cancer. Diagnostics, 8(3), 62.

Bacon, C. W., & D'Orso, I. (2019). CDK9: a signaling hub for transcriptional control. Transcription, 10(2), 57–75.

Bakr, A., Köcher, S., Volquardsen, J., Reimer, R., Borgmann, K., Dikomey, E., Rothkamm, K., & Mansour, W. Y. (2016). Functional crosstalk between DNA damage response proteins 53BP1 and BRCA1 regulates double strand break repair choice. Radiotherapy and Oncology, 119(2), 276–281.

Bakr, A., Oing, C., Köcher, S., Borgmann, K., Dornreiter, I., Petersen, C., Dikomey, E., & Mansour, W. Y. (2015). Involvement of ATM in homologous recombination after end resection and RAD51 nucleofilament formation. Nucleic Acids Research, 43(6), 3154–3166.

Bangma, C. H., & Roobol, M. J. (2012). Defining and predicting indolent and low risk prostate cancer. In Critical Reviews in Oncology/Hematology (Vol. 83, Issue 2, pp. 235–241).

Barbieri, C. E., Baca, S. C., Lawrence, M. S., Demichelis, F., Blattner, M., Theurillat, J. P., White, T. A., Stojanov, P., Van Allen, E., Stransky, N., Nickerson, E., Chae, S. S., Boysen, G., Auclair, D., Onofrio, R. C., Park, K., Kitabayashi, N., MacDonald, T. Y., Sheikh, K., Garraway, L. A. (2012). Exome sequencing identifies recurrent SPOP, FOXA1 and MED12 mutations in prostate cancer. Nature Genetics, 44(6), 685–689.

Barbieri, C. E., & Rubin, M. A. (2015). Genomic rearrangements in prostate cancer. In Current Opinion in Urology (Vol. 25, Issue 1, pp. 71–76).

Baumli, S., Lolli, G., Lowe, E. D., Troiani, S., Rusconi, L., Bullock, A. N., Debreczeni, J. É., Knapp, S., & Johnson, L. N. (2008). The structure of P-TEFb (CDK9/cyclin T1), its complex with flavopiridol and regulation by phosphorylation. EMBO Journal, 27(13), 1907–1918.

Belotserkovskii, B. P., Tornaletti, S., D'Souza, A. D., & Hanawalt, P. C. (2018). R-loop generation during transcription: Formation, processing and cellular outcomes. In DNA Repair (Vol. 71, pp. 69–81).

Berger, M. F., Lawrence, M. S., Demichelis, F., Drier, Y., Cibulskis, K., Sivachenko, A. Y., Sboner, A., Esgueva, R., Pflueger, D., Sougnez, C., Onofrio, R., Carter, S. L., Park, K., Habegger, L., Ambrogio, L., Fennell, T., Parkin, M., Saksena, G., Voet, D., Garraway, L. A. (2011). The genomic complexity of primary human prostate cancer. Nature, 470(7333), 214–220.

Beucher, A., Birraux, J., Tchouandong, L., Barton, O., Shibata, A., Conrad, S., Goodarzi, A. A., Krempler, A., Jeggo, P. A., & Löbrich, M. (2009). ATM and Artemis promote homologous recombination of radiation-induced DNA double-strand breaks in G2. EMBO Journal, 28(21), 3413–3427.

Bindra, R. S., Schaffer, P. J., Meng, A., Woo, J., Måseide, K., Roth, M. E., Lizardi, P., Hedley, D. W., Bristow, R. G., & Glazer, P. M. (2004). Down-Regulation of Rad51 and Decreased Homologous Recombination in Hypoxic Cancer Cells. Molecular and Cellular Biology, 24(19), 8504–8518.

Blattner, M., Liu, D., Robinson, B. D., Huang, D., Poliakov, A., Gao, D., Nataraj, S., Deonarine, L. D., Augello, M. A., Sailer, V., Ponnala, L., Ittmann, M., Chinnaiyan, A. M., Sboner, A., Chen, Y., Rubin, M. A., & Barbieri, C. E. (2017). SPOP Mutation Drives Prostate Tumorigenesis In Vivo through Coordinate Regulation of PI3K/mTOR and AR Signaling. Cancer Cell, 31(3), 436–451.

Boutros, R., Lobjois, V., & Ducommun, B. (2007). CDC25 phosphatases in cancer cells: Key players? Good targets? In Nature Reviews Cancer (Vol. 7, Issue 7, pp. 495–507).

Boysen, G., Barbieri, C. E., Prandi, D., Blattner, M., Chae, S.-S., Dahija, A., Nataraj, S., Huang, D., Marotz, C., Xu, L., Huang, J., Lecca, P., Chhangawala, S., Liu, D., Zhou, P., Sboner, A., de Bono, J. S., Demichelis, F., Houvras, Y., & Rubin, M. A. (2015). SPOP mutation leads to genomic instability in prostate cancer. ELife, 4.

Brandsma, I., & Gent, D. C. (2012). Pathway choice in DNA double strand break repair: Observations of a balancing act. In Genome Integrity (Vol. 3, Issue 1, pp. 1–10).

Brenner, J. C., & Chinnaiyan, A. M. (2011). Disruptive Events in the Life of Prostate Cancer. In Cancer Cell (Vol. 19, Issue 3, pp. 301–303).

Brookes, E., & Pombo, A. (2009). Modifications of RNA polymerase II are pivotal in regulating gene expression states. In EMBO Reports (Vol. 10, Issue 11, pp. 1213–1219).

Buenrostro, J. D., Giresi, P. G., Zaba, L. C., Chang, H. Y., & Greenleaf, W. J. (2013). Transposition of native chromatin for fast and sensitive epigenomic profiling of open chromatin, DNA-binding proteins and nucleosome position. Nature Methods, 10(12), 1213–1218.

Canman, C. E., Lim, D. S., Cimprich, K. A., Taya, Y., Tamai, K., Sakaguchi, K., Appella, E., Kastan, M. B., & Siliciano, J. D. (1998). Activation of the ATM kinase by ionizing radiation and phosphorylation of p53. Science, 281(5383), 1677–1679.

Christianson, J. C., & Ye, Y. (2014). Cleaning up in the endoplasmic reticulum: Ubiquitin in charge. In Nature Structural and Molecular Biology (Vol. 21, Issue 4, pp. 325–335).

Cleaver, J. E., Lam, E. T., & Revet, I. (2009). Disorders of nucleotide excision repair: The genetic and molecular basis of heterogeneity. In Nature Reviews Genetics (Vol. 10, Issue 11, pp. 756–768).

Corces, M. R., Trevino, A. E., Hamilton, E. G., Greenside, P. G., Sinnott-Armstrong, N. A., Vesuna, S., Satpathy, A. T., Rubin, A. J., Montine, K. S., Wu, B., Kathiria, A., Cho, S. W., Mumbach, M. R., Carter, A. C., Kasowski, M., Orloff, L. A., Risca, V. I., Kundaje, A., Khavari, P. A., Chang, H. Y. (2017). An improved ATAC-seq protocol reduces background and enables interrogation of frozen tissues. Nature Methods, 14(10), 959–962.

Core, L., & Adelman, K. (2019). Promoter-proximal pausing of RNA polymerase II: a nexus of gene regulation. Genes & Development, 33(15–16), 960–982.

Crossley, M. P., Bocek, M., & Cimprich, K. A. (2019). R-Loops as Cellular Regulators and Genomic Threats. Molecular Cell, 73(3), 398–411.

Cruz, C., Castroviejo-Bermejo, M., Gutiérrez-Enríquez, S., Llop-Guevara, A., Ibrahim, Y. H., Gris-Oliver, A., Bonache, S., Morancho, B., Bruna, A., Rueda, O. M., Lai, Z., Polanska, U. M., Jones, G. N., Kristel, P., de Bustos, L., Guzman, M., Rodríguez, O., Grueso, J., Montalban, G., Serra, V. (2018). RAD51 foci as a functional biomarker of homologous recombination repair and PARP inhibitor resistance in germline BRCA-mutated breast cancer. Annals of Oncology, 29(5), 1203–1210.

Dai, X., Gan, W., Li, X., Wang, S., Zhang, W., Huang, L., Liu, S., Zhong, Q., Guo, J., Zhang, J., Chen, T., Shimizu, K., Beca, F., Blattner, M., Vasudevan, D., Buckley, D. L., Qi, J., Buser, L., Liu, P., Wei, W. (2017). Prostate cancer-Associated SPOP

mutations confer resistance to BET inhibitors through stabilization of BRD4. Nature Medicine, 23(9), 1063–1071.

Davey, R. A., & Grossmann, M. (2016). Androgen Receptor Structure, Function and Biology: From Bench to Bedside. The Clinical Biochemist. Reviews, 37(1), 3–15.

David, S. S., O'Shea, V. L., & Kundu, S. (2007). Base-excision repair of oxidative DNA damage. In Nature (Vol. 447, Issue 7147, pp. 941–950).

Eid, W., Steger, M., El-Shemerly, M., Ferretti, L. P., Peña-Diaz, J., König, C., Valtorta, E., Sartori, A. A., & Ferrari, S. (2010). DNA end resection by CtIP and exonuclease 1 prevents genomic instability. EMBO Reports, 11(12), 962–968.

El Bezawy, R., Tripari, M., Percio, S., Cicchetti, A., Tortoreto, M., Stucchi, C., Tinelli, S., Zuco, V., Doldi, V., Gandellini, P., Valdagni, R., & Zaffaroni, N. (2020). SPOP deregulation improves the radiation response of prostate cancer models by impairing DNA damage repair. Cancers, 12(6), 1462.

Errington, W. J., Khan, M. Q., Bueler, S. A., Rubinstein, J. L., Chakrabartty, A., & Privé, G. G. (2012). Adaptor protein self-assembly drives the control of a cullin-RING ubiquitin ligase. Structure, 20(7), 1141–1153.

Escribano-Díaz, C., Orthwein, A., Fradet-Turcotte, A., Xing, M., Young, J. T. F., Tkáč, J., Cook, M. A., Rosebrock, A. P., Munro, M., Canny, M. D., Xu, D., & Durocher, D. (2013). A Cell Cycle-Dependent Regulatory Circuit Composed of 53BP1-RIF1 and BRCA1-CtIP Controls DNA Repair Pathway Choice. Molecular Cell, 49(5), 872–883.

Faber, G. P., Nadav-Eliyahu, S., & Shav-Tal, Y. (2022). Nuclear speckles - a driving force in gene expression. In Journal of cell science (Vol. 135, Issue 13).

Farlow, A., Meduri, E., & Schlötterer, C. (2011). DNA double-strand break repair and the evolution of intron density. Trends in Genetics, 27(1), 1–6.

Feher, J. M., Nagy, A., & Flasko, T. (1994). Epidemiology of prostate cancer. Magyar Urologia, 6(3), 229–232.

Fernandez-Capetillo, O., Lee, A., Nussenzweig, M., & Nussenzweig, A. (2004). H2AX: The histone guardian of the genome. In DNA Repair (Vol. 3, Issues 8–9, pp. 959–967).

Fialova, B., Luzna, P., Gursky, J., Langova, K., Kolar, Z., & Trtkova, K. S. (2016). Epigenetic modulation of AR gene expression in prostate cancer DU145 cells with the combination of sodium butyrate and 5'-Aza-2'-deoxycytidine. Oncology Reports, 36(4), 2365–2374.

Frank, S., Nelson, P., Vasioukhin, V., Antonarakis, E. S., & Hopkins, J. (2018). Recent advances in prostate cancer research: large-scale genomic analyses reveal novel driver mutations and DNA repair defects. F1000Research, 7, 1173.

Frappart, P. O., & McKinnon, P. J. (2006). Ataxia-telangiectasia and related diseases. In NeuroMolecular Medicine (Vol. 8, Issue 4, pp. 495–511).

Galganski, L., Urbanek, M. O., & Krzyzosiak, W. J. (2017). Nuclear speckles: molecular organization, biological function and role in disease. Nucleic Acids Research, 45(18), 10350–10368.

Gallagher, D. J., Gaudet, M. M., Pal, P., Kirchhoff, T., Balistreri, L., Vora, K., Bhatia, J., Stadler, Z., Fine, S. W., Reuter, V., Zelefsky, M., Morris, M. J., Scher, H. I., Klein, R. J., Norton, L., Eastham, J. A., Scardino, P. T., Robson, M. E., & Offit, K. (2010). Germline BRCA mutations denote a clinicopathologic subset of prostate cancer. Clinical Cancer Research, 16(7), 2115–2121.

Gan, W., Dai, X., Lunardi, A., Li, Z., Inuzuka, H., Liu, P., Varmeh, S., Zhang, J., Cheng, L., Sun, Y., Asara, J. M., Beck, A. H., Huang, J., Pandolfi, P. P., & Wei, W. (2015). SPOP Promotes Ubiquitination and Degradation of the ERG Oncoprotein to Suppress Prostate Cancer Progression. Molecular Cell, 59(6), 917–930.

Gao, K., Jin, X., Tang, Y., Ma, J., Peng, J., Yu, L., Zhang, P., & Wang, C. (2015). Tumor suppressor SPOP mediates the proteasomal degradation of progesterone receptors (PRs) in breast cancer cells. American Journal of Cancer Research, 5(10), 3210–3220.

García-Flores, M., Casanova-Salas, I., Rubio-Briones, J., Calatrava, A., Domínguez-Escrig, J., Rubio, L., Ramírez-Backhaus, M., Fernández-Serra, A., García-Casado, Z., & López-Guerrero, J. A. (2014). Clinico-pathological significance of the molecular alterations of the SPOP gene in prostate cancer. European Journal of Cancer, 50(17), 2994–3002.

García-Muse, T., & Aguilera, A. (2016). Transcription–replication conflicts: how they occur and how they are resolved. Nature Reviews Molecular Cell Biology 2016 17:9, 17(9), 553–563.

Gates, L. A., Foulds, C. E., & O'Malley, B. W. (2017). Histone Marks in the 'Driver's Seat': Functional Roles in Steering the Transcription Cycle. In Trends in Biochemical Sciences (Vol. 42, Issue 12, pp. 977–989).

Geis-Asteggiante, L., Dhabaria, A., Edwards, N., Ostrand-Rosenberg, S., & Fenselau, C. (2015). Top-down analysis of low mass proteins in exosomes shed by murine myeloid-derived suppressor cells. International Journal of Mass Spectrometry, 378, 264–269.

Geng, C., He, B., Xu, L., Barbieri, C. E., Eedunuri, V. K., Chew, S. A., Zimmermann, M., Bond, R., Shou, J., Li, C., Blattner, M., Lonard, D. M., Demichelis, F., Coarfa, C., Rubin, M. A., Zhou, P., O'Malley, B. W., & Mitsiades, N. (2013). Prostate cancer-associated mutations in speckle-type POZ protein (SPOP) regulate steroid receptor coactivator 3 protein turnover. Proceedings of the National Academy of Sciences of the United States of America, 110(17), 6997–7002.

Geng, C., Kaochar, S., Li, M., Rajapakshe, K., Fiskus, W., Dong, J., Foley, C., Dong, B., Zhang, L., Kwon, O. J., Shah, S. S., Bolaki, M., Xin, L., Ittmann, M., O'Malley, B. W., Coarfa, C., & Mitsiades, N. (2017). SPOP regulates prostate epithelial cell

proliferation and promotes ubiquitination and turnover of c-MYC oncoprotein. Oncogene, 36(33), 4767–4777.

Geng, C., Rajapakshe, K., Shah, S. S., Shou, J., Eedunuri, V. K., Foley, C., Fiskus, W., Rajendran, M., Chew, S. A., Zimmermann, M., Bond, R., He, B., Coarfa, C., & Mitsiades, N. (2014). Androgen Receptor Is the Key Transcriptional Mediator of the Tumor Suppressor SPOP in Prostate Cancer. Cancer Research, 74(19), 5631–5643.

GenScript.com. (2016). The CRISPR Genome Editing Revolution Evolution of Genome Editing Technology Discovery of CRISPR in Bacterial Immune Systems (Issue September). www.genscript.com/CRISPR-handbook.html

Globocan. (2020). Cancer Today. International Agency for Research. https://gco.iarc.fr/today/online-analysis/pie?v=2020&mode=cancer&mode_population=continents&population=900&populations=900&key=total&sex=1&cancer=39&type=0&statistic=5&prevalence=0&population_group=0&ages_group%5B%5D=0&ages_group%5B%5D=17&nb_items=7&group

Goodwin, J. F., Schiewer, M. J., Dean, J. L., Schrecengost, R. S., de Leeuw, R., Han, S., Ma, T., Den, R. B., Dicker, A. P., Feng, F. Y., & Knudsen, K. E. (2013). A hormone-DNA repair circuit governs the response to genotoxic insult. Cancer Discovery, 3(11), 1254–1271.

Grbesa, I., Augello, M. A., Liu, D., McNally, D. R., Gaffney, C. D., Huang, D., Lin, K., Ivenitsky, D., Goueli, R., Robinson, B. D., Khani, F., Deonarine, L. D., Blattner, M., Elemento, O., Davicioni, E., Sboner, A., & Barbieri, C. E. (2021). Reshaping of the androgen-driven chromatin landscape in normal prostate cells by early cancer drivers and effect on therapeutic sensitivity. Cell Reports, 36(10), 109625.

Groner, A. C., Cato, L., de Tribolet-Hardy, J., Bernasocchi, T., Janouskova, H., Melchers, D., Houtman, R., Cato, A. C. B., Tschopp, P., Gu, L., Corsinotti, A., Zhong, Q., Fankhauser, C., Fritz, C., Poyet, C., Wagner, U., Guo, T., Aebersold, R., Garraway, L. A., … Brown, M. (2016a). TRIM24 Is an Oncogenic Transcriptional Activator in Prostate Cancer. Cancer Cell, 29(6), 846–858.

Ha, M. (2020). Transcription boosting by nuclear speckles. Nature Reviews Molecular Cell Biology, 21(2), 64–65.

Haffner, M. C., De Marzo, A. M., Meeker, A. K., Nelson, W. G., & Yegnasubramanian, S. (2011). Transcription-induced DNA double strand breaks: Both oncogenic force and potential therapeutic target? In Clinical Cancer Research (Vol. 17, Issue 12, pp. 3858–3864).

Hamperl, S., Bocek, M. J., Saldivar, J. C., Swigut, T., & Cimprich, K. A. (2017). Transcription-Replication Conflict Orientation Modulates R-Loop Levels and Activates Distinct DNA Damage Responses. Cell, 170(4), 774-786.e19.

Helena, J., Joubert, A., Grobbelaar, S., Nolte, E., Nel, M., Pepper, M., Coetzee, M., & Mercier, A. (2018). Deoxyribonucleic Acid Damage and Repair: Capitalizing on Our

Understanding of the Mechanisms of Maintaining Genomic Integrity for Therapeutic Purposes. International Journal of Molecular Sciences, 19(4), 1148.

Helleday, T., Lo, J., van Gent, D. C., & Engelward, B. P. (2007). DNA double-strand break repair: From mechanistic understanding to cancer treatment. DNA Repair, 6(7), 923–935.

Helleday, T., Petermann, E., Lundin, C., Hodgson, B., & Sharma, R. A. (2008). DNA repair pathways as targets for cancer therapy. In Nature Reviews Cancer (Vol. 8, Issue 3, pp. 193–204).

Hernández-Llodrà, S., Segalés, L., Juanpere, N., Marta Lorenzo, T., Salido, M., Nonell, L., David López, T., Rodríguez-Vida, A., Bellmunt, J., Fumadó, L., Cecchini, L., & Lloreta-Trull, J. (2021). SPOP and CHD1 alterations in prostate cancer: Relationship with PTEN loss, tumor grade, perineural infiltration, and PSA recurrence. Prostate, 81(16), 1267–1277.

Hernández-Muñoz, I., Lund, A. H., Van Der Stoop, P., Boutsma, E., Muijrers, I., Verhoeven, E., Nusinow, D. A., Panning, B., Marahrens, Y., & Van Lohuizen, M. (2005). Stable X chromosome inactivation involves the PRC1 Polycomb complex and requires histone MACROH2A1 and the CULLIN3/SPOP ubiquitin E3 ligase. Proceedings of the National Academy of Sciences of the United States of America, 102(21), 7635–7640.

Hjorth-Jensen, K., Maya-Mendoza, A., Dalgaard, N., Sigurðsson, J. O., Bartek, J., Iglesias-Gato, D., Olsen, J. V., & Flores-Morales, A. (2018). SPOP promotes transcriptional expression of DNA repair and replication factors to prevent replication stress and genomic instability. Nucleic Acids Research, 46(18), 9484–9495.

Hopkins, J. L., Lan, L., & Zou, L. (2022). DNA repair defects in cancer and therapeutic opportunities. In Genes and Development (Vol. 34, Issues 5–6, pp. 278–293).

Hsin, J. P., & Manley, J. L. (2012). The RNA polymerase II CTD coordinates transcription and RNA processing. In Genes and Development (Vol. 26, Issue 19, pp. 2119–2137).

Huang, S., Gulzar, Z. G., Salari, K., Lapointe, J., Brooks, J. D., & Pollack, J. R. (2012). Recurrent deletion of CHD1 in prostate cancer with relevance to cell invasiveness. Oncogene, 31(37), 4164–4170.

Huang, Y., Tan, N., Jia, D., Jing, Y., Wang, Q., Li, Z., Zhang, J., Liu, L., Li, J., Chen, Z., & He, X. (2015). Speckle-type POZ protein is negatively associated with malignancies and inhibits cell proliferation and migration in liver cancer. Tumor Biology, 36(12), 9753–9761.

Irshad, S., Bansal, M., Castillo-Martin, M., Zheng, T., Aytes, A., Wenske, S., Le Magnen, C., Guarnieri, P., Sumazin, P., Benson, M. C., Shen, M. M., Califano, A., & Abate-Shen, C. (2013). A molecular signature predictive of indolent prostate cancer. Science Translational Medicine, 5(202).

Jackson, D. A., & Pombo, A. (1998). Replicon Clusters Are Stable Units of Chromosome Structure: Evidence That Nuclear Organization Contributes to the Efficient Activation and Propagation of S Phase in Human Cells. The Journal of Cell Biology, 140(6), 1285.

Jackson, S. P. (2002). Sensing and repairing DNA double-strand breaks. In Carcinogenesis (Vol. 23, Issue 5, pp. 687–696).

Jackson, S. P., & Bartek, J. (2009). The DNA-damage response in human biology and disease. Nature, 461(7267), 1071.

Jager, M., Blokzijl, F., Kuijk, E., Bertl, J., Vougioukalaki, M., Janssen, R., Besselink, N., Boymans, S., de Ligt, J., Pedersen, J. S., Hoeijmakers, J., Pothof, J., van Boxtel, R., & Cuppen, E. (2019). Deficiency of nucleotide excision repair is associated with mutational signature observed in cancer. Genome Research, 29(7), 1067–1077.

Jamaspishvili, T., Berman, D. M., Ross, A. E., Scher, H. I., De Marzo, A. M., Squire, J. A., & Lotan, T. L. (2018). Clinical implications of PTEN loss in prostate cancer. In Nature Reviews Urology (Vol. 15, Issue 4, pp. 222–234).

Janouskova, H., El Tekle, G., Bellini, E., Udeshi, N. D., Rinaldi, A., Ulbricht, A., Bernasocchi, T., Civenni, G., Losa, M., Svinkina, T., Bielski, C. M., Kryukov, G. V., Cascione, L., Napoli, S., Enchev, R. I., Mutch, D. G., Carney, M. E., Berchuck, A., Winterhoff, B. J. N., Theurillat, J. P. P. (2017). Opposing effects of cancer-Type-specific SPOP mutants on BET protein degradation and sensitivity to BET inhibitors. Nature Medicine, 23(9), 1046–1054.

Jao, C. Y., & Salic, A. (2008). Exploring RNA transcription and turnover in vivo by using click chemistry. Proceedings of the National Academy of Sciences of the United States of America, 105(41), 15779–15784.

Jarrard, D. F., Kinoshita, H., Shi, Y., Sandefur, C., Hoff, D., Meisner, L. F., Chang, C., Herman, J. G., Isaacs, W. B., & Nassif, N. (1998). Methylation of the androgen receptor promoter CpG island is associated with loss of androgen receptor expression in prostate cancer cells. Cancer Research, 58(23), 5310–5314.

Jeong, E. K., La, M., Kyu, H. O., Young, M. O., Gi, R. K., Jae, H. S., Sung, H. B., Chiba, T., Tanaka, K., Ok, S. B., Joe, C. O., & Chin, H. C. (2006). BTB domain-containing speckle-type POZ protein (SPOP) serves as an adaptor of Daxx for ubiquitination by Cul3-based ubiquitin ligase. Journal of Biological Chemistry, 281(18), 12664–12672.

Jiricny, J. (2006). The multifaceted mismatch-repair system. In Nature Reviews Molecular Cell Biology (Vol. 7, Issue 5, pp. 335–346).

Jonkers, I., & Lis, J. T. (2015). Getting up to speed with transcription elongation by RNA polymerase II. Nature Reviews Molecular Cell Biology, 16(3), 167–177.

Ju, L. G., Zhu, Y., Long, Q. Y., Li, X. J., Lin, X., Tang, S. B., Yin, L., Xiao, Y., Wang, X. H., Li, L., Zhang, L., & Wu, M. (2019). SPOP suppresses prostate cancer through

regulation of CYCLIN E1 stability. Cell Death and Differentiation, 26(6), 1156–1168.

Jung, S.-H., Shin, S., Kim, M. S., Baek, I.-P., Lee, J. Y., Lee, S. H., Kim, T.-M., Lee, S. H., & Chung, Y.-J. (2016). Genetic Progression of High Grade Prostatic Intraepithelial Neoplasia to Prostate Cancer. European Urology, 69(5), 823–830.

Kamoun, A., Cancel-Tassin, G., Fromont, G., Elarouci, N., Armenoult, L., Ayadi, M., Irani, J., Leroy, X., Villers, A., Fournier, G., Doucet, L., Boyault, S., Brureau, L., Multigner, L., Diedhiou, A., Roupret, M., Compérat, E., Blanchet, P., De Reyniès, A., & Cussenot, O. (2018). Comprehensive molecular classification of localized prostate adenocarcinoma reveals a tumour subtype predictive of non-aggressive disease. Annals of Oncology, 29(8), 1814–1821.

Kari, V., Mansour, W. Y., Raul, S. K., Baumgart, S. J., Mund, A., Grade, M., Sirma, H., Simon, R., Will, H., Dobbelstein, M., Dikomey, E., & Johnsen, S. A. (2016). Loss of CHD1 causes DNA repair defects and enhances prostate cancer therapeutic responsiveness. EMBO Reports, 17(11), 1609–1623.

Kastan, M. B., & Bartek, J. (2004). Cell-cycle checkpoints and cancer. In Nature (Vol. 432, Issue 7015, pp. 316–323).

Khanna, K. K., & Jackson, S. P. (2001). DNA double-strand breaks: Signaling, repair and the cancer connection. Nature Genetics, 27(3), 247–254.

Kim, N., & Jinks-Robertson, S. (2012). Transcription as a source of genome instability. In Nature Reviews Genetics (Vol. 13, Issue 3, pp. 204–214).

Köcher, S., Rieckmann, T., Rohaly, G., Mansour, W. Y., Dikomey, E., Dornreiter, I., & Dahm-Daphi, J. (2012). Radiation-induced double-strand breaks require ATM but not Artemis for homologous recombination during S-phase. Nucleic Acids Research, 40(17), 8336–8347.

Koelsche, C., Schrimpf, D., Stichel, D., Sill, M., Sahm, F., Reuss, D. E., Blattner, M., Worst, B., Heilig, C. E., Beck, K., Horak, P., Kreutzfeldt, S., Paff, E., Stark, S., Johann, P., Selt, F., Ecker, J., Sturm, D., Pajtler, K. W., von Deimling, A. (2021). Sarcoma classification by DNA methylation profiling. Nature Communications, 12(1), 498.

Kote-Jarai, Z., Jugurnauth, S., Mulholland, S., Leongamornlert, D. A., Guy, M., Edwards, S., Tymrakiewitcz, M., O'Brien, L., Hall, A., Wilkinson, R., Al Olama, A. A., Morrison, J., Muir, K., Neal, D., Donovan, J., Hamdy, F., Easton, D. F., & Eeles, R. (2009). A recurrent truncating germline mutation in the BRIP1/FANCJ gene and susceptibility to prostate cancer. British Journal of Cancer, 100(2), 426–430.

Kotsantis, P., Silva, L. M., Irmscher, S., Jones, R. M., Folkes, L., Gromak, N., & Petermann, E. (2016). Increased global transcription activity as a mechanism of replication stress in cancer. Nature Communications, 7(1), 1–13.

Labbé, D. P., & Brown, M. (2018). Transcriptional Regulation in Prostate Cancer. Cold Spring Harbor Perspectives in Medicine, 8(11), a030437.

Lakshminarasimhan, R., & Liang, G. (2016). The role of DNA methylation in cancer. Advances in Experimental Medicine and Biology, 945, 151–172.

Lavin, M. F. (2008). Ataxia-telangiectasia: From a rare disorder to a paradigm for cell signalling and cancer. In Nature Reviews Molecular Cell Biology (Vol. 9, Issue 10, pp. 759–769).

Lee, S. E., Moore, J. K., Holmes, A., Umezu, K., Kolodner, R. D., & Haber, J. E. (1998). Saccharomyces Ku70, Mre11/Rad50, and RPA proteins regulate adaptation to G2/M arrest after DNA damage. Cell, 94(3), 399–409.

Li, G., Ci, W., Karmakar, S., Chen, K., Dhar, R., Fan, Z., Guo, Z., Zhang, J., Ke, Y., Wang, L., Zhuang, M., Hu, S., Li, X., Zhou, L., Li, X., Calabrese, M. F., Watson, E. R., Prasad, S. M., Rinker-Schaeffer, C., White, K. P. (2014). SPOP promotes tumorigenesis by acting as a key regulatory hub in kidney cancer. Cancer Cell, 25(4), 455–468.

Li, J. J., Zhang, J. F., Yao, S. M., Huang, H., Zhang, S., Zhao, M., & Huang, J. A. (2017). Decreased expression of speckle-type POZ protein for the prediction of poor prognosis in patients with non-small cell lung cancer. Oncology Letters, 14(3), 2743–2748.

Li, L., Karanika, S., Yang, G., Wang, J., Park, S., Broom, B. M., Manyam, G. C., Wu, W., Luo, Y., Basourakos, S., Song, J. H., Gallick, G. E., Karantanos, T., Korentzelos, D., Azad, A. K., Kim, J., Corn, P. G., Aparicio, A. M., Logothetis, C. J., … Thompson, T. C. (2017). Androgen receptor inhibitor-induced “BRCAness” and PARP inhibition are synthetically lethal for castration-resistant prostate cancer. Science Signaling, 10(480).

Li, X., & Heyer, W. D. (2008). Homologous recombination in DNA repair and DNA damage tolerance. In Cell Research (Vol. 18, Issue 1, pp. 99–113).

Liu, X., Sun, G., & Sun, X. (2016). RNA interference-mediated silencing of speckle-type POZ protein promotes apoptosis of renal cell cancer cells. OncoTargets and Therapy, 9, 2393–2402.

Löbrich, M., & Jeggo, P. (2017). A Process of Resection-Dependent Nonhomologous End Joining Involving the Goddess Artemis. In Trends in Biochemical Sciences (Vol. 42, Issue 9, pp. 690–701).

Lu, X., Zhu, X., Li, Y., Liu, M., Yu, B., Wang, Y., Rao, M., Yang, H., Zhou, K., Wang, Y., Chen, Y., Chen, M., Zhuang, S., Chen, L. F., Liu, R., & Chen, R. (2016). Multiple P-TEFbs cooperatively regulate the release of promoter-proximally paused RNA polymerase II. Nucleic Acids Research, 44(14), 6853–6867.

Ma, J., Chang, K., Peng, J., Shi, Q., Gan, H., Gao, K., Feng, K., Xu, F., Zhang, H., Dai, B., Zhu, Y. Y., Shi, G., Shen, Y., Zhu, Y. Y., Qin, X., Li, Y., Zhang, P., Ye, D., & Wang, C. (2018). SPOP promotes ATF2 ubiquitination and degradation to suppress prostate cancer progression. Journal of Experimental & Clinical Cancer Research, 37(1).

Maekawa, M., & Higashiyama, S. (2020). The Roles of SPOP in DNA Damage Response and DNA Replication. International Journal of Molecular Sciences, 21(19), 7293.

Mailand, N., Falck, J., Lukas, C., Syljuåsen, R. G., Welcker, M., Bartek, J., & Lukas, J. (2000). Rapid destruction of human Cdc25A in response to DNA damage. Science, 288(5470), 1425–1429.

Maire, C. L., Fuh, M. M., Kaulich, K., Fita, K. D., Stevic, I., Heiland, Di. H., Welsh, J. A., Jones, J. C., Görgens, A., Ricklefs, T., Dührsen, L., Sauvigny, T., Joosse, S. A., Reifenberger, G., Pantel, K., Glatzel, M., Miklosi, A. G., Felce, J. H., Caselli, M., … Ricklefs, F. L. (2021). Genome-wide methylation profiling of glioblastoma cell-derived extracellular vesicle DNA allows tumor classification. Neuro-Oncology, 23(7), 1087–1099.

Malumbres, M. (2014). Cyclin-dependent kinases. Genome Biology, 15(6), 122.

Mansour, W. Y., Schumacher, S., Rosskopf, R., Rhein, T., Schmidt-Petersen, F., Gatzemeier, F., Haag, F., Borgmann, K., Willers, H., & Dahm-Daphi, J. (2008). Hierarchy of nonhomologous end-joining, single-strand annealing and gene conversion at site-directed DNA double-strand breaks. Nucleic Acids Research, 36(12), 4088–4098.

Mansour, W. Y., Tennstedt, P., Volquardsen, J., Oing, C., Kluth, M., Hube-Magg, C., Borgmann, K., Simon, R., Petersen, C., Dikomey, E., & Rothkamm, K. (2018). Loss of PTEN-assisted G2/M checkpoint impedes homologous recombination repair and enhances radio-curability and PARP inhibitor treatment response in prostate cancer. Scientific Reports, 8(1), 3947.

Mari, P. O., Florea, B. I., Persengiev, S. P., Verkaik, N. S., Brüggenwirth, H. T., Modesti, M., Giglia-Mari, G., Bezstarosti, K., Demmers, J. A. A., Luider, T. M., Houtsmuller, A. B., & Van Gent, D. C. (2006). Dynamic assembly of end-joining complexes requires interaction between Ku70/80 and XRCC4. Proceedings of the National Academy of Sciences of the United States of America, 103(49), 18597–18602.

Marshall, N. F., Peng, J., Xie, Z., & Price, D. H. (1996). Control of RNA polymerase II elongation potential by a novel carboxyl- terminal domain kinase. Journal of Biological Chemistry, 271(43), 27176–27183.

Mateo, J., Boysen, G., Barbieri, C. E., Bryant, H. E., Castro, E., Nelson, P. S., Olmos, D., Pritchard, C. C., Rubin, M. A., & de Bono, J. S. (2017). DNA Repair in Prostate Cancer: Biology and Clinical Implications. European Urology, 71(3), 417–425.

Menolfi, D., & Zha, S. (2020). ATM, DNA-PKcs and ATR: shaping development through the regulation of the DNA damage responses. Genome Instability & Disease, 1(2), 47–68.

Meyer, B., Voss, K. O., Tobias, F., Jakob, B., Durante, M., & Taucher-Scholz, G. (2013). Clustered DNA damage induces pan-nuclear H2AX phosphorylation mediated by ATM and DNA-PK. Nucleic Acids Research, 41(12), 6109–6118.

Meyer, F., Becker, S., Classen, S., Parplys, A. C., Mansour, W. Y., Riepen, B., Timm, S., Ruebe, C., Jasin, M., Wikman, H., Petersen, C., Rothkamm, K., & Borgmann, K. (2020). Prevention of DNA Replication Stress by CHK1 Leads to Chemoresistance Despite a DNA Repair Defect in Homologous Recombination in Breast Cancer. Cells, 9(1).

Millán-Zambrano, G., Burton, A., Bannister, A. J., & Schneider, R. (2022). Histone post-translational modifications — cause and consequence of genome function. In Nature Reviews Genetics (Vol. 23, Issue 9, pp. 563–580).

Moeglin, E., Desplancq, D., Conic, S., Oulad-Abdelghani, M., Stoessel, A., Chiper, M., Vigneron, M., Didier, P., Tora, L., & Weiss, E. (2019). Uniform widespread nuclear phosphorylation of histone H2AX is an indicator of lethal DNA replication stress. Cancers, 11(3).

Moore, L. D., Le, T., & Fan, G. (2013). DNA methylation and its basic function. In Neuropsychopharmacology (Vol. 38, Issue 1, pp. 23–38).

Nagai, Y., Kojima, T., Muro, Y., Hachiya, T., Nishizawa, Y., Wakabayashi, T., & Hagiwara, M. (1997). Identification of a novel nuclear speckle-type protein, SPOP. FEBS Letters, 418(1–2), 23–26.

Ni, Z., Saunders, A., Fuda, N. J., Yao, J., Suarez, J.-R., Webb, W. W., & Lis, J. T. (2008). P-TEFb Is Critical for the Maturation of RNA Polymerase II into Productive Elongation In Vivo. Molecular and Cellular Biology, 28(3), 1161–1170.

Nicholas, T. R., Metcalf, S. A., Greulich, B. M., & Hollenhorst, P. C. (2021). Androgen signaling connects short isoform production to breakpoint formation at Ewing sarcoma breakpoint region 1. NAR Cancer, 3(3).

Nientiedt, C., Budczies, J., Endris, V., Kirchner, M., Schwab, C., Jurcic, C., Behnisch, R., Hoveida, S., Lantwin, P., Kaczorowski, A., Geisler, C., Dieffenbacher, S., Falkenbach, F., Franke, D., Görtz, M., Heller, M., Himmelsbach, R., Pecqueux, C., Rath, M., Duensing, S. (2022). Mutations in TP53 or DNA damage repair genes define poor prognostic subgroups in primary prostate cancer. Urologic Oncology: Seminars and Original Investigations, 40(1), 8.e11-8.e18.

Nikiforova, M. N., Stringer, J. R., Blough, R., Medvedovic, M., Fagin, J. A., & Nikiforov, Y. E. (2000). Proximity of chromosomal loci that participate in radiation-induced rearrangements in human cells. Science, 290(5489), 138–141.

Oing, C., Tennstedt, P., Simon, R., Volquardsen, J., Borgmann, K., Bokemeyer, C., Petersen, C., Dikomey, E., Rothkamm, K., & Mansour, W. Y. (2018). BCL2-overexpressing prostate cancer cells rely on PARP1-dependent end-joining and are sensitive to combined PARP inhibitor and radiation therapy. Cancer Letters, 423, 60–70.

Ou, Y. H., Chung, P. H., Sun, T. P., & Shieh, S. Y. (2005). p53 C-terminal phosphorylation by CHK1 and CHK2 participates in the regulation of DNA-damage-induced C-terminal acetylation. Molecular Biology of the Cell, 16(4), 1684–1695.

Özturan, D., Morova, T., & Lack, N. A. (2022). Androgen Receptor-Mediated Transcription in Prostate Cancer. In Cells (Vol. 11, Issue 5, p. 898).

Parsels, L. A., Parsels, J. D., Tanska, D. M., Maybaum, J., Lawrence, T. S., & Morgan, M. A. (2018). The contribution of DNA replication stress marked by high-intensity, pan-nuclear γH2AX staining to chemosensitization by CHK1 and WEE1 inhibitors. Cell Cycle, 17(9), 1076–1086.

Peterlin, B. M., & Price, D. H. (2006). Controlling the Elongation Phase of Transcription with P-TEFb. In Molecular Cell (Vol. 23, Issue 3, pp. 297–305).

Petermann, E., & Caldecott, K. W. (2006). Evidence that the ATR/Chk1 pathway maintains normal replication fork progression during unperturbed S phase. In Cell Cycle (Vol. 5, Issue 19, pp. 2203–2209).

Polkinghorn, W. R., Parker, J. S., Lee, M. X., Kass, E. M., Spratt, D. E., Iaquinta, P. J., Arora, V. K., Yen, W. F., Cai, L., Zheng, D., Carver, B. S., Chen, Y., Watson, P. A., Shah, N. P., Fujisawa, S., Goglia, A. G., Gopalan, A., Hieronymus, H., Wongvipat, J., Sawyers, C. L. (2013). Androgen receptor signaling regulates DNA repair in prostate cancers. Cancer Discovery, 3(11), 1245–1253.

Poluri, R. T. K., & Audet-Walsh, É. (2018). Genomic Deletion at 10q23 in Prostate Cancer: More Than PTEN Loss? Frontiers in Oncology, 8(JUN), 246.

Proudfoot, N. J. (2016). Transcriptional termination in mammals: Stopping the RNA polymerase II juggernaut. In Science (Vol. 352, Issue 6291, p. aad9926).

Ramsden, D. A. (2011). Polymerases in nonhomologous end joining: Building a bridge over broken chromosomes. In Antioxidants and Redox Signaling (Vol. 14, Issue 12, pp. 2509–2519).

Rich, T., Allen, R. L., & Wyllie, A. H. (2000). Defying death after DNA damage. In Nature (Vol. 407, Issue 6805, pp. 777–783).

Richardson, C., & Jasin, M. (2000). Frequent chromosomal translocations induced by DNA double-strand breaks. Nature, 405(6787), 697–700.

Rinaldi, C., Pizzul, P., Longhese, M. P., & Bonetti, D. (2021). Sensing R-Loop-Associated DNA Damage to Safeguard Genome Stability. In Frontiers in Cell and Developmental Biology (Vol. 8).

Romanel, A., Garritano, S., Stringa, B., Blattner, M., Dalfovo, D., Chakravarty, Di., Soong, D., Cotter, K. A., Petris, G., Dhingra, P., Gasperini, P., Cereseto, A., Elemento, O., Sboner, A., Khurana, E., Inga, A., Rubin, M. A., & Demichelis, F. (2017). Inherited determinants of early recurrent somatic mutations in prostate cancer. Nature Communications, 8(1), 48.

Rose, N. R., & Klose, R. J. (2014). Understanding the relationship between DNA methylation and histone lysine methylation. In Biochimica et Biophysica Acta - Gene Regulatory Mechanisms (Vol. 1839, Issue 12, pp. 1362–1372).

Saksouk, N., Simboeck, E., & Déjardin, J. (2015). Constitutive heterochromatin formation and transcription in mammals. Epigenetics & Chromatin, 8(1), 3.

Scully, R., Panday, A., Elango, R., & Willis, N. A. (2019). DNA double-strand break repair-pathway choice in somatic mammalian cells. In Nature Reviews Molecular Cell Biology (Vol. 20, Issue 11, pp. 698–714).

Sebastian, R., & Oberdoerffer, P. (2017). Transcription-associated events affecting genomic integrity. Philosophical Transactions of the Royal Society B: Biological Sciences, 372(1731), 20160288.

Shannon, P., Markiel, A., Ozier, O., Baliga, N. S., Wang, J. T., Ramage, D., Amin, N., Schwikowski, B., & Ideker, T. (2003). Cytoscape: A software Environment for integrated models of biomolecular interaction networks. Genome Research, 13(11), 2498–2504.

Sheridan, R. M., Fong, N., D'Alessandro, A., & Bentley, D. L. (2019). Widespread Backtracking by RNA Pol II Is a Major Effector of Gene Activation, 5′ Pause Release, Termination, and Transcription Elongation Rate. Molecular Cell, 73(1), 107-118.e4.

Sidoli, S., Lopes, M., Lund, P. J., Goldman, N., Fasolino, M., Coradin, M., Kulej, K., Bhanu, N. V., Vahedi, G., & Garcia, B. A. (2019). A mass spectrometry-based assay using metabolic labeling to rapidly monitor chromatin accessibility of modified histone proteins. Scientific Reports, 9(1), 13613.

Smith, P. K., Krohn, R. I., Hermanson, G. T., Mallia, A. K., Gartner, F. H., Provenzano, M. D., Fujimoto, E. K., Goeke, N. M., Olson, B. J., & Klenk, D. C. (1985). Measurement of protein using bicinchoninic acid. Analytical Biochemistry, 150(1), 76–85.

Sollier, J., & Cimprich, K. A. (2015). Breaking bad: R-loops and genome integrity. In Trends in Cell Biology (Vol. 25, Issue 9, pp. 514–522).

Sollier, J., Stork, C. T., García-Rubio, M. L., Paulsen, R. D., Aguilera, A., & Cimprich, K. A. (2014). Transcription-Coupled Nucleotide Excision Repair Factors Promote R-Loop-Induced Genome Instability. Molecular Cell, 56(6), 777–785.

Song, Y., Xu, Y., Pan, C., Yan, L., Wang, Z. W., & Zhu, X. (2020). The emerging role of SPOP protein in tumorigenesis and cancer therapy. In Molecular Cancer (Vol. 19, Issue 1, p. 2).

Soulas-Sprauel, P., Rivera-Munoz, P., Malivert, L., Le Guyader, G., Abramowski, V., Revy, P., & De Villartay, J. P. (2007). V(D)J and immunoglobulin class switch recombinations: A paradigm to study the regulation of DNA end-joining. In Oncogene (Vol. 26, Issue 56, pp. 7780–7791).

Steurer, B., Janssens, R. C., Geijer, M. E., Aprile-Garcia, F., Geverts, B., Theil, A. F., Hummel, B., van Royen, M. E., Evers, B., Bernards, R., Houtsmuller, A. B., Sawarkar, R., & Marteijn, J. (2022). DNA damage-induced transcription stress

triggers the genome-wide degradation of promoter-bound Pol II. Nature Communications, 13(1), 3624.

Stork, C. T., Bocek, M., Crossley, M. P., Sollier, J., Sanz, L. A., Chédin, F., Swigut, T., & Cimprich, K. A. (2016). Co-transcriptional R-loops are the main cause of estrogen-induced DNA damage. ELife, 5(AUGUST).

Struve, N., Hoffer, K., Weik, A. S., Riepen, B., Krug, L., Cetin, M. H., Burmester, J., Ott, L., Liebing, J., Gatzemeier, F., Müller-Goebel, J., Gerbach, M., Bußmann, L., Parplys, A. C., Unger, K., Mansour, W. Y., Schüller, U., Rieckmann, T., Petersen, C., Kriegs, M. (2022). Increased replication stress and R-loop accumulation in EGFRvIII-expressing glioblastoma present new therapeutic opportunities.

Subramanian, A., Tamayo, P., Mootha, V. K., Mukherjee, S., Ebert, B. L., Gillette, M. A., Paulovich, A., Pomeroy, S. L., Golub, T. R., Lander, E. S., & Mesirov, J. P. (2005). Gene set enrichment analysis: A knowledge-based approach for interpreting genome-wide expression profiles. Proceedings of the National Academy of Sciences of the United States of America, 102(43), 15545–15550.

Sun, Y., McCorvie, T. J., Yates, L. A., & Zhang, X. (2020). Structural basis of homologous recombination. Cellular and Molecular Life Sciences, 77(1), 3–18.

Swami, U., Isaacsson Velho, P., Nussenzveig, R., Chipman, J., Sacristan Santos, V., Erickson, S., Dharmaraj, D., Alva, A. S., Vaishampayan, U. N., Esther, J., Hahn, A. W., Maughan, B. L., Antonarakis, E. S., & Agarwal, N. (2020). Association of SPOP Mutations with Outcomes in Men with De Novo Metastatic Castration-sensitive Prostate Cancer. European Urology, 78(5), 652–656.

Tachibana, M., Ueda, J., Fukuda, M., Takeda, N., Ohta, T., Iwanari, H., Sakihama, T., Kodama, T., Hamakubo, T., & Shinkai, Y. (2005). Histone methyltransferases G9a and GLP form heteromeric complexes and are both crucial for methylation of euchromatin at H3-K9. Genes and Development, 19(7), 815–826.

Takata, M., Sasaki, M. S., Sonoda, E., Morrison, C., Hashimoto, M., Utsumi, H., Yamaguchi-Iwai, Y., Shinohara, A., & Takeda, S. (1998). Homologous recombination and non-homologous end-joining pathways of DNA double-strand break repair have overlapping roles in the maintenance of chromosomal integrity in vertebrate cells. EMBO Journal, 17(18), 5497–5508.

Tan, M. E., Li, J., Xu, H. E., Melcher, K., & Yong, E. L. (2015). Androgen receptor: Structure, role in prostate cancer and drug discovery. In Acta Pharmacologica Sinica (Vol. 36, Issue 1, pp. 3–23).

Tarish, F. L., Schultz, N., Tanoglidi, A., Hamberg, H., Letocha, H., Karaszi, K., Hamdy, F. C., Granfors, T., & Helleday, T. (2015). Castration radiosensitizes prostate cancer tissue by impairing DNA double-strand break repair. Science Translational Medicine, 7(312), 312re11.

Tennstedt, P., Fresow, R., Simon, R., Marx, A., Terracciano, L., Petersen, C., Sauter, G., Dikomey, E., & Borgmann, K. (2013). RAD51 overexpression is a negative

prognostic marker for colorectal adenocarcinoma. International Journal of Cancer, 132(9), 2118–2126.

Theurillat, J.-P. P., Udeshi, N. D., Errington, W. J., Svinkina, T., Baca, S. C., Pop, M., Wild, P. J., Blattner, M., Groner, A. C., Rubin, M. A., Moch, H., Prive, G. G., Carr, S. A., & Garraway, L. A. (2014). Prostate cancer. Ubiquitylome analysis identifies dysregulation of effector substrates in SPOP-mutant prostate cancer. Science (New York, N.Y.), 346(6205), 85–89.

Toivanen, R., & Shen, M. M. (2017). Prostate organogenesis: Tissue induction, hormonal regulation and cell type specification. In Development (Cambridge) (Vol. 144, Issue 8, pp. 1382–1398).

Tomlins, S. A., Rhodes, D. R., Perner, S., Dhanasekaran, S. M., Mehra, R., Sun, X. W., Varambally, S., Cao, X., Tchinda, J., Kuefer, R., Lee, C., Montie, J. E., Shah, R. B., Pienta, K. J., Rubin, M. A., & Chinnaiyan, A. M. (2005). Recurrent fusion of TMPRSS2 and ETS transcription factor genes in prostate cancer. Science, 310(5748), 644–648.

Ui, A., Chiba, N., & Yasui, A. (2020). Relationship among DNA double-strand break (DSB), DSB repair, and transcription prevents genome instability and cancer. Cancer Science, 111(5), 1443–1451.

Uto, K., Inoue, D., Shimuta, K., Nakajo, N., & Sagata, N. (2004). Chk1, but not Chk2, inhibits Cdc25 phosphatases by a novel common mechanism. EMBO Journal, 23(16), 3386–3396.

Vamvakas, S., Vock, E. H., & Lutz, W. K. (1997). On the role of DNA souble-strand breaks in toxicity and carcinogenesis. In Critical Reviews in Toxicology (Vol. 27, Issue 2, pp. 155–174). Crit Rev Toxicol.

Van Geersdaele, L. K., Stead, M. A., Harrison, C. M., Carr, S. B., Close, H. J., Rosbrook, G. O., Connell, S. D., & Wright, S. C. (2013). Structural basis of high-order oligomerization of the cullin-3 adaptor SPOP. Acta Crystallographica Section D: Biological Crystallography, 69(9), 1677–1684.

Wahba, L., Amon, J. D., Koshland, D., & Vuica-Ross, M. (2011). RNase H and Multiple RNA Biogenesis Factors Cooperate to Prevent RNA:DNA Hybrids from Generating Genome Instability. Molecular Cell, 44(6), 978–988.

Wang, L., Pan, S., Zhu, B., Yu, Z., & Wang, W. (2021). Comprehensive analysis of tumour mutational burden and its clinical significance in prostate cancer. BMC Urology, 21(1), 29.

Watanabe, R., Maekawa, M., Hieda, M., Taguchi, T., Miura, N., Kikugawa, T., Saika, T., & Higashiyama, S. (2020). SPOP is essential for DNA-protein cross-link repair in prostate cancer cells: SPOP-dependent removal of topoisomerase 2A from the topoisomerase 2A-DNA cleavage complex. Molecular Biology of the Cell, 31(6), 478–490.

Wei Dai, Y. Y. (2014). Genomic Instability and Cancer. Journal of Carcinogenesis & Mutagenesis, 05(02).

Weterings, E., & Chen, D. J. (2007). DNA-dependent protein kinase in nonhomologous end joining: A lock with multiple keys? In Journal of Cell Biology (Vol. 179, Issue 2, pp. 183–186).

Wu, F., Dai, X., Gan, W., Wan, L., Li, M., Mitsiades, N., Wei, W., Ding, Q., & Zhang, J. (2017). Prostate cancer-associated mutation in SPOP impairs its ability to target Cdc20 for poly-ubiquitination and degradation. Cancer Letters, 385, 207–214.

Xu, J., Wang, F., Jiang, H., Jiang, Y., Chen, J., & Qin, J. (2015). Properties and Clinical Relevance of Speckle-Type POZ Protein in Human Colorectal Cancer. Journal of Gastrointestinal Surgery, 19(8), 1484–1496.

Yamaguchi, Y., Takagi, T., Wada, T., Yano, K., Furuya, A., Sugimoto, S., Hasegawa, J., & Handa, H. (1999). NELF, a multisubunit complex containing RD, cooperates with DSIF to repress RNA polymerase II elongation. Cell, 97(1), 41–51.

Yoshioka, K. I., Kusumoto-Matsuo, R., Matsuno, Y., & Ishiai, M. (2021). Genomic instability and cancer risk associated with erroneous dna repair. In International Journal of Molecular Sciences (Vol. 22, Issue 22, p. 12254).

Yu, K., Chedin, F., Hsieh, C. L., Wilson, T. E., & Lieber, M. R. (2003). R-loops at immunoglobulin class switch regions in the chromosomes of stimulated B cells. Nature Immunology, 4(5), 442–451.

Yurchenko, A. A., Padioleau, I., Matkarimov, B. T., Soulier, J., Sarasin, A., & Nikolaev, S. (2020). XPC deficiency increases risk of hematologic malignancies through mutator phenotype and characteristic mutational signature. Nature Communications, 11(1), 5834.

Zatreanu, D., Han, Z., Mitter, R., Tumini, E., Williams, H., Gregersen, L., Dirac-Svejstrup, A. B., Roma, S., Stewart, A., Aguilera, A., & Svejstrup, J. Q. (2019). Elongation Factor TFIIS Prevents Transcription Stress and R-Loop Accumulation to Maintain Genome Stability. Molecular Cell, 76(1), 57-69.e9.

Zeng, C., Wang, Y., Lu, Q., Chen, J., Zhang, J., Liu, T., Lv, N., & Luo, S. (2014). SPOP suppresses tumorigenesis by regulating Hedgehog/Gli2 signaling pathway in gastric cancer. Journal of Experimental and Clinical Cancer Research, 33(1).

Zhang, J., Bu, X., Wang, H., Zhu, Y., Geng, Y., Nihira, N. T., Tan, Y., Ci, Y., Wu, F., Dai, X., Guo, J., Huang, Y. H., Fan, C., Ren, S., Sun, Y., Freeman, G. J., Sicinski, P., & Wei, W. (2018). Cyclin D-CDK4 kinase destabilizes PD-L1 via cullin 3-SPOP to control cancer immune surveillance. Nature, 553(7686), 91–95.

Zhang, J., Chen, M., Zhu, Y., Dai, X., Dang, F., Ren, J., Ren, S., Shulga, Y. V., Beca, F., Gan, W., Wu, F., Lin, Y.-M., Zhou, X., DeCaprio, J. A., Beck, A. H., Lu, K. P., Huang, J., Zhao, C., Sun, Y., Wei, W. (2019). SPOP Promotes Nanog Destruction to Suppress Stem Cell Traits and Prostate Cancer Progression. Developmental Cell, 48(3), 329-344.e5.

Zhang, J., Gao, K., Xie, H., Wang, D., Zhang, P., Wei, T., Yan, Y., Pan, Y., Ye, W., Chen, H., Shi, Q., Li, Y., Zhao, S., Hou, X., Weroha, S. J., Wang, Y., Zhang, J., Karnes, R. J., He, H. H., … Huang, H. (2021). SPOP mutation induces DNA methylation via stabilizing GLP/G9a. Nature Communications, 12(1), 5716.

Zhang, L., Peng, S., Dai, X., Gan, W., Nie, X., Wei, W., Hu, G., & Guo, J. (2017). Tumor suppressor SPOP ubiquitinates and degrades EglN2 to compromise growth of prostate cancer cells. Cancer Letters, 390, 11–20.

Zhang, P., Gao, K., Jin, X., Ma, J., Peng, J., Wumaier, R., Tang, Y., Zhang, Y., An, J., Yan, Q., Dong, Y., Huang, H., Yu, L., & Wang, C. (2015). Endometrial cancer-associated mutants of SPOP are defective in regulating estrogen receptor-α protein turnover. Cell Death & Disease, 6(3), e1687–e1687.

Zhang, P., Wang, D., Zhao, Y., Ren, S., Gao, K., Ye, Z., Wang, S., Pan, C. W., Zhu, Y., Yan, Y., Yang, Y., Wu, D., He, Y., Zhang, J., Lu, D., Liu, X., Yu, L., Zhao, S., Li, Y., Huang, H. (2017). Intrinsic BET inhibitor resistance in SPOP-mutated prostate cancer is mediated by BET protein stabilization and AKT-mTORC1 activation. Nature Medicine, 23(9), 1055–1062.

Zhang, W., van Gent, D. C., Incrocci, L., van Weerden, W. M., & Nonnekens, J. (2020). Role of the DNA damage response in prostate cancer formation, progression and treatment. Prostate Cancer and Prostatic Diseases, 23(1), 24–37.

Zhao, F., Kim, W., Kloeber, J. A., & Lou, Z. (2020). DNA end resection and its role in DNA replication and DSB repair choice in mammalian cells. Experimental & Molecular Medicine, 52(10), 1705–1714.

Zhao, W., Zhou, J., Deng, Z., Gao, Y., & Cheng, Y. (2016). SPOP promotes tumor progression via activation of catenin/ TCF4 complex in clear cell renal cell carcinoma. International Journal of Oncology, 49(3), 1001–1008.

Zhou, B. B. S., & Elledge, S. J. (2000). The DNA damage response: putting checkpoints in perspective. Nature 2000 408:6811, 408(6811), 433–439.

Zhu, H., Ren, S., Bitler, B. G., Aird, K. M., Tu, Z., Skordalakes, E., Zhu, Y., Yan, J., Sun, Y., & Zhang, R. (2015). SPOP E3 Ubiquitin Ligase Adaptor Promotes Cellular Senescence by Degrading the SENP7 deSUMOylase. Cell Reports, 13(6), 1183–1193.

Zhu, K., Lei, P. J., Ju, L. G., Wang, X., Huang, K., Yang, B., Shao, C., Zhu, Y., Wei, G., Fu, X. D., Li, L., & Wu, M. (2017). SPOP-containing complex regulates SETD2 stability and H3K36me3-coupled alternative splicing. Nucleic Acids Research, 45(1), 92–105.

Zhuang, M., Calabrese, M. F., Liu, J., Waddell, M. B., Nourse, A., Hammel, M., Miller, D. J., Walden, H., Duda, D. M., Seyedin, S. N., Hoggard, T., Harper, J. W., White, K. P., & Schulman, B. A. (2009). Structures of SPOP-Substrate Complexes: Insights into Molecular Architectures of BTB-Cul3 Ubiquitin Ligases. Molecular Cell, 36(1), 39–50.

Zimmermann, M., Lottersberger, F., Buonomo, S. B., Sfeir, A., & De Lange, T. (2013). 53BP1 regulates DSB repair using Rif1 to control 5′ end resection. Science, 339(6120), 700–704.

https://www.takarabio.com/learning-centers/gene-function/gene-editing/gene-editing-tools-and-information/introduction-to-the-crispr/cas9-system.

https://www.activemotif.com/blog-atac-seq

## 9. Acknowledgements

In the name of God, almighty **Allah**, the merciful, the compassionate. Praise and thanks for the blessings, for empowering me to successfully finish this work and get through everything.

I am deeply indebted to my supervisor PD. Dr. **Wael Yassin Mansour** for his continuous support and guidance not just on the academic and professional level but also, on the personal side for whatever problems I faced in Germany.
As much I have tried to thank him, no words would ever be enough. I am so much grateful for giving me the opportunity to be part of his team, his patience, always giving me from his time despite his very busy schedule. Thanks a lot for the open discussions, sharing the knowledge and the brilliant ideas; in addition to, the open resources and funding.
I also would like to show my appreciation to him during the writing phase and all the discussions that I have learnt a lot from, not just on the scientific level, but also, on the interpersonal side.
I really appreciate a lot the continuous motivation, forward pushing and believing in me in the times I doubted my abilities. His guidance allowed me to be more oriented in understanding different fields and empowered me to better conduct my research and build different skills. I could have never wished for a better mentor.

I am sincerely thankful and grateful for Prof. Dr. **Kai Rothkamm**, the head of Laboratory of Radiobiology and experimental Radiooncology, for his continuous support, great brilliant suggestions and comments.

I am so grateful for the **DAAD** for giving me the opportunity to pursue my PhD in Germany by providing me a scholarship for the first 4 years of my study. In addition, I deeply appreciate the support from Dr. **Inga Melzer and MSNZ committee**, Hamburg, who provided me with fund to continue my PhD studies after my scholarship.

I am also thankful for **all my team and colleagues** in the Lab for their engaging and open atmosphere that helped me not only in my research, but also, to integrate in the German culture.

As for **Alexandra Zielinski,** I really can't thank her enough for everything. I am so grateful not just for her continuous help and technical support in the lab, but also, for being a real friend and supporting me like a family member. Thanks for helping and guiding me in whatever I needed in Germany and for the nice talks, outings and coffee breaks. I am lucky to get to know her.

Also, a special thanks for **Konstantin Hoffer**, **Fruzsina Gatzemeier**, **Stefanie Meien,** for their technical support whenever was needed.

My sincere thanks to PD. Dr. **Thorsten Rieckmann,** Dr. **Sabrina Köcher,** Dr. **Nina Struve,** Dr.med. **Christoph Oing**, for their nice support and lively discussions in meetings**.**

**Hannah voß,** I am so grateful for collaborating and performing the practical experiments for the proteomics part, as well as, the different analysis. In addition to, the support she provided to understand proteomics and guide through the data analysis, which helped me a lot to analyze the data and find my passion to omics. Moreover, thanks a lot for the guidance in writing the proteomics part.

To **my best friends** in Germany, I can't thank you enough for being my family here and supporting me in every possible way throughout the journey. I also would like to thank my Egyptian friends, who have been supporting me despite the long distance.

A special sincere thanks and appreciation to my dear mentors Prof. Dr. **Abdel-Hady Abdel-Wahab,** Prof. Dr. **Heba Moussa**, from NCI, Cairo university and Prof. Dr. **Hanan El- Abhar**, from Faculty of Pharmacy, Cairo University, for their continuous guidance and support since the day I met them; and for paving the way for me in the first place to start a career in Cancer research and pursue my PhD abroad.

Finally, I would like to give all the credit to my family, who without their support, I'd have never been able to pursue my journey. Thanks for supporting me to travel, and withstanding my absence and consequent troubles. **My father,** my role model, thanks for the everyday support. He is the reason behind my passion to my career. No words can describe how I am lucky to have him, can't thank him enough for being my mentor and best friend. My dearest sweetest **mother,** who always has a solution to any problem I face, thanks for the unconditional love and giving me strength through whatever obstacles I go through to reach my goals. My little **sister**, who has done nothing but loving me and being my backbone all the time and bringing **Lara** to life; who literally changed my life, and is the only reason for my smile in my most desperate depressive times.

## 10. Curriculum Vitae

## 11. Eidesstattliche Versicherung

Ich versichere ausdrücklich, dass ich die Arbeit selbständig und ohne fremde Hilfe verfasst, andere als die von mir angegebenen Quellen und Hilfsmittel nicht benutzt und die aus den benutzten Werken wörtlich oder inhaltlich entnommenen Stellen einzeln nach Ausgabe (Auflage und Jahr des Erscheinens), Band und Seite des benutzten Werkes kenntlich gemacht habe.
Ferner versichere ich, dass ich die Dissertation bisher nicht einem Fachvertreter an einer anderen Hochschule zur Überprüfung vorgelegt oder mich anderweitig um Zulassung zur Promotion beworben habe.

Ich erkläre mich einverstanden, dass meine Dissertation vom Dekanat der Medizinischen Fakultät mit einer gängigen Software zur Erkennung von Plagiaten überprüft werden kann.

Unterschrift: Shaimaa Fahmy